Summer 8-2012

The Effect of POSS Modified Montmorillonite On Elastomer Nanocomposites

Elana Celeste Lewis
University of Southern Mississippi

The University of Southern Mississippi

THE EFFECT OF POSS MODIFIED MONTMORILLONITE ON ELASTOMER NANOCOMPOSITES

by

Elana Celeste Lewis

A Thesis
Submitted to the Graduate School
of The University of Southern Mississippi
in Partial Fulfillment of the Requirements
for the Degree of Master of Science

Approved:

Dean of the Graduate School

August 2012

ABSTRACT

THE EFFECT OF POSS MODIFIED MONTMORILLONITE

ON ELASTOMER NANOCOMPOSITES

by Elana Celeste Lewis

August 2012

The goal of this thesis was to define the structural factors that determine performance in clay/rubber nanocomposites when polyhedral oligomeric silsesquioxane (POSS) is used as a dispersant. POSS has been shown previously to enhance clay, metal oxides, and carbon nanotube dispersion in thermoplastics matrices, but their performance in rubber systems has not yet been explored. There is little fundamental understanding of how POSS interacts with clay and how these modified fillers react with rubber matrices. This thesis aims to develop a greater understanding of the mechanisms of POSS-clay modification through the examination of two different POSS-clay systems and their effect on rubber matrices with varying functional groups.

In this thesis, an amino-based, closed cage POSS and an open-caged trisilanol POSS were used as modifiers of montmorillonite clay. A commercially available, organically modified clay was used as a control. These fillers were studied as a function of loading level in a hydrogenated nitrile butadiene rubber and a styrene butadiene rubber matrix. Both POSS systems successfully grafted onto the clay particles; however, the closed cage POSS produced an expanded interlayer spacing. The open cage POSS produced small particles with an increased surface area. When introduced into rubber matrices, both POSS-modified clay systems produced nanocomposites with improved properties. The trisilanolphenyl POSS-clay filler provided a 7°C increase in degradation

temperature, 136% increase in tensile modulus and an 800% improvement in storage modulus. Differences in performance are attributed to the cage structure, functional groups, and chemical and physical interactions of POSS with the rubber molecules

ACKNOWLEDGMENTS

I would like to thank my graduate research advisor, Dr. Sarah E. Morgan, for her constant support and guidance, and for the wonderful opportunities for collaboration and travel. I also thank my other committee members, Dr. Robert Y. Lochhead and Dr. Robson F. Storey. Financially, this work was supported by the Office of Naval Research.

I would like to thank Dr. Mithun Bhattacharya for his invaluable advice and support. Additionally, the help Qi Wu provided on TEM and Yingji Wu on microtoming is appreciated greatly. I had great opportunities for training at Sun Chemical as well as a month long research stint at the India Institute of Technology in Delhi.

TABLE OF CONTENTS

LIST OF TABLES

LIST OF ILLUSTRATIONS

Figure

CHAPTER I

INTRODUCTION

Literature Review

Organoclays

The use of clay as a filler in polymer matrices is a long-standing and popular area of industrial and academic research. Reinforcing fillers are of interest due to the increase in mechanical, thermal and barrier properties they can provide to a matrix (1). A variety of fillers have been used to improve properties and reduce the cost of plastics and elastomers. Nanofillers are defined as particles with at least one dimension in the nanometer size range (2). The introduction of nanofillers into matrices allows the properties of a nanocomposite to be tailored, starting during processing. Nanofillers are classified as rod/fiber, sheet/platelet or spherical/cubic types. Carbon nanotubes are an example of the fiber type of nanofiller. Carbon nanotubes have the unique properties of being highly isotropic, which provides high strength and semiconductive properties in nanocomposites. Carbon nanotubes are often functionalized to improve their compatibility with polymers. Platelet structures, such as layered silicates, are extremely useful fillers. Approximately 90% of the earth's crust is composed of silicates. The abundance of silicates provides a cost effective filler choice. Silicates are composed of silicon-oxygen tetrahedra. Silicates can range from single tetrahedron silicates known as nesosilicates to rings known as cyclosilicates, with many other varieties in between. The most common clays belong to the phyllosilicate structure, which is indicative of a sheet structure. The phyllosilicate subclass consists of materials with tetrahedra linked by shared oxygens to other tetrahedra. One of the materials of the subclass is clay. Within

the clay group, there are four subgroups: kaolinite, smectite, illite and chlorite. Within the smectite group is montmorillonite (MMT), a commonly used clay filler. MMT is composed of two silica-oxygen tetrahedral sheets sandwiching an aluminum or magnesium octahedral sheets (3). This Al or Mg ion is octahedrally coordinated to six hydroxyls or oxygens. Silicon is replaced by aluminum or the aluminum ions are replaced by magnesium. Either one of these replacements produces negatively charged MMT layers. In the case of sodium MMT, sodium cations are attracted to the MMT surface in order to neutralize the negative charges. MMT becomes hydrophilic due to the hydration of the sodium cations on the exchange sites. MMT is shown in the schematic below.

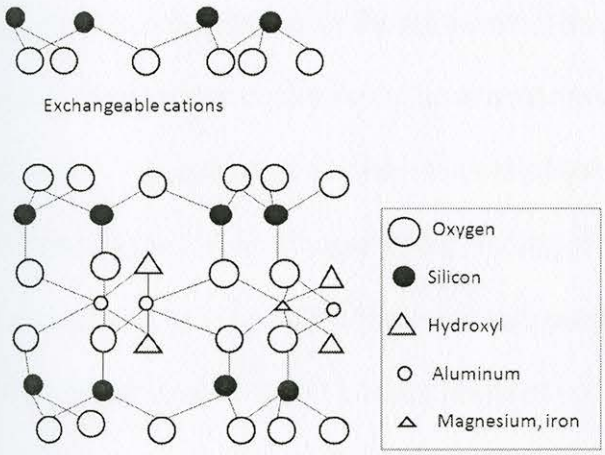

Figure 1. Structure of Montmorillonite clay (MMT (after (4)).

The hydrophilicity of unmodified MMT inhibits good interaction with hydrophobic polymer matrices (5). An ion exchange process of the sodium cations with alkyl ammonium compounds provides a hydrophobic surface coating to the clay and improves compatibility with hydrophobic polymers (6). The gap between two aluminosilicate layers is referred to as the interlayer. Relatively weak electrostatic forces hold the aluminosilicate layers together, thus the layers are easily expanded by cations or hydration. One of the common techniques to create a more hydrophobic clay is through

the expansion of this interlayer. By replacing the sodium cations at the exchange sites with alkyl ammonium ions, the MMT surface will become hydrophobic (7). Along with expanding the clay interlayer, interaction with hydrophobic polymers is increased and thermodynamic interactions improve with the ion exchange reaction. The layering of alkyl ammonium chains within the clay affects the spacing of the interlayer. Vaia et al. proposed that alkylammonium ions can layer in either a lateral monolayer, lateral bilayer, paraffin-type monolayer or a paraffin-type bilayer (8). In addition, trans or gauche conformers as well as the tilt of the ion can affect the spacing of the interlayer. FTIR studies monitoring the asymmetric CH_2 band have suggested that as the packing density or chain length decrease, or the temperature increases, that the intercalated chains have a more disordered structure due to an increase in mobility (8). A study by Xi examined the effects of the amount of alkylammonium added to MMT (3). XRD studies indicate that the packing behavior changes as the loading of alkylammonium is increased. The cation exchange capacity (CEC) is the maximum number of monovalent cations exchangeable per 100 grams of clay. At loading levels of 0.2 and 0.4 times the CEC, there is a lateral-monolayer. As the loading increases, a lateral bilayer occurs. At the highest loading levels of alkyl ammonium, the layering shifts to a pseudotrilayer arrangement. This study proposes that the largest interlayer spacing that the clay can achieve will translate into the best polymer-filler interaction. Osmana et al. studied the effect of altering the number of carbons in the alkyl chain (4, 8, or 18) and the area of the alkylammonium chain on clay layering (6). It was determined that short alkyl chains lay flat and remained disordered within the clay layers, while the longer chains provided increased clay layer spacing. At a certain length, the alkylammonium chains become ordered due to increased chain

interactions. MMT clay is commonly used as a polymer modifier due to its high swelling capacity courtesy of the small, easily hydrated sodium cations (9). This provides an easily accessible platelet surface for surfactant attachment. It is paramount that the modification of clays remains intact during addition into a polymer matrix. One way to ensure this is to rinse the modified clay with solvents such as ethanol or water. It has been shown that washing allows the physically adsorbed surfactant to be removed, without affecting the ion exchanged surfactant.

A study by Le Pluart et al. examined the influence of the exchange temperature on cation exchange process (1). It was reported that at 60°C, a paraffin structure developed, whereas at 80°C, the structure became a pseudotrilayer. The same study determined that the amine/clay ratio had no effect on the type of alkylammonium structure. However, it was also determined that an excess of amine is necessary to provide a complete layer of ions and create a strongly hydrophobic clay. Additionally, the polar component is higher for clays exchanged with short chain alkylammonium ions, as they provide lower hydrophobic coverage of the silicate surface.

POSS Polymer Composites

As an alternative to using an alkylammonium for ion exchange, an amino based polyhedral oligomeric silsesquioxane (POSS) can be used. POSS was first developed in 1946 and is a class of three-dimensional silsesquioxanes that are derived from the hydrolytic condensation of trifunctional organosilicon monomers (10). The inorganic-organic cage structure consists of a siloxane core to which organic groups are covalently attached at the corner silicon atoms. POSS molecules can be fully condensed or exist as an open cage structure. Figure 2 shows the structure of a closed cage POSS molecule.

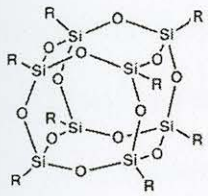

Figure 2. Schematic of closed cage POSS molecule, R represents organic substituent.

Changing the functional groups and the structure of the siloxane core of POSS molecules can increase compatibility with a variety of polymer matrices (11). POSS molecules with halide, epoxy, silanol, alcohol and a variety of other functional groups are available. POSS can be incorporated into copolymers both by grafting and copolymerization techniques. These copolymers exhibit enhanced modulus, stiffness, thermal stability and flame retardancy. The addition of POSS directly into polymer matrices is well explored. Dintcheva et al. reported that the POSS functionality and cage structure of POSS is related to the properties and structure of polystyrene (PS) nanocomposites (12). The authors suggest that POSS acts as a plasticizer in the PS. Additionally, the flexible open cage POSS provides the largest plasticizer effect due to the mobility of the chemical. Closed cage POSS with short aliphatic chains show a tendency towards aggregation while the longer alkyl chains increase the free volume of the composite. For PS in particular, the π-π stacking between the phenyl group of trisilanolphenyl POSS (TSP) and PS provide the greatest improvements in properties. Another study examining POSS and PS used nuclear magnetic resonance and theoretical solubility parameters to indicate that TSP provided better properties than octaisobutyl POSS in PS nanocomposites (13). The TSP showed greater interaction with the PS chain while the octaisobutyl POSS aggregated and exhibited surface segregation. POSS can

also be used as a dispersing agent for metal oxides. Wheeler et al. showed that the incorporation of POSS with nano- TiO_2 in polypropylene produces better dispersion compared to TiO_2 alone (14).

Additionally, studies have been conducted using POSS as a filler or crosslinking agent in rubber systems. Liu et al. used an epoxycyclohexyl POSS to bond to hydrogenated carboxylated nitrile butadiene rubber (15). Using *in situ* FTIR analysis, the authors determined that the carboxyl groups of the rubber chemically reacted with the epoxy groups of POSS during curing. The storage modulus, crosslink density and glass transition temperature increased with increasing POSS content due to increased chemical reactions with hydrogenated carboxylated nitrile butadiene rubber. In another study, polysiloxane and octaisobutyl POSS composites were prepared by melt blending (16). The study indicated that at high melt blending temperatures, the POSS dissolved in the polysiloxane and the dispersion increased. Additionally, the POSS was able to physically interact with the polymer chains, which resulted in a decrease in crosslink density. Sahoo examined the use of hydroxyl functionalized POSS as a crosslinking agent in fluorocarbon carboxylated nitrile butadiene (NBR) rubber (17). Increased mechanical and thermal properties with the use of POSS as a crosslinking agent indicated the success of this technique.

It is our hypothesis that clay dispersion in a rubber matrix can be improved through the use of appropriate POSS molecules as surface modifiers for clay. Additionally, the use of the exposed hydroxyl on open cage POSS systems may aid in crosslinking with rubber.

Amino-POSS clay

Our study has focused on two different POSS molecules for surface modification of MMT. The first approach involves using aminoethylaminopropylisobutyl POSS (AP) as an ion exchange agent. In a study by Perrin et al., three CEC of octa(ammoniumpropyl)octasilsesquioxane was added to MMT (18). Perrin hypothesized that all eight aminopropyl groups of POSS were able to ion exchange with MMT, producing an alignment of POSS in the clay interlayer. This study proposed monolayer arrangements of POSS at high concentration levels. The authors theorized that since all of the ammonium ions can ion exchange with the clay, the POSS is forced to lay flat and thus cannot form a bilayer. In another study by Toh et al., the POSS-clay synthesis was examined prior to use in a polymer matrix (19). This study began with chlorobenzyl-isobutyl POSS and chlorobenzyl-ethyl-isobutyl POSS which were then transformed into an imidazolium salt with the addition of 1,2-dimethylimidazole. By studying two POSS systems, the flexibility of the POSS was examined. For both POSS-MMT products, a tilted bilayer packing was reported with the long axes of the molecules tilted with respect to the basal plane. This bilayer packing conflicts with the monolayer packing noted by Perrin (18). Based on XRD and differential scanning calorimetry data, the authors concluded that the more flexible chlorobenzyl-ethyl-isobutyl POSS formed an ordered structure within the MMT layers while the more rigid chlorobenzyl-isobutyl POSS had a more disordered structure.

Liu et al. explored the addition of octaaminopropyl POSS modified clay in an epoxy resin (20). The study reported XRD results that indicated the successful intercalation of POSS in between MMT layers. The increase in interlayer spacing of 0.4

nm suggested a monolayer stacking. DGEBA and POSS-MMT were first mixed at 80°C for 12 hours before DDM was added. The cured composite was examined using XRD, and no peaks were observed. The authors suggested, based on this result, that the silicate layers were significantly delaminated. TEM studies indicated a good dispersion of intercalated and exfoliated POSS-clay platelets. The authors concluded that the addition of POSS-clay to epoxy improves the thermal stability.

A study by Teo et al. examined different POSS-clay fillers in an epoxy network (21). A dimethyl, benzylheptaisobutyl POSS was used to ion exchange with MMT. Additionally, POSS by itself was added into a different epoxy matrix. The authors reported that sub-micron and nano scale POSS domains were formed that acted as physical crosslinks that hindered polymer chain motion and improved the modulus in the glassy region. Large increases in reinforcement were reported and were attributed to effective stress transfer between POSS in the network and POSS that is attached to the clay surface. This dual filler system was reported to produce a decrease in the coefficient of thermal expansion as well as a reduction in the cure temperature. Zhao et al. examined POSS-clay in a polypropylene matrix (22). The authors studied aminopropylisooctyl POSS with MMT with an alkyl ammonium ion as a second surfactant. When 0.4 CEC or higher of POSS was added to MMT, the authors noted a bilayer packing structure. However, it was reported that thermal gravimetric analysis (TGA) indicated that MMT was only partially exchanged with POSS. The authors hypothesized that this is due to the large size and rigidity of POSS. In order to improve the compatibility with polypropylene, an alkyl ammonium surfactant was added. It was reported that this surfactant increased the clay interlayer spacing and provided better dispersion than with

POSS and clay alone. The authors attributed the dispersion to the successful control of hydrophobicity and polarity between the modified clay and the PP.

When the matrix is changed to PS, the addition of POSS and clay provide changes in thermal stability. Yei et al. looked at adding three weight percent of modified clay into a PS matrix, using aminopropylisobutyl POSS to modify MMT (23). When compared to MMT modified with a cetylpyridinium chloride salt, the interlayer spacing of POSS modified clay was reported to be smaller than that of cetylpyridinium chloride and MMT. However, PS more easily intercalated and exfoliated between the layers of the POSS treated MMT. This exfoliation of the clay in PS resulted in a reported increase in the glass transition temperature (T_g) of 8°C. A study by Fu et al. examined the same POSS in a PS matrix (24). This study reconfirmed the improvements in thermal stability with the addition of POSS modified clay. Authors reported that the dispersion of the exfoliated clay resulted in an increase in the T_g and thermal decomposition temperature as well as a reduction in the coefficient of thermal expansion.

When POSS modified clay was added into a polyamide matrix, mechanical and structural changes were observed. For example, Zhao et al. examined hydrophilic octammonium POSS and aminopropylisooctyl POSS in conjunction with MMT (25). Ditallow dimethyl-ammonium chloride was used as a second surfactant. The authors reported that as seen with a polypropylene matrix, POSS is able to partially exchange with silicates. The addition of a secondary surfactant improved the exchange ratio as well as dispersion. The lower interfacial free energy of the secondary surfactant improved compatibility with the polyamide matrix. Additionally, the strong dispersion led to an increase in tensile modulus and yield strength. The authors concluded that compatibility

between polymer and filler, thermal stability, and interlayer spacing are all indicators for good dispersion of a filler into a polyamide matrix. A study by Fox et al. attempted to incorporate POSS modified clay into polyamide with no secondary surfactant (26). This study reported that the clay had a mix of intercalation and exfoliation with small tactoid size. Nanofiller dispersion was studied using fluorescently tagged POSS modified clay. The authors concluded that at lower ratios of POSS to clay, the size of the clay tactoids decreased but no change in dispersion or interlayer spacing was observed. Overall, this study indicates that POSS aggregation inhibits the POSS modified clay from exfoliating completely in a polyamide matrix.

Silane-POSS-clay

Silane based molecules are another common choice to modify MMT clay. Organosilanes can be grafted onto the edges of clay platelets (1). The organic groups of the silane can be altered to improve compatibility with the chosen polymer matrix. Silanes can undergo a condensation reaction with the hydroxyl groups present on the edges and surfaces of the clay and form covalent bonds. Since there is no grafting in the interlayer of the clay, the interlayer spacing of the clay is not expanded before addition to a polymer matrix. We were able to find only one mention of a silane POSS being used to modify MMT (24). In this case, a trisilanolisobutyl POSS was used to modify clay, shown below in Figure 3.

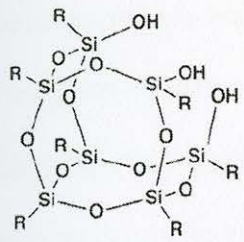

Figure 3. Schematic of open cage "trisilanol" POSS where R is isobutyl.

However, the POSS was used as an intermediate to produce a closed cage, benzyl chloride POSS. This modified POSS was then ion exchanged with MMT. To our knowledge, there have been no literature reports of using an open caged POSS to directly modify MMT through silane grafting. There have been numerous reports regarding silane grafting of MMT through various silane molecules. A study by Ianchis et al. examined the wettability of MMT through the grafting of a variety of silanes (27). Contact angle studies indicated that the hydrophobicity of the clay was increased with silane modification. Similar polarity of the filler and the polymer matrix is essential to avoid aggregation of fillers in a polymer matrix. Another study by Ianchis used dynamic light scattering and microscopy techniques to examine the aggregation of silane modified clays (28). It was determined that grafting with silanes reduced the tendency of MMT to aggregate within a styrene polymer matrix.

The addition of aminopropyltriethoxysilane onto MMT was examined in numerous studies. This method combines intercalation of amino groups with the grafting of silanes. One study by Choi et al. compared an unmodified MMT, MMT modified with silane grafting and an ammonium salt substituted MMT in an epoxy matrix (29). This study compared the expansion of the interlayer of MMT created by an ion exchange process to that caused by the chemical bonding to epoxies that silane grafting can accomplish. The study determined that the interlayer spacing produced by the ion

exchange process was larger than that of silane grafting. However, it was reported that silane grafting did occur within the clay platelets, since the interlayer was expanded more than with pristine MMT. On addition to the epoxy matrix, the silane grafted MMT did not expand further. However, the aminosilane modified clay reacted with the epoxy. Better mechanical properties were exhibited for the silanol-modified clay epoxy than for the alkylammonium salto-modified clay system. Authors concluded that the restriction of molecular motion of the clay in the epoxy caused an increase in the glass transition temperature of all samples, and that the greatest increase was in the silane modified clay due to the chemical, rather than physical, interactions with the epoxy. Another study investigated aminopropyltriethoxysilane when grafted to two varieties of MMT (30). Authors reported that in the natural MMT, the silane created a parallel bilayer packing, while in a synthetic fluorohectorite, a parallel monolayer was observed. For both clay systems, the authors proposed that the silane molecules are first intercalated into the clay layer, and then a condensation reaction occurs between the silanes and the clay layer surface.

A study by Shen et al. investigated the same amino-silane and compared the results to a trimethoxychlorosilane modified MMT (31). It was reported that the amino-silane effectively intercalated between the clay layers in a bilayer arrangement, while the chlorosilane provided a slight increase in the interlayer spacing due to monolayer packing. The chloride on the trimethoxychlorosilane prompted an ion exchange reaction to occur, however, large interlayer expansion was not observed with this method. A study by Zhang took a slightly different approach (32). This study used silane to modify an MMT that had already been modified with an alkylammonium salt. XRD analysis

indicated that with silane grafting, the interlayer spacing actually decreased. The method of combining ion exchange and silane grafting was suggested to permit both the interlayer and the edges of the clay to become organophilic and thus compatible with non-polar polymer matrices. A study by Song et al. investigated MMT silane grafted with octadecyltrichlorosilane (33). They reported that XRD studies indicated no shift in the diffraction angle, implying that the silane was grafted to the outer surfaces and edges of the clay via condensation reactions. Authors suggested that the addition of silanes on the outside of MMT provides a hydrophobic encapsulation that limits diffusion through the clay. Research has indicated that an expansion of the clay interlayer prior to addition in a polymer matrix is not necessary (34). The shear adsorption model suggested by Rooj et al. provides evidence that the shear created by mechanical mixing can cause the polymer to intercalate or exfoliate the clay layers, regardless of their prior gallery spacing.

Rubber Nanocomposites

Traditionally, carbon black has been used as a filler for rubbers (35). However, very high loading levels of carbon black are needed to achieve property improvements. The production of carbon black is petroleum based and creates pollution. The large amount of carbon black needed to improve rubber properties also results in decreased processability (36). In order to limit cost as well as to alleviate environmental concerns, clay has been considered as a replacement for carbon black (37). The ability of a polymer to intercalate between the clay layers is paramount to a good rubber-clay composite. The intercalation of a polymer implies that the clay structure is separated but parallel. Exfoliation occurs when the polymer intercalates the clay and forces the layers to separate and high levels of nanoscale dispersion occur. Complete exfoliation of clays is

very uncommon, and a mixture of intercalation and exfoliation generally occurs. As long as the clay surface area remains high, good polymer-filler interactions can still occur.

Rubber clay nanocomposites are commonly prepared with three different techniques. Solution blending, melt blending and latex compounding are all capable of producing nanocomposites (38). Solution blending consists of a dry rubber being dissolved in a solvent along with the clay, or the clay can be added after being dissolved in a separate solvent. Melt blending is accomplished with melt blending in an internal mixer (37, 39). The latex compounding method, which has been used in our study, is a water based reaction. Clays can be added directly into the rubber latex, which is an aqueous dispersion of rubber particles, or they can be added as a slurry (water and clay) (40). Layered silicates are readily dispersed in water since water acts as a swelling agent. The water provides hydration to the sodium interlayer cations of MMT. Latex blending has been used to overcome the poor dispersion of clays when melt mixing is used. Additionally, latex compounding provided improved mechanical properties and increased glass transition temperature of a natural rubber clay nanocomposite when compared to properties produced through melt blending techniques (41). Combination techniques of latex compounding and melt blending are also available (42).

Hydrogenated Nitrile Butadiene Rubber Clay Nanocomposites

HNBR and NBR are popular rubbers for industrial uses due to their strong resistance to oil and fluids (43). HNBR is resistant to degradation, even in hot and humid environments. Applications include hosing and tubing in the automotive industry. HNBR is a polar molecule owing to the nitrile group, while the hydrogenation increases the saturation of the hydrocarbon polymer backbone (44). Increased resistance to solvents

and temperature is correlated to the presence of the nitrile group and the saturated nature of the elastomer (45). Hydrogenated Nitrile Butadiene Rubber (HNBR) is shown in Figure 4.

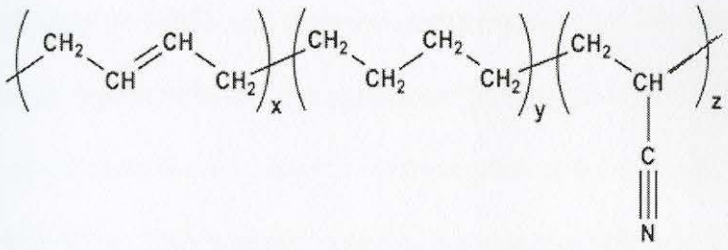

Figure 4. Structure of HNBR.

Numerous studies have been conducted using modified clays as fillers in HNBR, NBR and carboxylated NBR. A study by Wang et al. investigated HNBR with organically modified clays (46). By using melt blending and a peroxide curing system, microstructural changes were observed. This study determined that the use of high temperature and high pressure vulcanization techniques has a large impact on clay microstructure. During mixing, the clays had an exfoliated structure. This structure was thermodynamically unstable, and upon vulcanization, the structure changed into a mixture of exfoliation, intercalation and aggregations of clay. The authors theorized that the structure change is due to the molecular relaxation of HNBR and aliphatic chains during high heat and pressure conditions.

A study by Choudhary examined accelerated aging resistance of HNBR with organoclays (43). The long-term thermooxidative stability and lifetime use was compared to that of HNBR. It was reported that HNBR with no clay fillers experienced cross-linking reactions that led to embrittlement and failure. The incorporation of organoclays was reported to provide a significant improvement in degradation properties. Nanofillers successfully prevented HNBR from the surface rupture that is caused by oxidation. The

addition of 8 phr of an alykylammonium modified clay resulted in a three-fold increase in the service temperature range of HNBR. Gatos et al. examined the effect of the modified clay aspect ratio on HNBR nanocomposite properties (47). The addition of octadecylamine to MMT and fluorohectorite resulted in very different aspect ratios. The difference in aspect ratio did not significantly affect the amount of HNBR that could intercalate between the clay layers. However, for both clay systems, a collapse of the clay gallery was noted. This was attributed to the reaction between the amine intercalant and the zinc of the curing agent. Despite this collapse, both clays were well dispersed in HNBR. Transmission electron microscopy (TEM) analysis indicated the intercalation, exfoliation, confined and deintercalated structures of the clay within HNBR. Tensile experimentation showed that the clay with the higher aspect ratio demonstrated higher stiffness characteristics. Oxygen permeation studies demonstrated the most evidence of the effect aspect ratio. Authors concluded that the fluorohectorite created a more tortuous path than the MMT due to the higher aspect ratio. Similar results were reported when oxygen permeation was conducted in a humid environment.

An investigation by Sadhu studied the effect of the acrylonitrile (ACN) content of HNBR on clay nanocomposite properties (48). Lower content of ACN was reported to provide better clay intercalation due to the larger amount of butadiene. The lower ACN caused a decrease in polarity, which is compatible with the non-polar modified clays. Additionally, it was reported that the nitrile groups of HNBR are capable of forming hydrogen bonds with the clay surface. Authors suggested that the nitrile groups must first saturate the exposed hydroxyls before becoming intercalated. With higher ACN levels, the rubber may be bonded to the outside of the clay, but the intercalated amine and the

rubber are less likely to form hydrogen bonds. The non-polar nature of HNBR provides an increase in strength when compared to more polar rubbers such as styrene butadiene rubber (SBR). As the nitrile content increases and the glass transition increases, the strength of the rubber-clay nanocomposite tends to increase. The exfoliation and high surface area of the clays result in a higher tensile strength as ACN content increases. Additionally, an ideal loading level of clay was reported. Authors reported that higher loading levels promoted aggregation while lower loadings had a lower surface area and thus poorer polymer-filler interactions.

Latex compounding has been used in studies with carboxylated NBR and clay (49). Reported TEM and XRD experiments indicated the delamination and intercalation of clay within carboxylated NBR. After compounding on an open mill, the intercalation remained. This study found no percolation threshold when loading levels were up to 40 weight percent. This was attributed to the reduction of aspect ratio and the layer alignment during the open mill processing. This study concluded that latex compounding prior to open mill compounding produces nanocomposites where the clays do not experience an interlayer gap collapse. A comparison study prepared HNBR nanocomposites with either two-dimensional MMT or zero-dimensional nanosilica (50). It was reported that nanosilica provided an improvement in thermal stability greater than that of the modified MMT. This was attributed to the fact that silica nanofillers contain more surface hydroxyl groups than MMT that can interact with the polar groups of HNBR. At loading levels above 4 phr, the MMT provided thermal stability while the nanosilica did not.

Styrene Butadiene Rubber Clay Nanocomposites

Wu et al. examined styrene butadiene rubber (SBR) and organoclays produced with the latex compounding method (51). This study determined that a 'separated' structure of clay existed that is in between that of intercalated and exfoliated. This separated structure is defined as silicate layer aggregates of nanometer thickness without aggregation and without the intercalation of a polymer into the clay galleries resulting from reaggregation. This structure resulted in an increase in Tg and a tensile strength increase of six times. Additionally, the gas permeability was decreased by half. The authors suggested that this study demonstrates the success of the latex compounding technique regardless of the separated structure. Additional studies with NBR clay nanocomoposites were performed. The permeation of oxygen in SBR with clay was much higher than with NBR and clay, attributed by the authors to a better polymer-filler interaction with NBR. Zhang examined the mechanical properties of SBR with organoclays with the latex compounding method (52). It was reported that the organoclays dispersed into bundles with a thickness of 4-10 nm. It was found that the use of latex compounding provided improved mechanical properties than those obtained by just adding clay directly. The study noted poor interfacial adhesion of the polymer and filler due to the lack of available hydroxyl groups. When comparing the latex blending method to solution blending, similar results were obtained. Authors claimed that the ease of use and lack of solvents make latex blending an accepted choice for rubber-clay nanocomposites. SBR is a common rubber used in the automotive industry for tires.

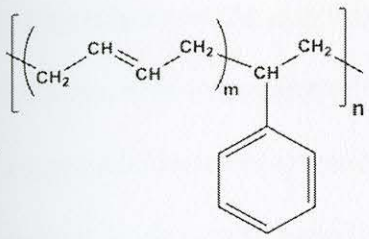

Figure 5. Structure of SBR.

Silane grafted clay has been studied in an SBR latex rubber (53). Authors suggested that the use of 3-aminopropyltrimethoxysilane allows for ion exchange to enlarge the clay layer and the silane allows for a condensation reaction on the outside of the clay to promote further hydrophobicity. It was hypothesized that the organosilane attached onto the surface of layers in suspension via NH_3^+, and at the same time, the Si-OR groups changed to Si-OH groups due to a hydrolysis reaction. The compatibility in polarity of SBR and the modified clay resulted in well dispersed filler particles. During vulcanization, bis(triethoxysilyl-propy)tetrasulfide was added to improve interfacial interaction. This two step method provided SBR with an eight times higher modulus at 300% strain and a seven times higher tensile strength compared to unfilled SBR. The authors suggested that the use of organosilane contributed to these properties, however, the secondary addition during vulcanization promoted a chemical bridge between the clay and rubber which improved the interfacial strength.

Motivation and Contribution to Research

Clay nanofillers are capable of improving the viscoelastic, thermal, and mechanical properties of a rubber polymer matrix. Clay is a cost-effective material with reduced environmental impact in comparison to traditional carbon black. The challenge with using clay nanofillers is the difficulty in obtaining consistent, nanoscale dispersion of the clay within the rubber matrix. Surface treatment of clays increases the

hydrophobicity of the clay surface to promote dispersion in hydrophobic rubber matrices. POSS has been demonstrated as an effective dispersing agent for metal oxide nanoparticles in thermoplastic matrices. Amino-functional POSS molecules have been explored as clay surface modifiers to improve dispersion in selected rubber matrices. To our knowledge, there have been no reports of examination of trisilanol POSS surface modification of nanoclays for rubber nanocomposites. We hypothesize that trisilanol POSS with appropriate functionality can be used to effectively modify clay surfaces and improve intercalation and exfoliation in selected rubber matrices. The organic functionalization of POSS provides the potential to precisely tailor POSS molecules for interaction with and improved performance in desired clay/rubber systems.

Research Objectives

The objectives of this research are as follows:

- Modify MMT clay with two different types of POSS;
- Determine the effect of POSS on the interlayer spacing, hydrophobicity and chemical bonding of clay;
- Use POSS modified clays as fillers in an HNBR and SBR matrix;
- Determine how POSS modification of clay fillers effects the dispersion and structure of the filler in the rubber matrix;
- Compare thermal, mechanical, viscoelastic, rheological, morphological and adsorption properties of POSS modified clays to a commercially available modified clay; and
- Define structure-property relationships that determine the effect of POSS modification on nanocomposite properties

REFERENCES

1. Le Pluart, L.; Duchet, J.; Sautereau, H.; Gerard, J. F., Surface Modifications of Montmorillonite For Tailored Interfaces in Nanocomposites. *The Journal of Adhesion* **2002,** *78*, 645-662.

2. Maiti, M.; Bhattacharya, M.; Bhowmick, A., Elastomer Nanocomposites. *Rubber Chemistry and Technology* **2008,** *81*, 384-469.

3. Xi, Y.; Ding, Z.; He, H.; Frost, R., Structure of organoclays- an X-ray diffraction and thermogravimetric analysis study. *Journal of Colloid and Interface Science* **2004,** *277*, 116-120.

4. Volzone, C.; Rinaldi, J. O.; Ortiga, J., N2 and CO2 Adsorption by TMA- and HDP-Montmorillonites. *Materials Research* **2002,** *5*, 475-479.

5. Xi, Y.; Martens, W.; He, H.; Frost, R. L., Thermogravimetric analysis of organoclays intercalated with the surfactant octadecyltrimethylammonium bromide. *Journal of Thermal Analysis and Calorimetry* **2005,** *81*, 91-97.

6. Osman, M. A.; Ploetze, M.; Skrabal, P., Structure and Properties of Alkylammonium Monolayers Self-Assembled on Montmorillonite Platelets. *Journal of Physical Chemistry B* **2004,** *108*, 2850-2588.

7. Tiwari, R.; Khilar, K.; Natarajan, U., Synthesis and characterization of novel organo-montmorillonites. *Applied Clay Science* **2008,** *38*, 203-208.

8. Vaia, R. A.; Teukolsky, R. K.; Giannelis, E. P., Interlayer Structure and Molecular Environment of Alkylammonium Layered Silicates. *Chem Mater* **1994,** *6* (7), 1017-1022.

9. Vazquez, A.; Lopez, M.; Kortaberria, G.; Martin, L.; Mondragon, I., Modification of montmorillonite with cationic surfactants. Thermal and chemical analysis including CEC determination. *Applied Clay Science* **2008,** *41*, 24-36.

10. Feher, F., Polyhedral Oligosilsesquioxanes and Heterosilsesquioxanes.

11. Fina, A.; Tabuani, D.; Peijs, T.; Camino, G., POSS grafting on PPgMA by one-step reactive blending. *Polymer* **2009,** *50* (1), 218-226.

12. Dintcheva, N. T.; Morici, E.; Arrigo, R.; La Mantia, F. P.; Malatesta, V.; Schwab, J. J., Structure-properties relationships of polyhedral oligomeric silsesquioxane (POSS) filled PS nanocomposites. *Express Polymer Letter* **2012,** *6* (7), 561-571.

13. Misra, R.; Alidedeoglu, A. H.; Jarrett, W. L.; Morgan, S. E., Molecular miscibility and chain dynamics in POSS/polystyrene blends: Control of POSS preferential dispersion states. *Polymer* **2009,** *50* (13), 2906-2918.

14. Wheeler, P. A.; Misra, R.; Cook, R. D.; Morgan, S. E., Polyhedral Oligomeric Silsesquioxane Trisilanols as Dispersants for Titanium Oxide Nanopowder. *Journal of Applied Polymer Science* **2008,** *108*, 2503-2508.

15. Liu, Q.; Ren, W.; Zhang, Y.; Zhang, Y., Curing reactions and properties of organic-inorganic composites from hydrogenated carboxylated nitrile rubber and epoxycyclohexyl polyhedral oligomeric silsesquioxanes. *Polymer Internationsl* **2010,** *60*, 422-429.

16. Liu, L.; Tian, M.; Zhang, W.; Zhang, L.; Mark, J. E., Crystallization and morphology study of polyhedral oligomeric silsesquioxane (POSS)/polysiloxane elastomer composites prepared by melt blending. *Polymer* **2007,** *48* (11), 3201-3212.

17. Sahoo, S.; Bhowmick, A., Polyhedral Oligomeric Silsesquioxane (POSS) Nanoparticles as New Crosslinking Agent for Functionalized Rubber. *Rubber Chemistry and Technology* **2007,** *80*, 826-837.

18. Perrin, F. X.; Bruzaud, S.; Grohens, Y., Structure and thermal behaviour of polyhedral oligomeric silsesquioxane modified montmorillonite. *Applied Clay Science* **2010,** *49* (3), 113-119.

19. Toh, C.; Xi, L.; Lau, S.; Pramoda, K. P.; Chua, Y.; Lu, X., Packing Behaviors of Structurally Different Polyhedral Oligomeric Silsesquioxane-Imidazolium Surfactants in Clay. *Journal of Physical Chemistry B* **2009**.

20. Liu, H.; Zhang, W.; Zheng, S., Montmorillonite intercalated by ammonium of octaaminopropyl polyhedral oligomeric silsesquioxane and its nanocomposites with epoxy resin. *Polymer* **2005,** *46* (1), 157-165.

21. Teo, J.; Toh, C.; L, X., Catalytic and reinforcing effects of polyhedral oligomeric silsesquioxane (POSS)-imidazolium modified clay in an anhydride-cured epoxy. *Polymer* **2011,** *52*, 1975-1982.

22. Zhao, F.; Wan, C.; Bao, X.; Kandasubramanian, B., Modification of montmorillonite with aminopropylisooctyl polyhedral oligomeric silsequioxane. *Journal of Colloid and Interface Science* **2009,** *333* (1), 164-170.

23. Yei, D.-R.; Kuo, S.-W.; Su, Y.-C.; Chang, F.-C., Enhanced thermal properties of PS nanocomposites formed from inorganic POSS-treated montmorillonite. *Polymer* **2004,** *45* (8), 2633-2640.

24. Fu, H.-K.; Kuo, S.-W.; Yeh, D.-R.; Chang, F.-C., Properties Enhancement of PS Nanocomposites through the POSS Surfactants. *Journal of Nanomaterials* **2008,** *2008*, 1-7.

25. Zhao, F.; Bao, X.; McLauchlin, A. R.; Gu, J.; Wan, C.; Kandasubramanian, B., Effect of POSS on morphology and mechanical properties of polyamide 12/montmorillonite nanocomposites. *Applied Clay Science* **2010,** *47*, 249-256.

26. Fox, D. M.; Harris, R. H.; Bellayer, S.; Gilman, J. W.; Gelfer, M. Y.; Hsaio, B. S.; Maupin, P. H.; Trulove, P. C.; De Long, H. C., The pillaring effect of the 1,2-dimethyl-3(benzyl ehtyl iso-butyl POSS) imidazolium cation in polymer/montmorillonite nanocomposites. *Polymer* **2011,** *52*, 5335-5343.

27. Ianchis, R.; Cinteza, L.; Donescu, D.; Petcu, C.; Corobea, M. C.; Somoghi, R.; Ghiurea, M.; Spataru, C., Implications of silylated montmorillonite on montmorillonite-polyacrylate nanocomposites. *Applied Clay Science* **2011,** *52*, 96-103.

28. Ianchis, R.; Donescu, D.; Petcu, C.; Anghel, D. F.; Stanga, G.; Marcu, A., Surfactant-free emulsion polymerization of styrene in the presence of silylated montmorillonite. *Applied Clay Science* **2009,** *45*, 164-170.

29. Choi, Y.; Lee, S.; Ryu, S., Effect of silane functionalization of montmorillonite on epoxy/montmorillonite nanocomposite. *Polymer Bulletin* **2009,** *63*, 47-55.

30. He, H.; Duchet, J.; Galy, J.; Gerard, J.-F., Grafting of swelling clay materials with 3-aminopropyltriethoxysilane. *Journal of Colloid and Interface Science* **2005,** *288* (1), 171-176.

31. Shen, W.; He, H.; Zhu, J.; Yuan, P.; Frost, R., Grafting of montmorillonite with different functional silanes via two different reaction systems. *Journal of Colloid and Interface Science* **2007,** *313*, 268-273.

32. Zhang, J.; Gupta, R. K.; Wilkie, C. A., Controlled silylation of montmorillonite and its polyethylene nanocomposites. *Polymer* **2006,** *47*, 4537-4543.

33. Song, K.; Sandi, G., Characterization of Montmorillonite Surfaces After Modification by Organosilane. *Clay and Clay Minerals* **2001,** *49* (2), 119-125.

34. Rooj, S.; Das, A.; Sto¨ckelhuber, K. W.; Reuter, U.; Heinrich, G., Highly Exfoliated Natural Rubber/Clay Composites by ''Propping-Open Procedure'': The Influence of Fatty-Acid Chain Length on Exfoliation. *Macromolecular Materials Engineering* **2012,** *297*, 369-383.

35. Bhattacharya, M.; Bhowmick, A., Synergy in carbon black-filled natural rubber nanocomposites. Part I: Mechanical, dynamic mechanical properties and morphology. *Journal of Materials Science* **2010**.

36. Varghese, S.; Karger-Kocsis, J., Natural rubber-based nanocomposites by latex compounding with layered silicates. *Polymer* **2003,** *44*, 4921-4927.

37. Samadi, A.; Kashani, M. R., Effects of Organo-Clay Modifier on Physical-Mechanical Properties of Butyl-Based Rubber Nano-Composites. *Journal of Applied Polymer Science* **2010,** *116*, 2101-2109.

38. Shen, Z.; Simon, G. P.; Cheng, Y.-B., Comparison of solution intercalation and melt intercalation of polymer-clay nanocomposites. *Polymer* **2002,** *43*, 4251-4260.

39. Razzaghi-Kashani, M.; Hasankhani, H.; Kokabi, M., Improvement in Physical and Mechanical Properties of Butyl Rubber with Montmorillonite Organo-clay. *Iranian Polymer Journal* **2007,** *16* (10), 671-679.

40. (a) Sengupta, R.; Chakraborty, S.; Bandyopadhyay, S.; Dasgupta, S.; Mukhopadhyay, R., A Short Review on Rubber/Clay Nanocomposites With Emphasis on Mechanical Properties. *Polymer Engineering and Science* **2007,** *47* (11), 1956-1974; (b) Wang, Y.; Zhang, H.; Wu, Y.; Yang, J.; Zhang, L., Structure and Properties of Strain-Induced Crystallization Rubber-Clay Nanocomposites by Co-coagulating the Rubber Latex and Clay Aqueous Suspension. *Journal of Applied Polymer Science* **2005,** *96*, 318-323.

41. Bhowmick, A.; Bhattacharya, M.; Mitra, S., Exfoliation of Nanolayer Assemblies for Inmproved Natural Rubber Properties: Methods and THeory. *Journal of Elastomers and Plastics* **2010,** *00*, 1-21.

42. Bhowmick, A.; Bhattacharya, M.; Mitra, S.; Kumar, K. D.; Maji, P. K.; Choudhury, A.; George, J. J.; Basak, G. C., Morphology-Property Relationship in Rubber-Based Nanocomposites: Some Recent Developments. *Advanced Polymer Science* **2010,** *239*, 1-83.

43. Choudhury, A.; Bhowmick, A.; Soddemann, M., Effect of organo-modified clay on accelerated aging resistance of hydrogenated nitrile rubber nanocomposites and their life time prediction. *Polymer Degradation and Stability* **2010,** *95*, 2555-2562.

44. Choudhury, A.; Bhowmick, A.; Ong, C., Novel role of polymer-solvent and clay-solvent interaction parameters on the thermal, mechanical and optical properties of polymer nanocomposites. *Polymer* **2009,** *50*, 201-210.

45. Perraud, S.; Vallat, M.-F.; David, M.-O.; Kuczynski, J., Network characteristics of hydrogenated nitrile butadiene rubber networks obtained by radiation crosslinking by electron beam. *Polymer Degradation and Stability* **2010,** *95* (9), 1495-1501.

46. Wang, X.; Huang, A.; Jia, D.; Li, Y., From exfoliation to intercalation- changes in morphology of HNBR/organoclay nanocomposites. *European Polymer Journal* **2008,** *44*, 2784-2789.

47. Gatos, K. G.; Karger-Kocsis, J., Effect of the aspect ratio of silicate platelets on the mechanical and barrier properties of hydrogenated acrylonitrile butadiene rubber (HNBR)/layered silicate nanocomposites. *European Polymer Journal* **2007,** *43*, 1097-1104.

48. Sadhu, S.; Bhowmick, A. K., Preparation and Properties of Nanocomposites Based on Acrylonitrile-Butadiene Rubber, Styrene-Butadiene Rubber, and Polybutadiene Rubber. *Journal of Polymer Science: Part B: Polymer Physics* **2004,** *42*, 1573-1585.

49. Wu, Y.-P.; Zhang, L.-Q.; Wang, Y.-Q.; Liang, Y.; Yu, D.-S., Structure of Carboxylated Acrylonitrile-Butadiene Rubber (CNBR)-Clay Nanocomposites by Co-coagulating Rubber Latex and Clay Aqueous Suspension. *Journal of Applied Polymer Science* **2001,** *82*, 2842-2848.

50. Choudhury, A.; Bhowmick, A.; Ong, C., Effect of Different Nanoparticles on Thermal, Mechanical and Dynamic Mechanical Properties of Hydrogenated Nitrile Butadiene Rubber Nanocomposites *Journal of Applied Polymer Science* **2009,** *116*, 1428-1441.

51. Wu, Y.-P.; Wang, Y.-Q.; Zhang, H.-F.; Wang, Y.-Z.; Yu, D.-S.; Zhang, L.-Q.; Yang, J., Rubber–pristine clay nanocomposites prepared by co-coagulating rubber latex

and clay aqueous suspension. *Composites Science and Technology* **2005,** *65* (7–8), 1195-1202.

52. Zhang, L.; Wang, Y.; Wang, Y.; Sui, Y.; Yu, D., Morphology and Mechanical Properties of Clay/Styrene-Butadiene Rubber Nanocomposites. *Journal of Applied Polymer Science* **2000,** *78*, 1873-1878.

53. Jia, Q.-X.; Wu, Y.-P.; Wang, Y.-Q.; Lu, M.; Zhang, L.-Q., Enhanced interfacial interaction of rubber/clay nanocomposites by a novel two-step method. *Composites Science and Technology* **2008,** *68*, 1050-1056.

CHAPTER II

EXPERIMENTAL

Materials

Sodium montmorillonite clay (Cloisite Na+, cation exchange capacity (CEC) = 92 mmol/100 g, denoted by MMT) was purchased from Southern Clay Products Co. (Gonzales, Texas). Cloisite 15A was donated by Southern Clay Products Co. (Gonzales, Texas). Cloisite 15A, denoted by 15A, is sodium montmorillonite modified by a quaternary ammonium salt and dimethyl dihydrogenated tallow (2M2HT) with approximately 65% C18, 30% C16, 5% C14 with CEC =125 mmol/100 g. The particle size ranges from 2 μm to 13 μm. Aminoethylaminopropylisobutyl POSS (AP) and trisilanolphenyl POSS (TSP) were donated by Hybrid Plastics, Inc. (Hattiesburg, Mississippi). The AP structure is shown in Figure 6. TSP is shown in Figure 9. Ethanol (anhydrous, 200 proof, ≥99.5) and tetrahydrofuran (THF) were purchased from Sigma Aldrich (St. Louis, Missouri). Glacial acetic acid and hydrochloric acid were purchased from Fisher Scientific (USA). All chemicals were used as received. Styrene butadiene latex (Taktene® Latex S62 denoted by SBR) was donated by Lanxess. Taktene is an aqueous dispersion with 68% of solids produced by cold emulsion polymerization and 24% styrene content. Chemisat LCH- 7272, a hydrogenated nitrile butadiene rubber latex (HNBR), was donated by Zeon Chemicals (Hattiesburg, Mississippi). HNBR has a 38% acrylonitrile (ACN) content and 34% solids. This HNBR has proprietary antioxidants and stabilizers. Additionally, both cis and trans conformations occur randomly in the polymer. T-2000, a curative package consisting of zinc oxide, sulfur, accelerator and antioxidant, was donated by Tiarco Chemical (Dalton, Georgia).

APMMT Synthesis

AP-MMT fillers were prepared using the following technique: AP and MMT were both dried in an oven at 80°C for 2 days. 5 g of MMT was added to 250 mL of deionized water. This solution was stirred for 2 hours at 25 °C. 0.6 CEC of AP was dissolved in 10 mL of THF. 5 mL of ethanol and 5 mL acetic acid was added to this solution. This solution was added dropwise to the clay slurry and stirred overnight at 70°C. The solution was then filtered and rinsed three times with a 33:33:33 v:v:v of deionized water, ethanol and THF. The product was dried in an oven at 80°C for two days. Before characterization and use in the nanocomposite, the sample was crushed into a powder using a mortar and pestle.

TSPMMT Synthesis

TSPMMT composites were prepared using the following technique: TSP was dried in an oven at 110 °C and MMT dried in an oven at 80 °C for 2 days. 5 g of the clay was added to 200 mL of ethanol. This solution was stirred for 2 hours at 25 °C. 0.6 CEC of TSP was dissolved in 10 mL of ethanol. 5 mL of hydrochloric acid was added to this solution. This solution was then added dropwise to the clay slurry and stirred overnight at 70 °C. The solution was then filtered and rinsed three times with ethanol. The product was dried in an oven at 80 °C for two days. Before characterization and use in nanocomposites, the sample was crushed into a powder using a mortar and pestle. 15A was heated at 80 °C for 2 days before use.

Nanocomposite Preparation

A 2% aqueous dispersion of the filler in deionized water was stirred for 30 minutes at RT. 1, 4 or 7 parts per hundred rubber (phr) of filler and 1 phr of T-2000

curative cure were added to the HNBR latex and mixed for 30 minutes at RT. 1 phr of filler and 1 phr of T-2000 curative were added to the SBR latex and mixed for 30 minutes at RT. 1, 2 or 3 phr of TSPMMT and 1 phr T-2000 cure package were added to the SBR latex and mixed for 30 minutes at RT. The decrease in loading level of the filler in SBR is due to the high solids content of the SBR. The nanocomposite was poured into a film and dried at room temperature until excess water was removed. The composite was then vulcanized at 70 °C in a vacuum oven for 45 hours.

Wide Angle X-ray Diffraction

Wide angle x-ray diffraction (XRD) studies were conducted on AP and TSP to determine their crystallinity peaks. XRD studies of the fillers were used to determine the interlayer spacing. Additionally, XRD studies of the composite films were conducted to determine the exfoliation and intercalation of the nanocomposites. Diffraction patterns were obtained using a Rigaku D/MAXUltima-III diffractometer (Woodlands, Texas). XRD was conducted in transmission mode at room temperature using Cu Ka (λ=0.1542 nm) radiation at a tube current of 44 mA and an acceleration voltage of 40 kV. The scan range was 2°–10° at a step interval of 0.1 ° and a scanning rate of 0.5 °/min. Data analysis was conducted using OriginPro 8 software.

Thermogravimetric Analysis

Thermogravimetric analysis (TGA) was performed on a TA Instruments Q500 (New Castle, Delaware). Fillers and nanocomposite films of 10-15 mg were heated in a Pt cell at 10°C/min heating rate from ambient temperature to 800°C in nitrogen at a nitrogen flow rate of 40 mL/min. The temperature of maximal degradation were recorded

for each sample. The amount of POSS attached to MMT was calculated using TGA data. Data analysis was conducted using the OriginPro 8 software suite.

Fourier Transform Infrared Spectroscopy

Fourier transform infrared spectroscopy (FTIR) was used to determine the bonding mechanisms of the modified fillers. IR spectra were obtained using a Thermo Instrument Nicolet 6700 in attenuated total reflectance (1) mode (USA). 32 scans were collected at a spectral resolution of 2 cm^{-1}. The surfaces of each modified filler was analyzed using a 2-mm germanium (Ge) crystal with a 45° angle maintaining constant contact pressure between the crystal and the powders. Data analysis was conducted using the OriginPro 8 software suite.

Rheology

Parallel plate rheology was conducted on uncured nanocomposite samples in dynamic mode on a TA Instruments ARES rheometer (New Castle, Delaware). Isothermal frequency sweeps were conducted at 120 °C in the frequency range of 0.1 to 100 rad/s at 1% strain. Parallel plate geometry plates (25 mm diameter plates) with a gap in the range of 1.0 to 2.0 mm were used in order to generate the storage modulus, loss modulus and complex viscosity with data collected at five points per decade. Data analysis was conducted using the OriginPro 8 software suite. Similar experiments were conducted on cured SBR nanocomposites.

Dynamic Mechanical Analysis

Dynamic mechanical analysis (DMA) was used to determine the storage modulus, loss modulus and the tan delta values of the vulcanized HNBR nanocomposites using the TA Q800 (New Castle, Delaware). Multi-frequency strain sweeps were conducted at a

temperature range of -60 °C to 80 °C at 1 hertz frequency, 0.01% strain at 2°C/min. Data analysis was conducted using the OriginPro 8 software suite.

Mechanical Testing

An MTS Insight (Eden Prairie, Minnesota) was used to perform tensile testing to determine stress strain curves of HNBR nanocomposites. The crosshead speed was set at 500 mm/min and tests were conducted at room temperature. The average of three tests for each composite is reported.

Water Vapor Sorption

Water vapor sorption analysis was performed using a TA Instruments Q5000SA to determine the hydrophobicity of the fillers and composites (New Castle, Delaware). Testing on modified and unmodified fillers was performed by first removing excess water with 80 °C heat at 0 % RH for approximately 250 minutes. After this time, the humidity was increased to 90 % and the temperature was decreased to 25 °C, and the sample was held for another 250 minutes. HNBR and SBR nanocomposites were tested using an isohume test at a humidity of 90% at 25 °C. The change in mass was recorded for all fillers. The time to reach equilibrium and the equilibrium mass was recorded for all nanocomposites.

Swelling Studies

The equilibrium volume fraction of rubber was determined by immersing the HNBR nanocomposite film in a polar solvent such as methyl ethyl ketone (MEK). SBR was studied with placement in toluene. The sample was removed every half hour, patted dry and weighed. The sample was then placed back in solvent. The Flory-Rehner equation was used to determine the volume fraction, V_r, of rubber at equilibrium.

$$V_r = \frac{(D-FT)\rho_r^{-1}}{(D-FT)\rho_r^{-1}+A_0\rho_s^{-1}} \quad (1)$$

Where D= deswollen weight, F= weight fraction of the insoluble component, T= weight of the test specimen, ρ_r= density of rubber, ρ_s= density of solvent and A_0= amount of solvent absorbed (2).

The molecular weight between crosslinks was determined using the following equation (2b).

$$-[\ln(1-V_r)+V_r)+\chi V_r^2] = \frac{\rho_r V(V_r^{\frac{1}{3}}-\frac{V_r}{2})}{2M_c} \quad (2)$$

Where χ = Flory-Huggins interaction parameter; 0.42: for SBR- toluene system (3); V= molar volume of swelling solvent; Mc= number average molecular weight of the chain between two crosslinks; 1/2Mc = Apparent crosslink density, in mol/cc of rubber hydrocarbon. The following equation was used to determine the χ parameter for the HNBR- MEK system (4).

$$\chi = 0.501 + 0.273V_r \quad (3)$$

Scanning Electron Microscopy

The FEI Quanta 200 Scanning Electron Microscopy (SEM) was used to probe the structure of fillers (Hillsboro, Oregon). Powder samples were placed onto carbon adhesive tabs and then gold coated for three minutes. SEM was conducted in environmental mode at a voltage of 20 kV and 1 torr of pressure.

Transmission Electron Microscopy

Transmission electron microscopy (TEM) was conducted on selected nanocomposite films on a JEOL JEM 2100 ultra high resolution transmission electron microscope (JEOL, Tokyo, Japan) at an accelerating voltage of 200 kV to determine bulk

morphology. Nanocomposites were examined to determine the dispersion of fillers and the extent of exfoliation and intercalation of the fillers in the composite. Ultrathin sections, about 100 nm thick, were prepared by cryoultramicrotoming the samples with a diamond knife using a Leica EM UC6 cryomicrotome at -90°C. The ultrathin sections were collected on a 600-mesh copper grid prior to examination. Nanocomposites were examined to determine the extent of exfoliation and intercalation of the fillers in the composite.

Atomic Force Microscopy

Morphology of cured nanocomposites were determined with the Dimension ICON atomic force microscope (AFM) from Bruker (Santa Barbara, CA) using ScanAsyst Air technology. Height and inphase images were taken with a ScanAsyst probe in air. Probes were purchased from Bruker, (Santa Barbara, CA). A ScanAsyst Air silicon probe with 115 μm long silicon cantilever, nominal force constant of 0.4 N/m and resonance frequency of 70 KHz was used for tapping mode surface and fracture surface topography studies. AFM studies were conducted under ambient conditions in a temperature (27°C) and humidity (40–45%) controlled room. Surface topographies of the nanocomposites and the fracture surface bulk regions of HNBR nanocomposites were studied on 2 μm x 2 μm scan areas with an image resolution of 512 x 512 pixels at a scan rate of 0.9 Hz. Fracture surfaces were obtained by cutting the samples with sharp scissors in order to eliminate any artifacts of fracture. SBR nanocomposites were studied on 5 μm x 5 μm scan areas with an image resolution of 512 x 512 pixels at a scan rate of 0.9 Hz. Multiple areas were imaged and figures show representative morphology. Surface roughness analysis was performed using NanoScope Analysis version 1.40 image

analysis software. The reported roughness is the root mean square average roughness in nm. Two sets of readings were taken for each sample and an average value is reported. The differences between the two readings were less than 1%. Image J software was used to determine the average particle size and standard deviation of the fillers within the composite.

Solubility Parameters

Solubility parameters of POSS were determined using the Hoy and van Krevelen method. Both methods employ the formula:

$$\delta = \frac{\rho \Sigma G_i}{M_0} \tag{4}$$

where δ is the theoretical solubility parameter, ρ is the material density, G_i is a molar attraction constant representing one of the various structural groups present in the molecule, and *Mo* is the molecular weight of the material (5).

Nomenclature

To provide clarity throughout the thesis, certain nomenclature will be used. Table 1 shows common words and phrases as well as their abbreviations.

Table 1

Nomenclature

	Abbreviation
Acrylonitrile	ACN
Atomic Force Microscopy	AFM

Table 1 (continued).

	Abbreviation
Aminopropylaminoethylisobutyl POSS	AP
Attenuated Total Reflectance	ATR
Cation exchange capacity	CEC
Dynamic Mechanical Analysis	DMA
Fourier Transform Infrared Spectroscopy	FTIR
Hydrogenated Nitrile Butadiene Rubber	HNBR
Montmorillonite	MMT
Nitrile Butadiene Rubber	NBR
Polyhedral oligomeric silsesquioxane	POSS
Polystyrene	PS
Styrene Butadiene Rubber	SBR
Scanning Electron Microscopy	SEM
Glass transition temperature	Tg
Transmission Electron Microscopy	TEM
Thermal Gravimetric Analysis	TGA
Trisilanolphenyl POSS	TSP
X-ray Diffraction	XRD

REFERENCES

1. Guimarães, J. L.; Peralta-Zamora, P.; Wypych, F. Covalent Grafting of Phenylphosphonate Groups onto the Interlamellar Aluminol Surface of Kaolinite. *Journal of Colloid and Interface Science* **1998,** *206* (1), 281-287.

2. (a) Rooj, S.; Das, A.; Sto¨ckelhuber, K. W.; Reuter, U.; Heinrich, G. Highly Exfoliated Natural Rubber/Clay Composites by ''Propping-Open Procedure'': The Influence of Fatty-Acid Chain Length on Exfoliation. *Macromolecular Materials Engineering* **2012,** *297*, 369-383; (b) Flory, P. J.; Rehner, J. H. Statistical mechanics of crosslinked polymer networks II. Swelling. *Journal of Chem Phys* **1943,** *11*, 521-526.

3. Bhattacharya, M.; Maiti, M.; Bhowmick, A. K. Tailoring properties of styrene butadiene rubber nanocomposite by various nanofillers and their dispersion. *Polymer Engineering & Science* **2009,** *49* (1), 81-98.

4. Maciejewska, M.; Zaborski, M.; Krzywania-Kaliszewska, A. Mineral oxides and layered minerals in combination with itaconic acid as coagents for peroxide crosslinking of hydrogenated acrylonitrile- butadiene elastomer. *Comptes Rendus Chimie* **2012**, 15 (5), 414-423.

5. (a) van Krevelen, D. W. *Cohesive properties and solubility*.Elsevier: New York, 2009; (b) Misra, R.; Fu, B. X.; Plagge, A.; Morgan, S., POSS-Nylon 6 Nanocomposites: Influence of POSS Structure on Surface and Bulk Properties. *Journal of Polymer Science: Part B: Polymer Physics* **2009,** *47*, 1088-1102.

CHAPTER III

FILLER CHARACTERIZATION

MMT, because of its abundance, relatively low cost and ease of use, is an attractive nanofiller for polymer matrices. However, due to its hydrophilic nature, it is difficult to disperse in hydrophobic polymers, and generally must undergo surface modification to improve its compatibility with the chosen polymer matrix. The most common MMT surface modification approach involves cation exchange with alkylammonium salts or amines (1). These organocations exchange with the sodium cations present in the MMT gallery layers to produce an organophilic clay (2). In this study, AP was used as an ion exchange material with MMT. The structure of AP is shown in Figure 6.

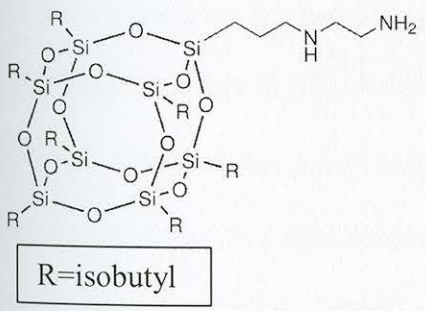

Figure 6. Schematic of aminopropylaminoethylisobutyl POSS (AP), where R is isobutyl.

A space filling model of AP is shown in Figure 7. In the model, yellow represents silicon, red represents oxygen, white is hydrogen, grey is carbon and blue is nitrogen. This simulated model accounts for Van der Waals bonding and the radii of the atoms and helps elucidate the space filling nature of the isobutyl groups on the amino-POSS. The aliphatic groups produce a nanostructured chemical that has a diameter of approximately 1.89 nm. The model indicates that the amino groups are available on the periphery of the

molecule for ion exchange, while the isobutyl groups appear to shield the cage and present a hydrophobic corona.

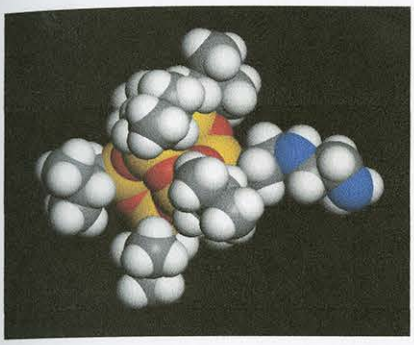

Figure 7. Space filling simulation of AP.

Previous reports have shown that by first protonating POSS, and then adding it to MMT, ion exchange occurs (3). POSS is a useful modifier of MMT due to its high thermal stability and tendency to disperse (4). In the case of AP, the presence of two amine functional groups provides two possible sites for ion exchange to occur. We hypothesize that this structure will provide a greater level of POSS ion exchange with the clay. This cation exchange not only creates an expanded interlayer, it also makes the clay more hydrophobic, and thus more compatible with polymer matrices. We hypothesize that the large diameter of AP will be able to intercalate and expand the clay layers.

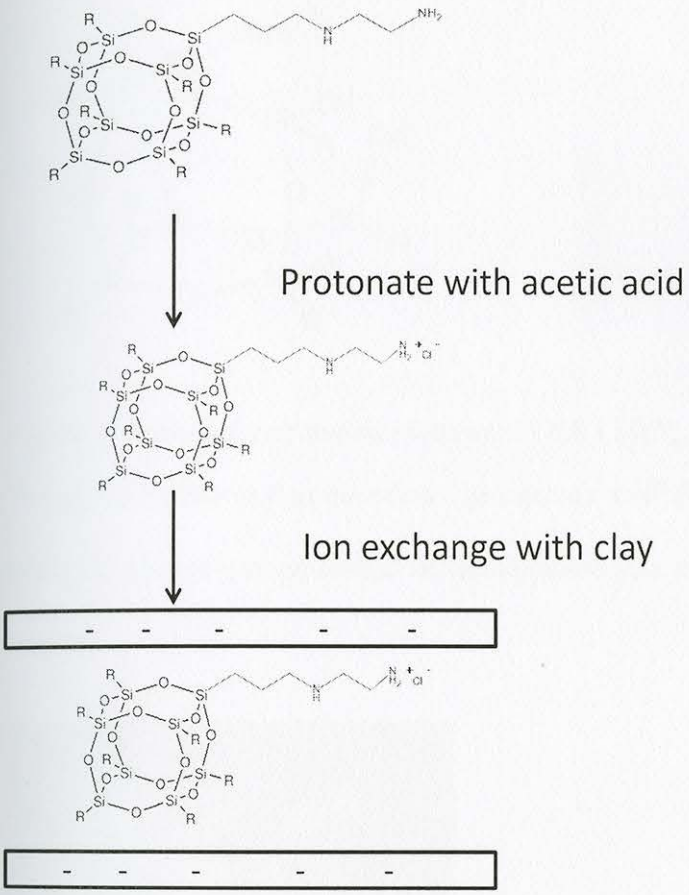

Figure 8. Suggested mechanism of AP with MMT.

Another common technique to modify clays before use as a filler in a polymer matrix is the reaction with a silane. In this study, we have used TSP as a modifier for MMT. TSP is an "open cage" (not fully condensed) molecule whose structure is shown in Figure 9 and space filling model is shown in Figure 10.

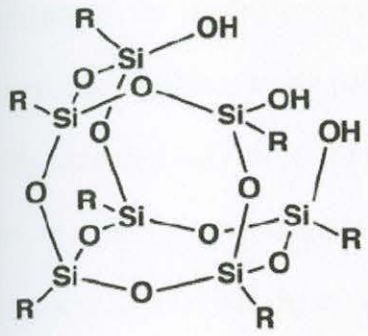

Figure 9. Schematic of trisilanolphenyl POSS (TSP), where R is phenyl. The model indicates that the silanol groups are available for interaction with the clay, while the phenyl groups extend on the opposite side of the cage to present a hydrophobic corona.

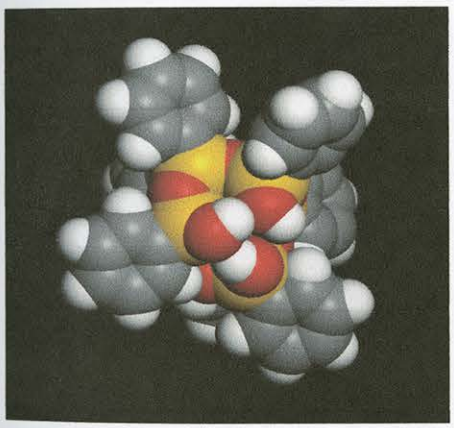

Figure 10. Space filling simulation of TSP.

Silanes are thought to undergo condensation reactions with the hydroxyl groups of clay, making the filler more hydrophobic. Grafting of silane molecules on the surface of clay can occur at three possible sites due to the reactive hydroxyl groups present in clay at the edges, external surfaces and the interlayer (5). If silanization occurs at the interlayer or the edges, the distance between the layers will increase (6). In our study, we chose to use TSP to modify MMT because of the availability of three silanol groups.

Additionally, the phenyl group on the TSP provides hydrophobicity to the clay to improve dispersability in the polymer matrix. Once on the clay surface, the silanes form an oligomer film on the outside of the clay, which improves the compatibility with rubber matrices during the vulcanization process. It can also be hypothesized that siloxane oligomers can react with hydroxyl groups of neighboring clays, creating chemical crosslinking between clay layers (5b). The suggested scheme is shown below. This chapter will provide evidence to support this hypothesis.

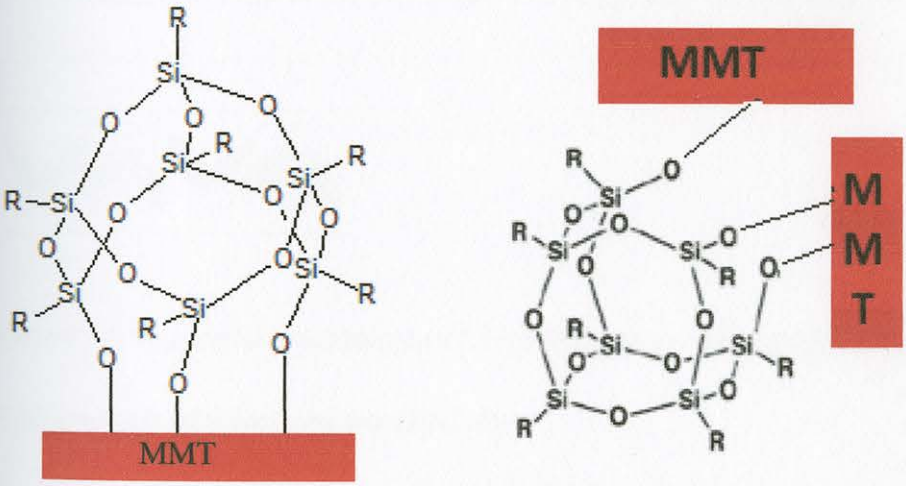

Figure 11. Suggested mechanism of TSP interaction with MMT.

Finally, a commercially available modified MMT, 15A, was used as a control for clay fillers in polymer matrices. The figures below illustrate 15A as well as the hydrogenated tallow portion of the clay.

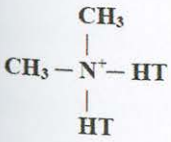

Figure 12. Schematic of 15A clay, where HT is hydrogenated tallow.

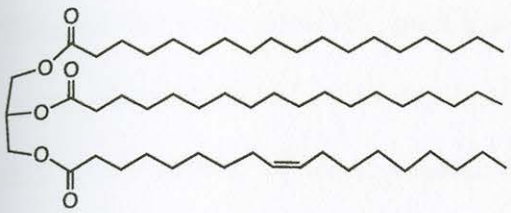

Figure 13. Schematic of hydrogenated tallow.

15A uses the same cation exchange method as APMMT, except instead of using AP to intercalate and ion exchange, the ammonium ions come from the quaternary ammonium salt. Attached to the ammonium is the long chain fatty acid which is thought to intercalate and expand the clay layer. The suggested scheme is shown below.

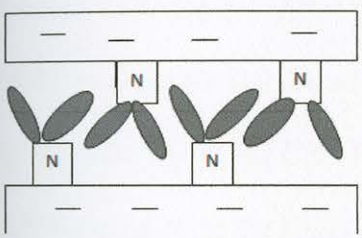

Figure 14. Suggested mechanism of 15A where grey ovals represent the fatty acid.

XRD analysis of fillers and modified clays

The effect of fillers in a rubber matrix must first be characterized in order to determine their individual properties. A common technique to determine whether MMT has been successfully modified is to use XRD. XRD is capable of indicating the interlayer spacing. In this case, the (001) plane of the unmodified or modified MMT is under investigation. As shown in Figure 15, XRD indicates a shifting of the (001) plane when comparing unmodified MMT to AP modified MMT. MMT has a peak at 7.56 2θ. Bragg's law: $n\lambda=2d\sin(\theta)$, can be using to correlate the angular spacing to a numerical spacing. For MMT, the spacing between planes is 1.17 nm. Pure AP shows numerous strong peaks which are due to the crystalline nature of the nanostructured chemical (3a).

The modified filler (APMMT) peak indicates the shifting of the (001) peak to lower 2θ values. The shift to 2.25 2θ corresponds to 3.93 nm spacing between the clay layers. This shift is indicative of AP being intercalated between the MMT layers(3c). The diameter of the POSS molecule was calculated from dynamic simulations to be 1.89 nm. The difference between the spacing of MMT and APMMT is 2.76 nm. Since the interlayer spacing is greater than a single layer of POSS but less than a bilayer, it can be concluded that the spacing is a modified bilayer. A modified, or tilted, bilayer represents an overlapping bilayer arrangement. Two layers of POSS are tilted at an angle with some degree of overlap (7). XRD was used to determine the necessary amount of AP to add to MMT in order for full ion exchange. The figure below shows the XRD spectra of neat MMT, MMT with 0.2 CEC APMMT, MMT with 0.6 CEC AP and MMT with 1.0 CEC AP. By examining the (001) plane, it can be determined that with 0.2 CEC AP in MMT, the spacing is 6.23 2θ, or 1.42 nm which implies a monolayer packing. With 0.6 CEC APMMT, the spacing increases 2.25 2θ, or 3.93 nm. Thus, it is at 0.6 CEC APMMT that the tilted bilayer packing first occurs. With 1.0 CEC APMMT, the (001) plane does not shift, suggesting that the clay interlayer has reached its maximum expansion.

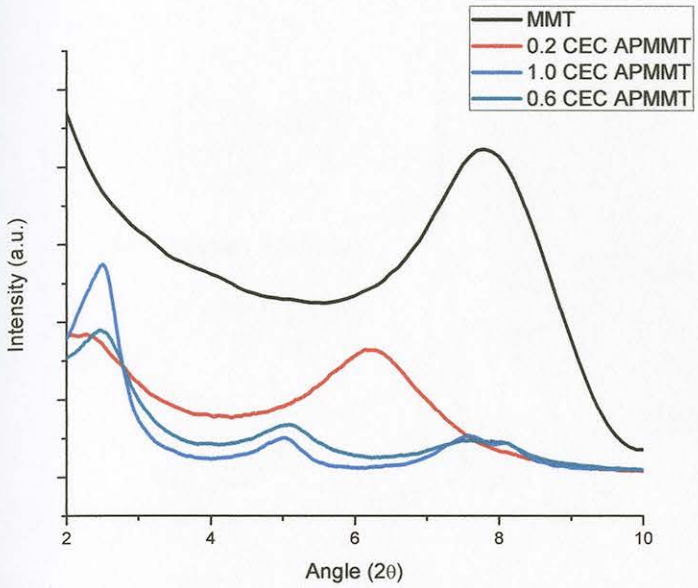

Figure 15. XRD spectra of loading levels of AP in MMT.

The (002) and (003) planes of APMMT are located at 5.05 2θ and 7.75 2θ respectively. These planes represent the b and c axes of the APMMT structure. The spacing of 1.75 nm and 1.14 nm respectively refer to the spacing in the y and z directions.

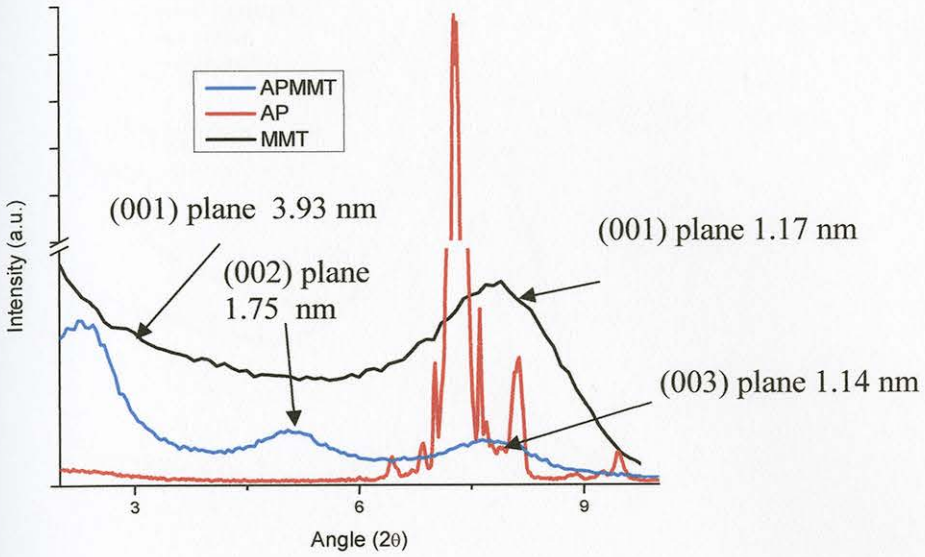

Figure 16. XRD spectra of AP, MMT, and APMMT

Examining the effect of trisilanolphenyl POSS (TSP) on MMT indicates a different mechanism of attachment as shown in Figure 17. The unmodified MMT has an interlayer spacing of 7.56 2θ which corresponds to 1.17 nm clay layer spacing. Pure TSP has multiple peaks which are indicative of the strong crystallinity of POSS (3a). When TSP is incorporated into MMT, the TSPMMT modified filler has an interlayer spacing of 7.15 2θ which corresponds to 1.24 nm interlayer spacing. This very slight increase in interlayer spacing with the addition of TSP implies that the silanol POSS is fixed on the outer surfaces of the clay. This finding indicates that the POSS undergoes condensation reactions with the edges of the clay, but does not react with the interlayer of the clay (8).

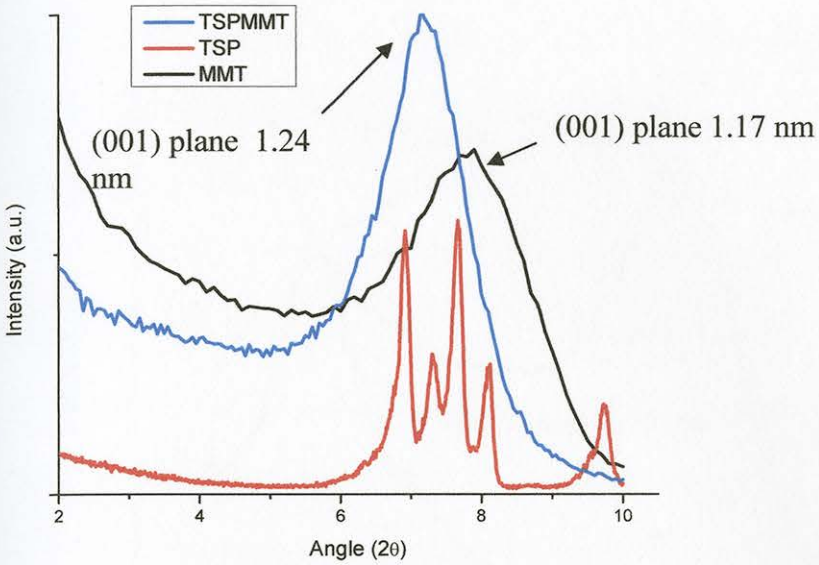

Figure 17. XRD spectra of TSP, MMT, and TSPMMT.

XRD of the commercially available modified clay, Cloisite 15A, is shown in Figure 18. MMT has an interlayer spacing of 1.17 nm. 15A has an interlayer spacing of 2.66 2θ which corresponds to an interlayer spacing of 3.32 nm. The difference in spacing is 2.15 nm, which implies intercalation of the tallow of 15A (9). The (002) and (003) plane of 15A are located at 4.14 2θ and 6.86 2θ respectively, representing the b and c planes of the modified clay. In comparison to APMMT, the (002) and (003) planes of 15A are present at higher interlayer spacings. The lower interlayer spacing of the b and c planes of APMMT imply restriction of the modified filler. This restriction may cause less rubber to become intercalated between its layers.

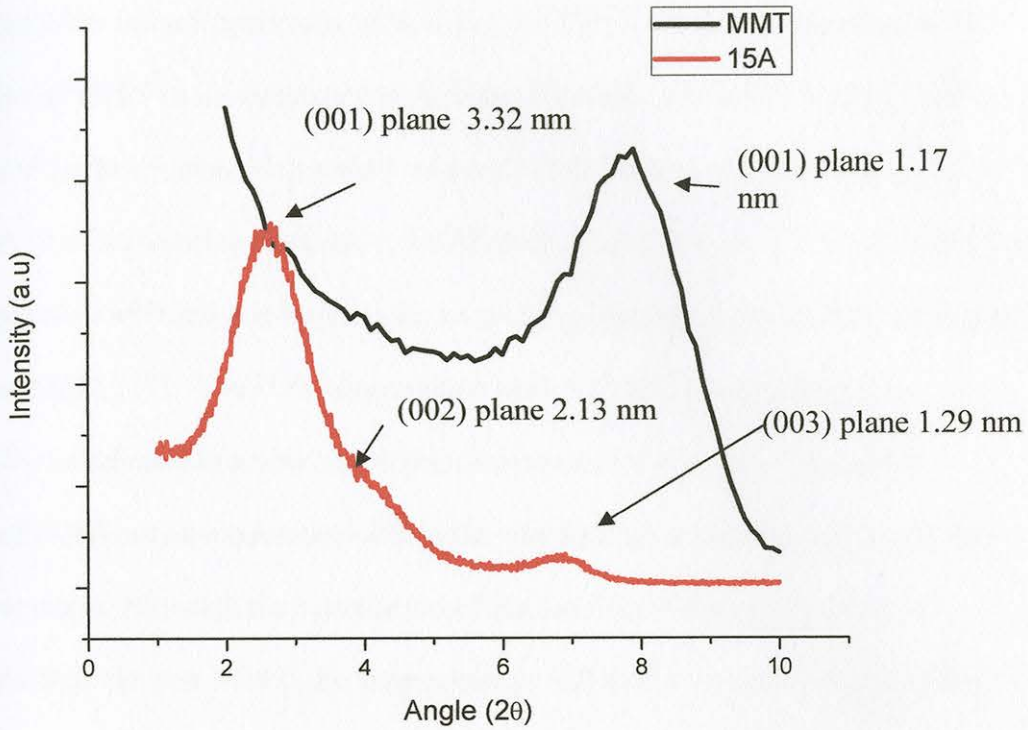

Figure 18. XRD spectra of MMT and 15A.

TGA Analysis

Thermogravimetric analysis can be used to determine the amount of POSS on MMT as well as the thermal stability of the filler. Figure 19 shows the TGA derivative weight curves obtained for MMT, AP and APMMT under nitrogen flow. Pure sodium MMT experiences two main degradation steps. The first slight mass loss before 200 °C is due to the removal of the physically adsorbed water molecules on the MMT. The TGA plot shows only a small mass loss below 200°C. Another mass loss peak occurs at 635°C which is due to dehydroxylation of structural water in MMT (3a). AP has two strong degradation peaks at 269°C and 394°C. The first peak is attributed to the degradation of the functional groups as they are removed from the POSS cage, while the second degradation step is due to the sublimation of the POSS cage (10). The AP modified MMT

filler shows three degradation steps in nitrogen. Below 200°C, mass loss is due to excess water in the filler as seen previously with MMT. At 392°C, the mass loss is due to the degradation of POSS in the interlayer of the clay. The mass loss at 519°C is due to the loss of the dehydroxylation of structural water of MMT as seen in the mass loss of pure MMT (3a). The degradation peak due to MMT shifts from 635°C to 519°C, implying that the incorporation of POSS has lowered the temperature necessary to eliminate structural water from MMT (11). The POSS degradation peak at 269°C is eliminated. This elimination is attributed to a now single degradation step of AP, since the organic moieties of POSS are now contained within the clay interlayer and cannot decompose at low temperatures. Although the degradation of the modified filler occurs at a lower temperature than the neat MMT, the temperature is still well above normal processing temperatures of the rubber matrices used in this study (12).

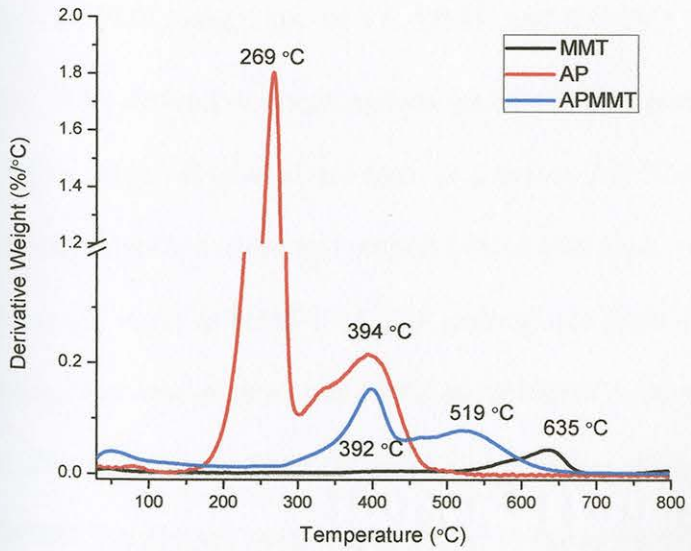

Figure 19. TGA derivative weight of AP, MMT, and APMMT in nitrogen.

The TGA percent weight loss curves of MMT, AP and APMMT are shown in Figure 20. Neat MMT has a weight loss of 5.87% at 800°C. AP completely degrades with

no remaining char. The APMMT modified filler indicates the incorporation of POSS onto MMT. Accounting for the mass loss of MMT, the AP contributes 22.84 weight % to the modified filler (3b). This corresponds to 25.43 molar % due to AP degradation. This high efficiency will be examined further with water sorption studies.

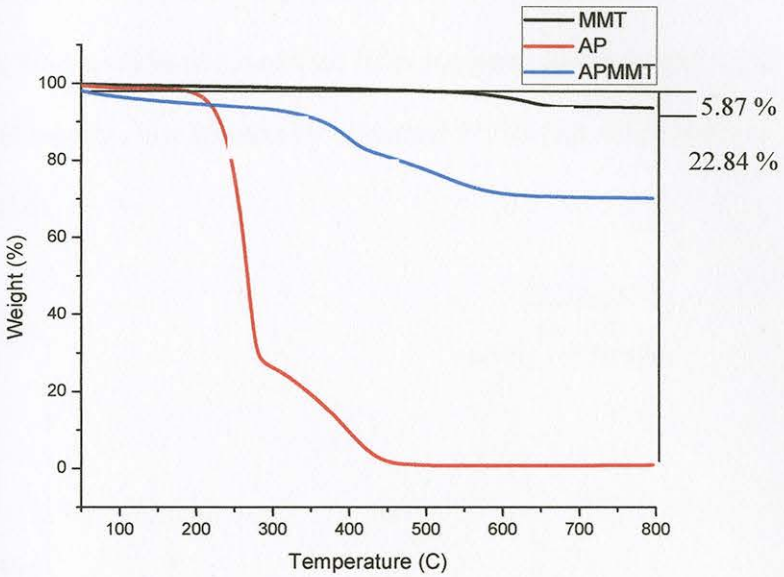

Figure 20. TGA weight loss of AP, MMT, and APMMT in nitrogen.

TGA derivative weight curves for MMT, TSP and TSPMMT are shown in Figure 21. Again, MMT displayed one mass loss before 200 °C due to the decomposition of the physically adsorbed water and second a mass loss peak at 635°C due to dehydroxylation of structural water in MMT (3a). TSP undergoes a three step degradation process in nitrogen. The first mass loss at 234°C is attributed to the condensation of the open POSS cage. The mass loss at 501°C is assigned to the degradation of the functional groups on the POSS. Finally, the mass loss at 595°C is due to the partial degradation of the POSS cage (13). The TSPMMT modified filler undergoes a two step degradation process in nitrogen. The first mass loss at 414°C can be assigned to the degradation of the condensed POSS molecules on the outside of the MMT. Common silanols used to modify

MMT have degradation temperatures of 130°C. Thus, the use of a POSS silanol increases the use temperature of silanol modified clay fillers in polymer matrices (14). The mass loss at 234°C due to the degradation of the POSS functional groups is not observed, implying the chemical attachment of POSS to the MMT. The final degradation peak of TSPMMT occurs at 592°C and is due to the dehydroxylation of water on the MMT. The lack of a third peak in the modified filler suggests that the washing of the filler with ethanol eliminates any physically adsorbed POSS that might have remained on the clay surface (14).

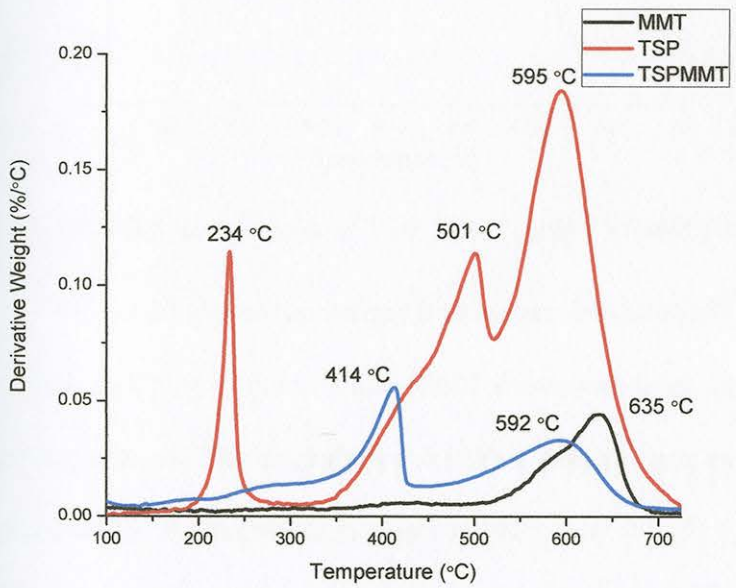

*Figure 21.*TGA derivative weight of TSP, MMT, and TSPMMT in nitrogen.

The TGA percent mass loss curves for the TSP system are shown in Figure 22. The MMT alone contributes a mass loss of 5.87%. Accounting for this percentage, the filler consists of 5.18 weight %, or 8.11 mole % TSP. This amount is considerably lower than the 25.43 mole % contribution of AP to APMMT. This implies that the TSPMMT condensation reaction is less efficient than the cation exchange reaction of APMMT. This

efficiency rate will have a profound effect on water sorption, as will be explained later in the chapter.

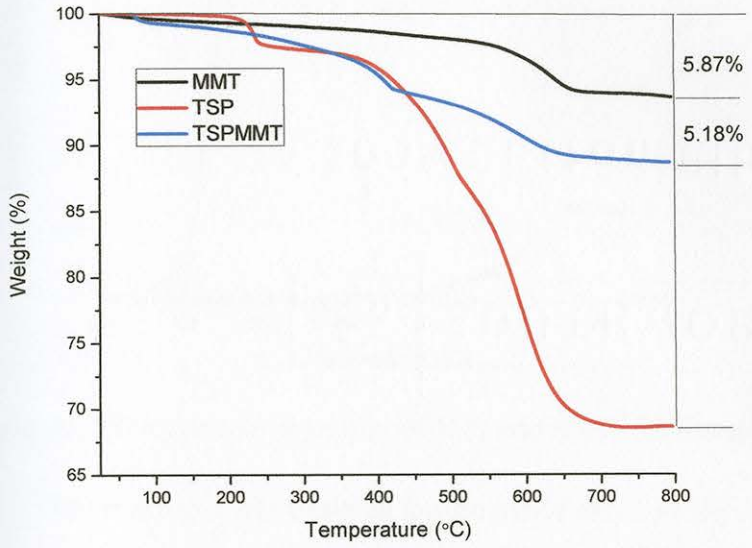

Figure 22. TGA weight loss of TSP, MMT, and TSPMMT in nitrogen.

Figure 23 shows the weight loss curves for the MMT and the commercially modified 15A clay system. While MMT shows two mass losses, 15A experiences a three stage degradation. The degradation of tallow residue and unexchanged surfactant are responsible for the degradation peaks at 291°C and 401°C, respectively. The peak at 517°C is the decomposition of the structural water of the 15A (15).

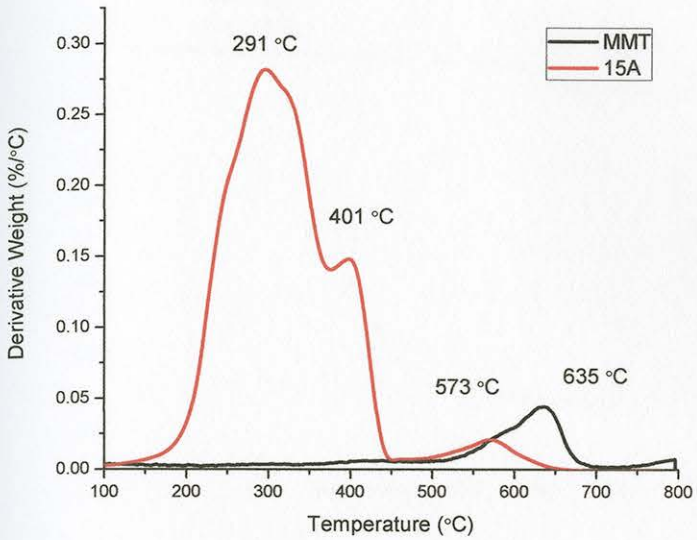

Figure 23. TGA derivative weight of 15A and MMT in nitrogen.

The mass loss TGA curves for the MMT and 15A clays are shown in Figure 24. MMT contributes a mass loss of 5.87%. Accounting for this percentage, 15A consists of 39.63 weight %, or 44.42 molar % organic modifier. This amount is considerably higher than the 25.43 molar % contribution of AP to APMMT. The exchange ratio of the ion exchanged clays was calculated using:

$$X(\%) = \frac{R*CEC*MW_{surfactant}}{100+R*CEC*(MW_{surfactant})} * 100 \quad (5)$$

Where R is the exchange ratio, X is the organic weight loss determined by TGA, and $MW_{surfactant}$ is the molecular weight of the modifier. X takes into account the mass loss of the MMT (16). For 15A, the addition of the surfactant to the clay results in an exchange ratio of 0.27. The addition of AP to MMT has an efficiency of 0.38. This exchange values indicates that 27% of the available cations are exchanged in the production of 15A. The use of AP as an ion exchange surfactant with MMT, results in 38% of the cations being exchanged with POSS.

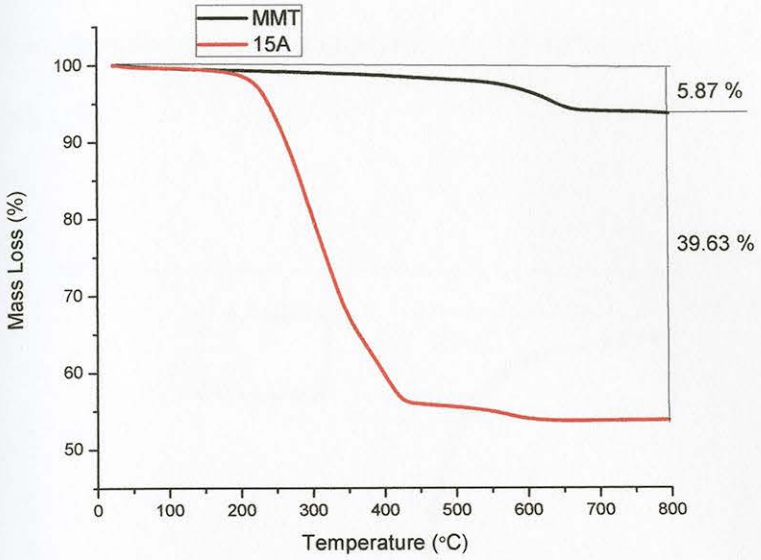

Figure 24. TGA weight loss of 15A and MMT in nitrogen.

Water sorption studies

Water sorption studies were conducted to determine the hydrophobicity of the unmodified and modified fillers. Hydrophobicity of fillers is a key property influencing the compatibility with polymer matrices. The measured water sorption of fillers prior to modification is shown in Figure 25. AP has a water uptake of 2.0%, TSP 0.2% and MMT 24.7%. These results are indicative of the hydrophobic nature of AP POSS and the hydrophilic nature of unmodified clay. However, the low water uptake of TSP is unexpected due to the exposed hydroxyl groups in its structure. Literature has shown that uncondensed POSS molecules such as TSP, can condense to form dimers in the presence of water, thus reducing the hydrophilic content (17). MMT has the highest water uptake levels due to the hydrophilic nature of clays from the hydration of inorganic cations on exchange sites (14). While both types of POSS have a much lower water vapor sorption, the increased water sorption level of the AP is attributed to its polar amine groups (18). The phenyl groups of TSP appear to effectively reduce the water uptake for this POSS

molecule. The commercially modified clay, 15A has a sorption of 4.9%. This fivefold decrease in water sorption compared to MMT is due to the replacement of exchanged cations (19).

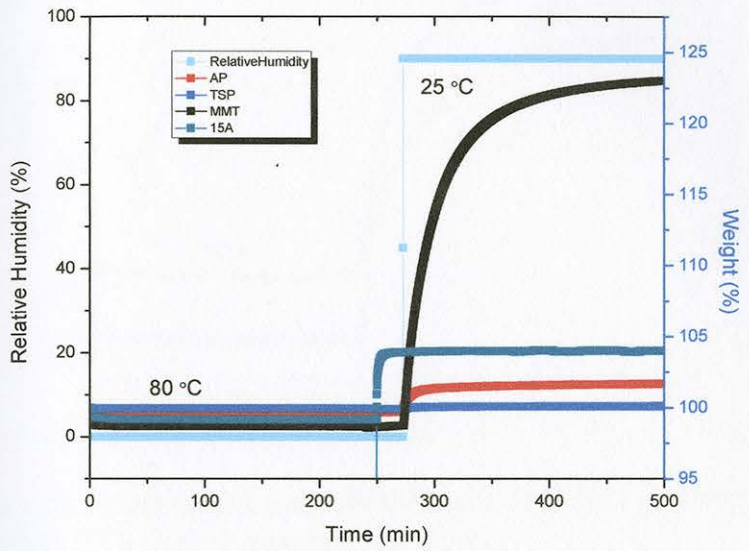

Figure 25. Water sorption of AP, TSP, MMT, and 15A at 80°C and 10% relative humidity shifted to 90% relative humidity and 25°C.

The effect of POSS modification of clay on water vapor uptake is seen in Figure 26. After equilibration at 0% RH, TSPMMT gains 17.4% in weight while APMMT gains 10.7%. The hydrophobic nature of TSP contributes to the reduction of water uptake. However, the low level of TSP incorporation in MMT, as shown by TGA, results in only a small decrease in water uptake. This suggests that not all of the exposed hydroxyl groups of TSP have reacted with the hydroxyl groups of MMT. The incorporation of AP in MMT produces hydrophobicity due to the ion exchange process, similar to the process of modification in15A (20). The difference in water uptake of APMMT and 15A is once again attributed to the amount of organic modifier present on the clay. Due to the smaller

amount of AP (25 mole%) to 15A (54 mole%), the decrease in water uptake is smaller with APMMT.

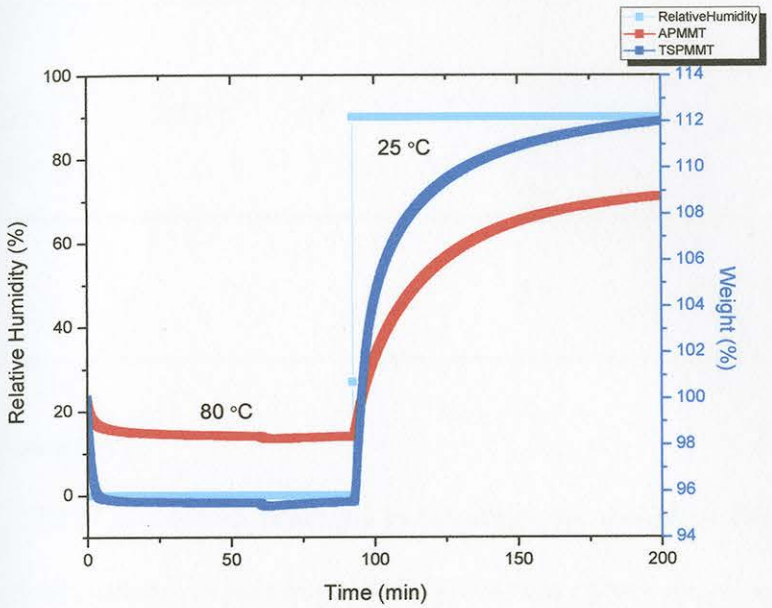

Figure 26. Water sorption of APMMT and TSPMMT at 80°C and 10% relative humidity shifted to 90% relative humidity and 25°C.

The table below summarizes the water uptake of the various unmodified and modified fillers. It is evident that the additions of either AP or TSP result in a more hydrophobic filler. This hydrophobicity is evidence of a successful filler modification since one of the goals of a clay filler is to decrease the hydrophilicity of clay in order to become more compatible with a polymer matrix.

Table 2

Percent mass gain of fillers in 90% relative humidity and 25°C environment

% Mass Gain	MMT	AP	TSP	15A	APMMT	TSPMMT
	24.7	2.0	0.2	4.9	10.7	17.4

FTIR analysis

FTIR is a useful technique to determine the chemical shifts that take place upon filler modification. In particular, ATR FTIR was chosen due to its ease of use on bulk powder samples. Figure 27 shows the ATR FTIR spectra of MMT, AP and APMMT. MMT has a peak at 3628 cm^{-1} which is characteristic of structural OH present in the clay. The Si-O-Si stretch of MMT occurs at 990 cm^{-1}. AP has a peak at 1076 cm^{-1} which is due to the Si-O-Si stretch. Aliphatic stretching of AP can be seen at 2800 to 3000 cm^{-1} (3c). FTIR is most useful in the determination of the bonding that occurs when MMT and AP are chemically combined. The aliphatic stretching region of AP remains present in the modified filler as well. This provides further evidence that AP was not washed off during the synthesis process and that it remains chemically bonded to the clay. The aliphatic region of the FTIR spectra can be probed in order to understand the order or disorder of the system. Well ordered layers show aliphatic stretches at higher wavenumbers (21). At lower wavenumbers such as 2924 cm^{-1} and 2856 cm^{-1} for CH_2 stretching, a completely disordered structure is discovered. A peak at 2924 cm^{-1} develops when AP is bonded to MMT. This peak suggests that the POSS in between the MMT layers is in a disordered

state. In the modified filler, the structural OH of MMT shifts to 3630 cm^{-1}. The Si-O-Si stretch of MMT shifts to 1009 $cm^{-1}$and the Si-O-Si stretch of AP shifts to 1110 cm^{-1} (3c). Both the AP and the MMT components of the filler shift to lower wavenumbers. This is indicative of the disorder of the surfactants already present inside the layer structures (21). This is evidenced with XRD spectra.

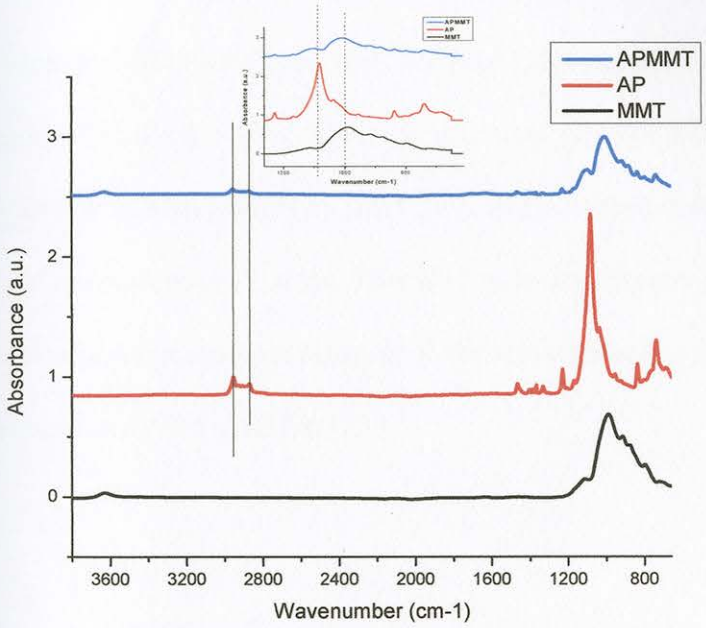

Figure 27. FTIR spectra of AP, MMT, and APMMT.

One of the concerns in the mechanism of modifying MMT with silanes such as TSP is the unclear bonding mechanism. It has been shown that silanes can be physically adsorbed onto the clay surface. These silanes are not sufficiently bonded to the clay and will not remain affixed during addition with a polymer (22). Thus, FTIR is a useful technique to determine whether POSS is truly condensed onto MMT or merely physically adsorbed. In our sample preparation, TSPMMT was rinsed multiple times with ethanol. TSP should not be coating and adsorbing to the clay surface. If this were the case, there would be no change in the IR spectra since adsorption corresponds to a relatively weak

combination between the clay and the silane (23). When chemical bonding of silanes to MMT occur, changes in the IR spectra will be seen. Figure 28 shows the ATR FTIR spectra of MMT, TSP and TSPMMT. A peak at 2964 cm^{-1} is visible in TSP due to the stretching of the phenyl groups of TSP. This peak decreased in intensity, but is still visible in TSPMMT. Phenyl aromatic stretching of TSP can be seen at 1400 to 1600 cm^{-1}. The Si-O-Si stretch of TSP is located at 1076 cm^{-1}. Due to the small amount of TSP that has been grafted to MMT (as seen via TGA), the peaks of the modified filler are small, but visible. In the modified filler, the structural OH of MMT shifts to 3636 cm^{-1}. The Si-O-Si stretch of MMT shifts to 1003 cm^{-1}. Si-O-Si stretch of TSP shifts to 1110 cm^{-1} (3c). Both of the components of the filler shift to lower wavenumbers. The shift to lower wavenumbers can indicate disorder of the surfactants due to the disturbance of the conformation of the modifier (21).

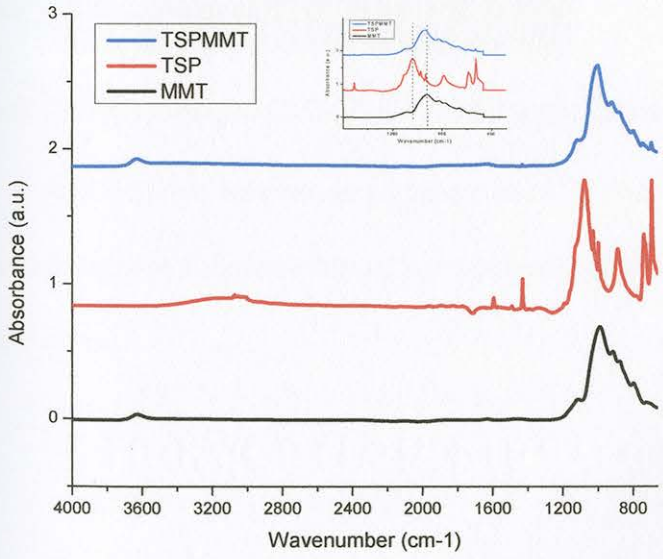

Figure 28. FTIR spectra of TSP, MMT, and TSPMMT.

SEM Analysis

The unmodified and modified fillers were examined using scanning electron microscopy. The visual examination of fillers can indicate the size as well as structure. These properties are important factors in determining the compatibility with a polymer matrix. Images were taken at 5000x magnification. Figure 29 shows unmodified MMT. The 25 micron size of MMT will be compared with the other fillers.

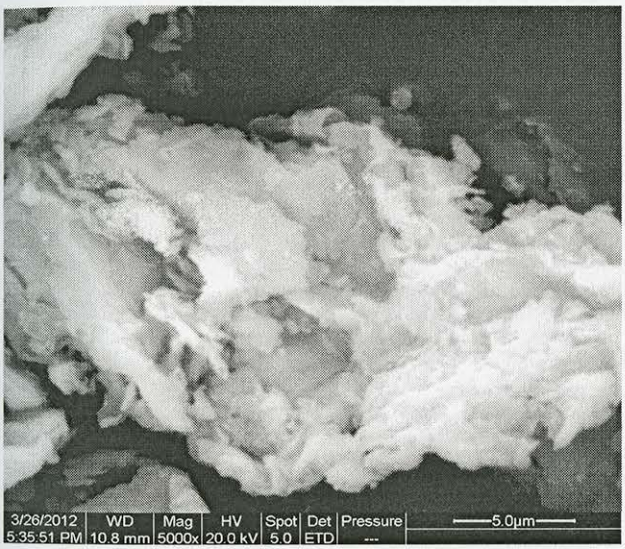

Figure 29. SEM image of MMT at 5000x magnification.

APMMT has an average particle size of 20 microns as seen in Figure 30. Although there is a slight decrease in particle size, the structure has lost some of its 'flaky' nature.

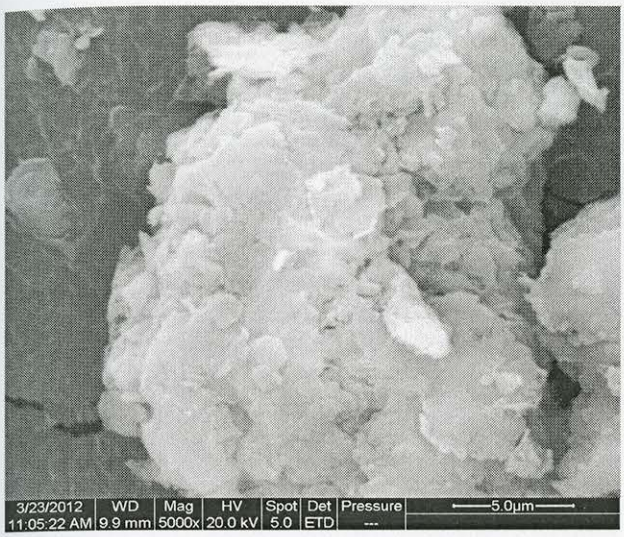

Figure 30. SEM image of APMMT at 5000x magnification.

TSPMMT has an average particle size of 4 microns as seen in Figure 31. Due to the mechanical shearing used to modify the clay with silanes, the modified clay is much smaller than the original MMT. The smaller particle size allows for easier dispersion and a higher surface area (24).

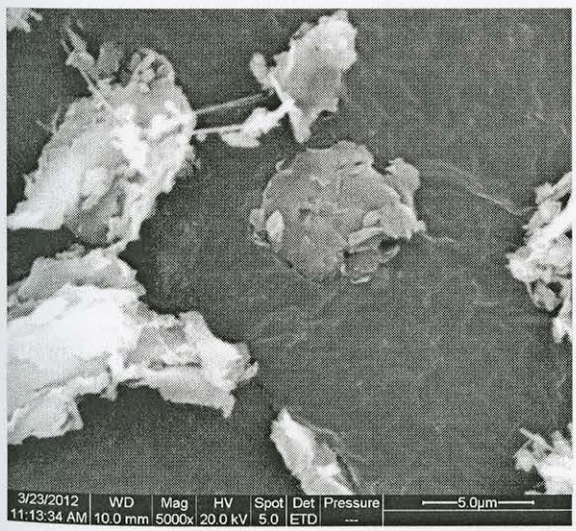

Figure 31. SEM image of TSPMMT at 5000x magnification.

The commercially available 15A shows a flakier surface and the average particle size decreases to 7 microns as seen in Figure 32. The large surface area of 15A suggests a successful interface with a polymer matrix.

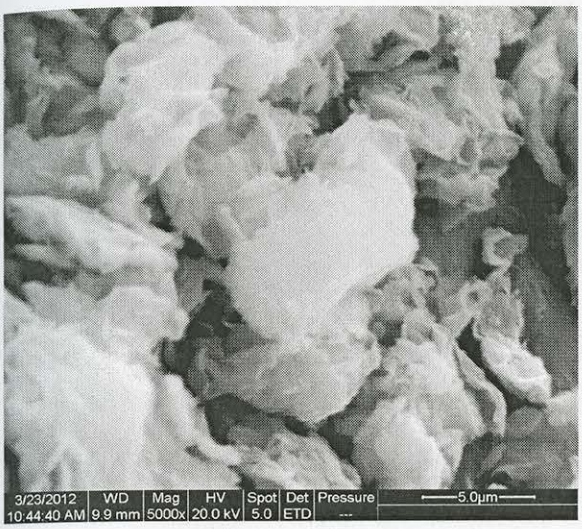

Figure 32. SEM image of 15A at 5000x magnification.

Microscopy is a useful technique to determine the physical compatibility of fillers with a matrix. We hypothesize that the small size and flaky nature of both TSPMMT and 15A could aid in their dispersion in a polymer matrix.

Conclusions

The results of the aforementioned characterization techniques allow us to confidently suggest a mechanism for the addition of AP to MMT. XRD indicates a shift of the (001) plane between MMT and APMMT. This shift from 1.17 nm to 3.93 nm suggests that AP has become intercalated between the MMT layers. Additionally, a tilted bilayer arrangement of POSS in between the clay layers is hypothesized based upon the POSS size. Cation exchange of the sodium of the MMT with the chlorine of the protonated POSS allows for this intercalation. More evidence is found in the TGA results. Additional mass losses beyond that of MMT are due to AP being degraded. Additionally, the loss of the second degradation peak of AP when combined with MMT suggests that the organic substituents of POSS are entrapped between the clay layers. FTIR spectra imply that peaks relative to both POSS and MMT are present in the

modified filler spectra. FTIR also suggests that the POSS is disordered within the clay layers. All of this data was collected after the sample had been rinsed with water, ethanol and THF to remove any residual POSS on the surface of the clay. The synthesis of TSPMMT is a product of a silanol condensation reaction. XRD data indicates no intercalation of the POSS between the MMT layers. This suggests that the POSS is condensed onto the outside edges and sides of the MMT. TGA weight loss confirms that POSS has been successfully attached to the MMT, even after rinsing thoroughly with ethanol. Additionally, FTIR spectra indicate the presence of TSP on MMT. Water sorption studies indicate the decrease in hydrophilicity of MMT with the addition of the hydrophobic TSP.

REFERENCES

1. Vazquez, A.; Lopez, M.; Kortaberria, G.; Martin, L.; Mondragon, I. Modification of montmorillonite with cationic surfactants. Thermal and chemical analysis including CEC determination. *Applied Clay Science* **2008,** *41*, 24-36.

2. Xie, W.; Gao, Z.; Liu, K.; Pan, W.-P.; Vaia, R. A.; Hunter, D.; Singh, A. Thermal characterization of orgnically modified montmorillonite. *Thermochimica Acta* **2001,** *367*, 339-350.

3. (a) Zhao, F.; Wan, C.; Bao, X.; Kandasubramanian, B. Modification of montmorillonite with aminopropylisooctyl polyhedral oligomeric silsequioxane. *Journal of Colloid and Interface Science* **2009,** *333* (1), 164-170; (b) Perrin, F. X.; Bruzaud, S.; Grohens, Y. Structure and thermal behaviour of polyhedral oligomeric silsesquioxane modified montmorillonite. *Applied Clay Science* **2010,** *49* (3), 113-119; (c) Yei, D.-R.; Kuo, S.-W.; Su, Y.-C.; Chang, F.-C. Enhanced thermal properties of PS nanocomposites formed from inorganic POSS-treated montmorillonite. *Polymer* **2004,** *45* (8), 2633-2640.

4. Liu, H.; Zhang, W.; Zheng, S. Montmorillonite intercalated by ammonium of octaaminopropyl polyhedral oligomeric silsesquioxane and its nanocomposites with epoxy resin. *Polymer* **2005,** *46* (1), 157-165.

5. (a) Park, M.; Shim, I.-K.; Jung, E.-Y.; Choy, J.-H. Modification of external surface of laponite by silane grafting. *Journal of Physics and Chemistry of Solids* **2004,** *65* (2–3), 499-501; (b) Negrete-Herrera, N.; Putaux, J.-L.; Bourgeat-Lami, E. Synthesis of polymer/Laponite nanocomposite latex particles via emulsion

polymerization using silylated and cation-exchanged Laponite clay platelets. *Progress in Solid State Chemistry* **2006,** *34* (2–4), 121-137.

6. Guimarães, J. L.; Peralta-Zamora, P.; Wypych, F. Covalent Grafting of Phenylphosphonate Groups onto the Interlamellar Aluminol Surface of Kaolinite. *Journal of Colloid and Interface Science* **1998,** *206* (1), 281-287.

7. (a) Vaia, R. A.; Teukolsky, R. K.; Giannelis, E. P. Interlayer Structure and Molecular Environment of Alkylammonium Layered Silicates. *Chem Mater* **1994,** *6* (7), 1017-1022; (b) Zhu, J.; He, H.; Guo, J.; Yang, D.; Xie, X. Arrangement models of alkylammonium cations in the interlayer of HDTMA pillared montmorillonites. *Chinese Science Bulletin* **2003,** *48* (4), 368-372.

8. Song, K.; Sandi, G. Characterization of Montmorillonite Surfaces After Modification by Organosilane. *Clay and Clay Minerals* **2001,** *49* (2), 119-125.

9. Xi, Y.; Ding, Z.; He, H.; Frost, R. Structure of organoclays- an X-ray diffraction and thermogravimetric analysis study. *Journal of Colloid and Interface Science* **2004,** *277*, 116-120.

10. Bolln, C.; Tsuchida, A.; Frey, H.; Mulhaupt, L. Thermal Properties of the Homologous Series of 8-fold Alkyl-Substituted Octasilsesquioxane. *Chem Mater* **1997,** *9*, 1475-1479.

11. Xi, Y.; Martens, W.; He, H.; Frost, R. L. Thermogravimetric analysis of organoclays intercalated with the surfactant octadecyltrimethylammonium bromide. *Journal of Thermal Analysis and Calorimetry* **2005,** *81*, 91-97.

12. Sadhu, S.; Bhowmick, A. K. Preparation and Properties of Nanocomposites Based on Acrylonitrile-Butadiene Rubber, Styrene-Butadiene Rubber, and

Polybutadiene Rubber. *Journal of Polymer Science: Part B: Polymer Physics* **2004,** *42*, 1573-1585.

13. (a) Feher, F. Polyhedral Oligosilsesquioxanes and Heterosilsesquioxanes; (b) Mantz, R. A.; P.F., J.; Chaffee, K. P.; Lichtenhan, J. D.; Gilman, J. W. Thermolysis of Polyhedral Oligomeric Silsesquioxane (POSS) Macromers and POSS-Siloxane Copolymers. *Chem Mater* **1996,** *8*, 1250-1259.

14. Shen, W.; He, H.; Zhu, J.; Yuan, P.; Frost, R. Grafting of montmorillonite with different functional silanes via two different reaction systems. *Journal of Colloid and Interface Science* **2007,** *313*, 268-273.

15. Golebiewski, J.; Galeski, A. Thermal stability of nanoclay polypropylene composites by simultaneous DSC and TGA. *Composites Science and Technology* **2007,** *67* (15–16), 3442-3447.

16. Toh, C.; Xi, L.; Lau, S.; Pramoda, K. P.; Chua, Y.; Lu, X. Packing Behaviors of Structurally Different Polyhedral Oligomeric Silsesquioxane-Imidazolium Surfactants in Clay. *Journal of Physical Chemistry B* **2009,** *114* (1), 207-214.

17. Liu, H.; Kondo, S.-i.; Tanaka, R.; Oku, H.; Unno, M. A spectroscopic investigation of incompletely condensed polyhedral oligomeric silsesquioxanes (POSS-mono-ol, POSS-diol and POSS-triol): Hydrogen-bonded interaction and host–guest complex. *Journal of Organometallic Chemistry* **2008,** *693* (7), 1301-1308.

18. Zhou, Q.; Pramoda, K. P.; Lee, J.-M.; Wang, K.; Loo, L. S. Role of interface in dispersion and surface energetics of polymer nanocomposites containing

hydrophilic POSS and layered silicates. *Journal of Colloid and Interface Science* **2010,** *355*(1), 222-230.

19. Barshad, I. Adsorptive and Swelling Properties of Clay-Water System. *Clays and Clay Technology*, 70-77.

20. Fu, H.-K.; Kuo, S.-W.; Yeh, D.-R.; Chang, F.-C. Properties Enhancement of PS Nanocomposites through the POSS Surfactants. *Journal of Nanomaterials* **2008,** *2008*, 1-7.

21. Rooj, S.; Das, A.; Sto¨ckelhuber, K. W.; Reuter, U.; Heinrich, G. Highly Exfoliated Natural Rubber/Clay Composites by ''Propping-Open Procedure'': The Influence of Fatty-Acid Chain Length on Exfoliation. *Macromolecular Materials Engineering* **2012,** *297*, 369-383.

22. Mittal, V.; Herle, V. Physical adsorption of organic molecules on the surface of layered silicate clay platelets: A thermogravimetric study. *Journal of Colloid and Interface Science* **2008,** *327* (2), 295-301.

23. Ianchis, R.; Cinteza, L.; Donescu, D.; Petcu, C.; Corobea, M. C.; Somoghi, R.; Ghiurea, M.; Spataru, C. Implications of silylated montmorillonite on montmorillonite-polyacrylate nanocomposites. *Applied Clay Science* **2011,** *52*, 96-103.

24. Dai, J.; Huang, J. Surface modification of clays and clay-rubber composite. *Applied Clay Science* **1999,** *15*, 51-65.

CHAPTER IV

HYDROGENATED NITRILE BUTADIENE RUBBER NANOCOMPOSITES

HNBR nanocomposites were prepared with APMMT, TSPMMT and 15A modified clays. Rheological studies of the uncured filled latex were performed to analyze clay/rubber interactions. The cured composites were analyzed by XRD, AFM, TEM and DMA techniques. The HNBR used in this study contains 38% ACN content (Figure 33). The nitrile groups of the acrylonitrile segment provide polarity to the rubber. This nitrile segment is capable of hydrogen bonding with exposed hydroxyl groups of the clay. Additionally, there is a possibility that hydrogen bonding may occur between the ammonium ion of the intercalated amine and the nitrile group of HNBR (1).

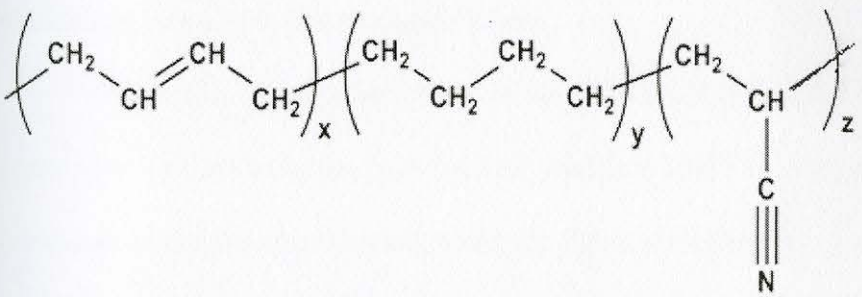

Figure 33. Structure of HNBR.

Uncured Composite Rheology

The rheological properties of uncured HNBR latex were examined as a function of filler type and loading level. Studies were conducted at a constant low strain of 1%, where morphological changes were evaluated as a function of time. Figure 34 shows storage modulus as a function of frequency for uncured HNBR latex with 1 phr loading of the three fillers evaluated. It is apparent that all of the fillers produced an increase in storage modulus as compared to the unfilled matrix.

TSPMMT and 15A fillers provided an almost three-fold increase in storage modulus, while the APMMT gave slightly less than a doubling of the modulus. The larger increases in storage modulus observed in 15A and TSPMMT blends are attributed to the exfoliation of the clay, which results in increased surface area of the fillers and the opportunity for increased clay/rubber interaction. This surface area promotes formation of physical connectivity of the modified clay with the HNBR matrix. We hypothesize that this connectivity is improved by the hydrogen bond formation between the hydroxyls of TSPMMT and the nitrile group of HNBR. The previous chapter discussed the likelihood of TSPMMT maintaining hydroxyl groups after synthesis. However, these exposed hydroxyl groups are not present on APMMT or 15A, eliminating this bonding mechanism possibility for these two fillers.

While the AP modified MMT in the absence of HNBR latex appeared to have a greater level of intercalation than the TSP modified MMT as determined by XRD studies presented in the previous chapter, when the fillers were dispersed in HNBR latex the TSP appears to have greater interaction and exfoliation, as evidenced by the rheological storage modulus results. XRD and TEM analysis of the uncured HNBR filled blends presented later in this chapter will provide further evidence of the relative exfoliation and dispersion levels of the three fillers. The smaller enhancement in modulus observed for APMMT in uncured HNBR latex is attributed to poorer dispersion and agglomeration of APMMT in the HNBR matrix (2). This indicates that little hydrogen bonding between the amine of the APMMT and the nitrile group of HNBR occurs.

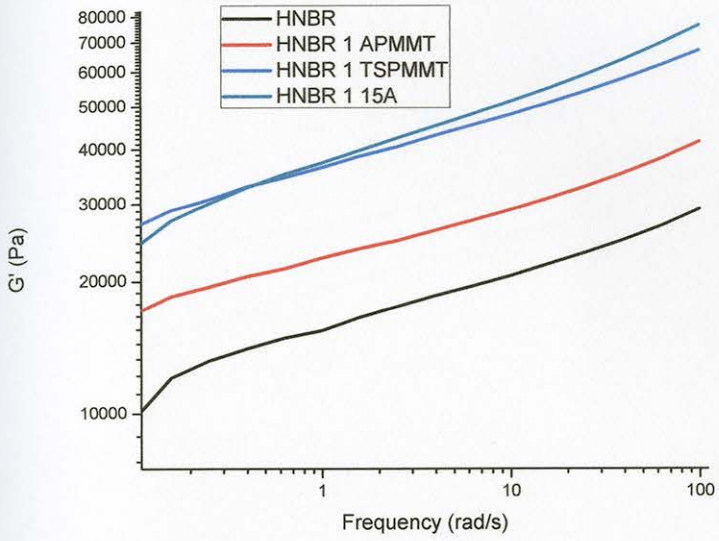

Figure 34. 120°C parallel plate rheology storage modulus results as a function of frequency for uncured HNBR composites with 1 phr filler loading .

When the amount of filler is increased to 4 phr loading, the storage modulus of both APMMT and TSPMMT increase, as seen in Figure 35. This is expected due to the increase in interfacial area of the filler in the polymer matrix. However, when the loading level of 15A is increased to 4 weight percent, the storage modulus decreased by 10 kPa. This large decrease is attributed to aggregation of the modified clay at higher loading levels, which results in a decrease in surface area, and an inhibited interaction with the HNBR (3).

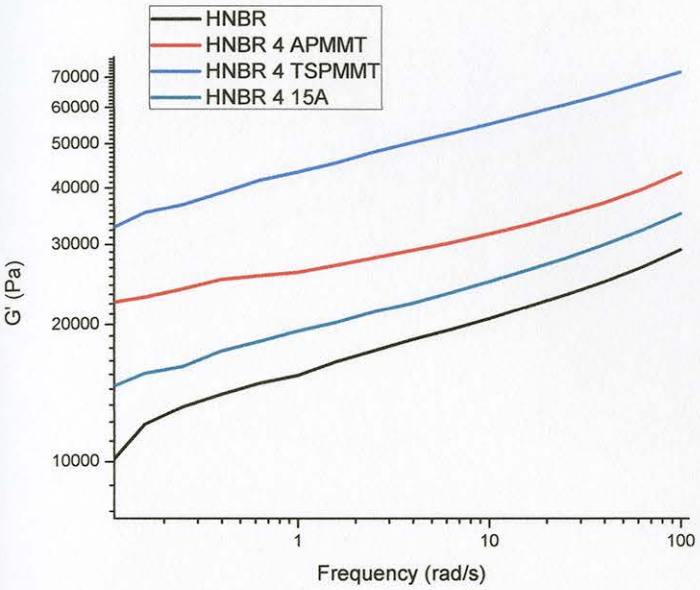

Figure 35. 120°C parallel plate rheology storage modulus results as a function of frequency for uncured HNBR composites with 4 phr filler.

The effect of higher loading levels of TSPMMT on cured HNBR composites' storage modulus is examined below. At loading levels higher than 4 phr, no further increase in storage modulus is observed (Figure 36). This finding indicates that there is no further increase in interfacial area or physical interactions between TSPMMT and HNBR above 4 phr loading, and a critical volume fraction for percolation of the filler in the matrix has been reached (4).

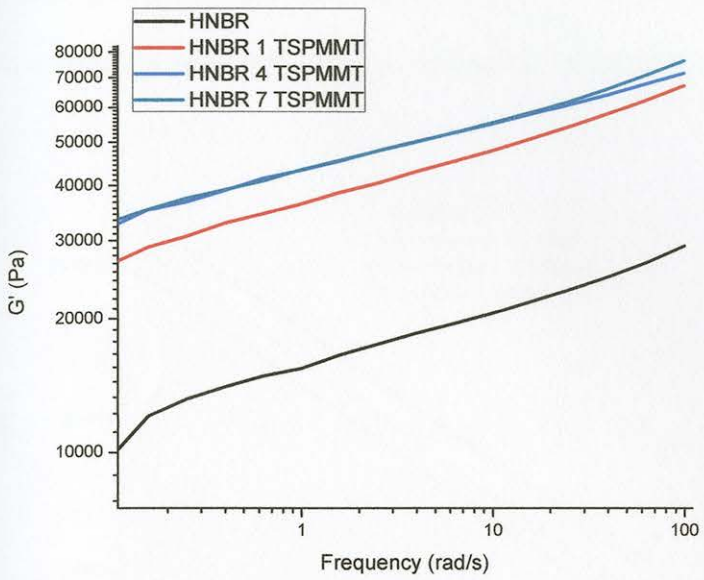

Figure 36. 120°C parallel plate rheology storage modulus results as a function of frequency for uncured HNBR composites with loading variation of TSPMMT.

Complex viscosity curves for the neat and filled uncured HNBR latex are shown in Figure 37. All of the fillers increased the viscosity relative to the gum rubber over the shear regime tested, and all systems showed shear thinning behavior. The resistance to shear deformation that is signified by an increase in viscosity is indicative of exfoliated platelets. As the number of platelets per unit volume is increased, the viscosity will increase. While all fillers produced an increase in viscosity due to the addition of a solid powder to a liquid resin, the effect was more pronounced with the well dispersed 15A and TSPMMT. Inhibition of mobility of the filler-rubber interface increases the viscosity, and this is a function of the interfacial area available and the degree of interaction between the filler and the matrix. TSPMMT and 15A decrease polymer chain mobility to a greater degree due to the higher clay surface area and greater degree of interaction with the rubber (5). Additionally, the viscosity increase with the addition of TSPMMT reinforces

the concept of hydrogen bonding of TSPMMT with HNBR. The shear thinning behavior of the filled systems indicates clay alignment in the direction of increasing shear (6).

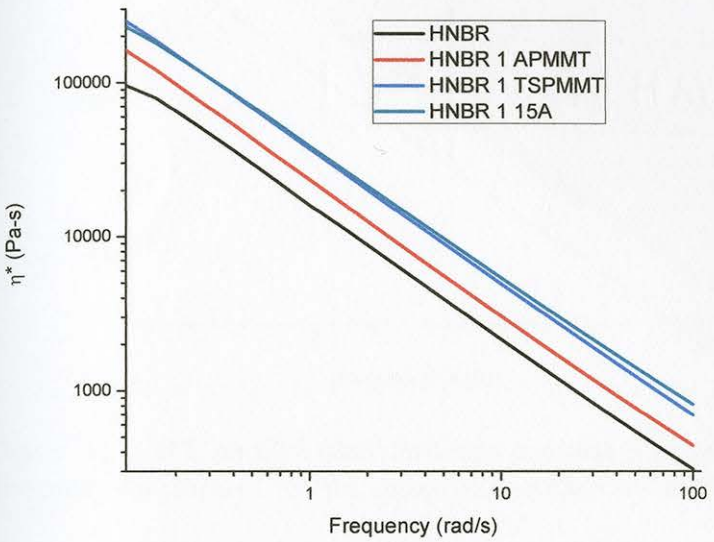

Figure 37. 120°C parallel plate rheology complex viscosity results as a function of frequency for uncured HNBR composites with 1 phr filler.

The effect of increased loading levels of TSPMMT in HNBR on complex viscosity is shown in Figure 38. Indication of a saturation level of TSPMMT is shown by the overlap in viscosity for 4 and 7 phr loadings. This overlap signifies that the filler weight fraction has reached a critical value above which the viscosity has a clay-concentration independent behavior (2).

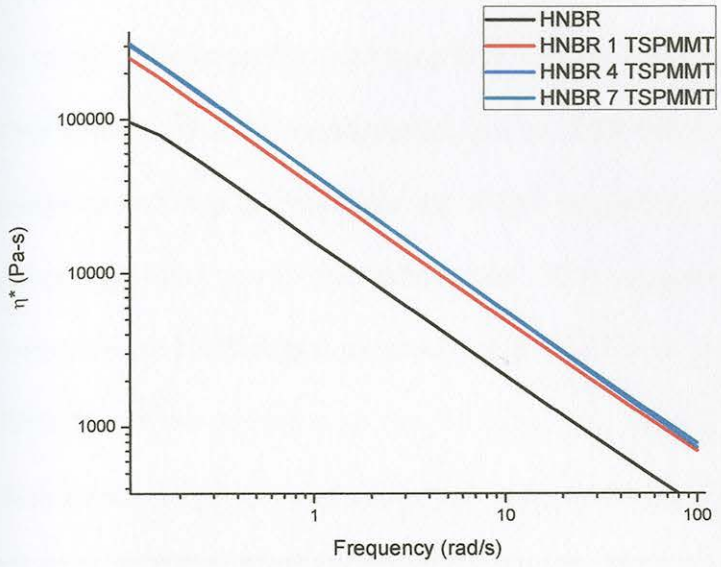

Figure 38. 120°C parallel plate rheology complex viscosity results as a function of frequency for uncured HNBR composites with loading variation of TSPMMT.

The complex viscosity is assumed to follow power law behavior as a function of frequency in the shear-thinning regime (7). The linear log-log relationship between frequency and viscosity follows a non-Newtonian power law model:

$$\eta^* = K(\omega)^{n-1} \tag{6}$$

Where η* is the complex viscosity, K is the consistency coefficient (Pa s^n), ω is the frequency (rad/s) and n is the power law index. Calculated power law parameters for the uncured HNBR-filler blends are shown in Table 3. K is a measure of viscosity at the intercept of log (η*) and log (frequency), in this case, a frequency of 10 rad/s. The consistency coefficient decreases with a decrease in viscosity. The K values ranged from 4.20 to 4.80 Pa s^n with varying filler loadings. With no filler added, HNBR had a K of 4.20 Pa s^n. The addition of fillers increased that value. The higher K value is indicative of increasing polymer-filler interactions due to the inhibition of flow (8). The power law index, n, provides a quantitative measure of flow behavior. The power law index, n,

ranged from 0.862 to 0.91. When n is less than one, flow is pseudoplastic, and the smaller the n value, the larger the departure from Newtonian behavior (8). As fillers are added to HNBR, the n value increases, implying a more Newtonian flow behavior. The one exception to this is the 1 phr loading of 15A in HNBR, where the n value decreases, indicating a more pseudoplastic behavior. This suggests that the fillers with the greatest dispersion inhibit flow and result in blends with lower pseudoplasticity (8).

Table 3

Consistency coefficient and power law index of uncured HNBR nanocomposites

	K (Pa s^n)	n	R^2
HNBR	4.20	0.86	0.99
HNBR 1 APMMT	4.36	0.87	0.99
HNBR 4 APMMT	4.42	0.89	0.99
HNBR 7 APMMT	4.41	0.87	0.99
HNBR 1 TSPMMT	4.57	0.87	0.99
HNBR 4 TSPMMT	4.51	0.89	0.99
HNBR 7 TSPMMT	4.64	0.88	0.99
HNBR 1 15A	4.58	0.841	0.99
HNBR 4 15A	4.29	0.87	0.99
HNBR 7 15A	4.80	0.91	0.99

Cured HNBR modified MMT composites

Post-cure composite characteristics help to define the structure-property relationships governing filler/rubber interactions. XRD indicates the extent of exfoliation and intercalation of clay in HNBR nanocomposites. Figure 39 shows the XRD spectra for cured HNBR nanocomposites with 1 phr filler loading. All fillers produce a similar peak at approximately 2.6 2θ which is indicative of HNBR intercalation between the clay layers and expansion of the filler interlayer. This is especially notable for HNBR with TSPMMT, since the filler originally did not have an expanded interlayer. The TSP was condensed onto the edges of the clay and had a strong bond with MMT. This increase in interlayer spacing can be explained with the 'adsorption-shear mechanism'. The 'adsorption-shear' mechanism suggests that the polymer first is adsorbed on the surface of the filler and expands the clay interlayer during the shear mixing process. After a gap is created, further polymer chains are able to intercalate and push the layers farther apart (9).

Peaks corresponding to the (002) and (003) planes are seen with HNBR/TSPMMT blends which indicate strong interaction with the HNBR. A higher signal intensity indicates the existence of clay-polymer interaction, seen with the HNBR/TSPMMT composite (5a, 10). Both 15A and APMMT have small peaks visible which indicate interaction with HNBR, but the lower intensity indicates the interactions are smaller than those observed with TSPMMT.

It is important to note that sulfur vulcanization does not appear to have an effect on the intercalation of the APMMT nanocomposites. Wang et al. reported that a zinc-sulfur complex is capable of being formed that causes a collapse of the gallery spacing

(11). This has been attributed to the primary amine intercalants of the organoclay interacting with the sulfur curatives. This collapse is not evident with the addition of 15A or APMMT, perhaps due to the use of vacuum oven curing rather than compression molding curing. The lack of high temperature and pressure curing has been shown to inhibit the collapse of the gallery spacing (11).

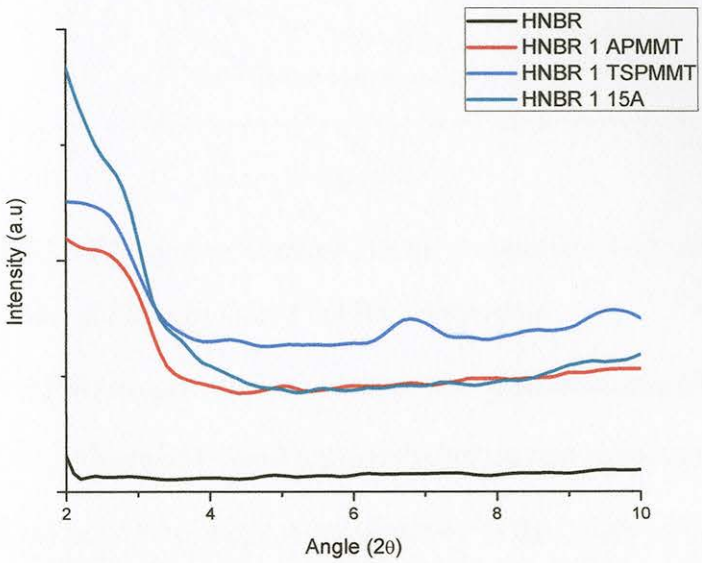

Figure 39. XRD spectra of cured HNBR composites with 1 phr of filler.

Since TSPMMT appears to have the best dispersion and compatibility with the HNBR matrix, higher loading levels were examined in more detail in Figure 40. In line with the arguments presented above, the higher signal intensity of 7 phr loading is indicative of good dispersion, even at high loading levels. Additionally, strong peaks at 3.0 2θ indicate that HNBR is still intercalated within the clay interlayer. The XRD results indicate that higher loading levels of TSPMMT may be effective at producing improved thermal and mechanical properties due to the expansion of the interlayer and the lack of aggregation.

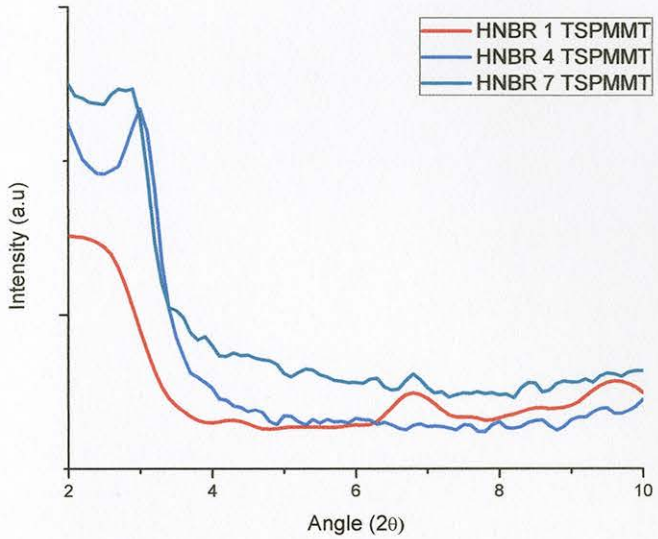

Figure 40. XRD spectra of cured HNBR composites with loading variation of TSPMMT.

Dispersion of Filler in Cured HNBR Composites

AFM images of the as-cured rubber and nanocomposite surfaces are shown in Figure 41. Figures 41 a and b show the height and phase images respectively of the neat HNBR surface. The bright areas observed in the height image are attributed to zinc-oxide aggregates that are formed from residual components of the rubber curing package. Surface images of the 1phr APMMT HNBR cured composite are shown in Figure 41 c, d. The large (~300 nm), bright areas observed in the height image are attributed to APMMT aggregates on the surface, which indicate poor dispersion and surface segregation of the APMMT aggregates. The 1 phr TSPMMT HNBR surface appears smoother, with smaller particles of approximately 10 nm in diameter (Figure 41 e, f). The images indicate a finer dispersion for the TSPMMT/HNBR composite, and provide further evidence of the greater interaction of TSP with the HNBR matrix. The 1phr 15A/HNBR composite surface image shows features consistent with aggregation of the platelet structure. (Figure

41 e, f). In the lower right corner of the figure, an area of agglomerated clay platelets can be seen.

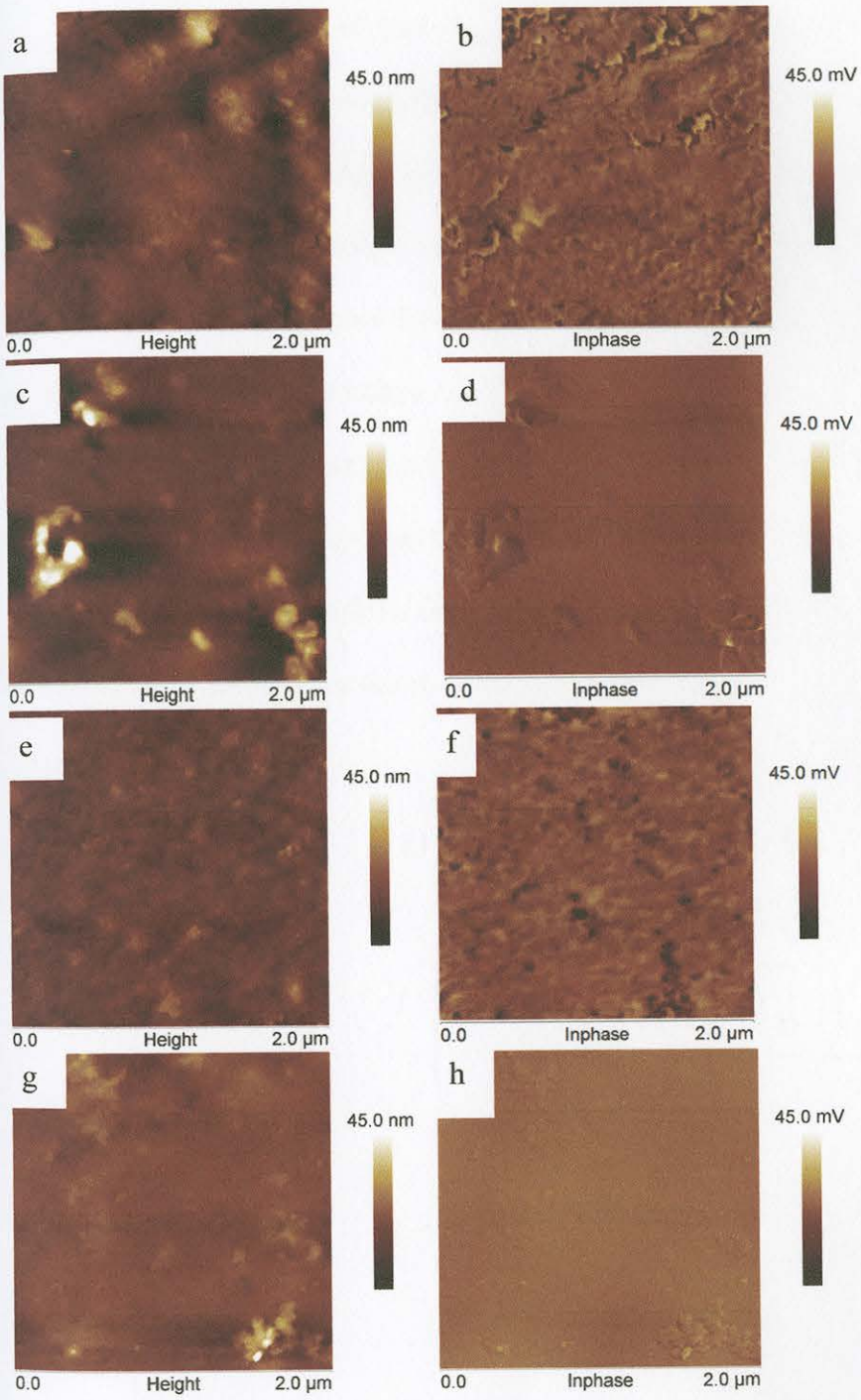

Figure 41. AFM images of surface of (a) height of cured HNBR, (b) inphase of cured HNBR, (c) height of cured HNBR with 1 phr APMMT, (d) inphase of cured HNBR with 1 phr APMMT, (e) height of cured HNBR with 1 phr TSPMMT, (f) inphase of cured HNBR with 1 phr APMMT, (g) height of cured HNBR with 1 phr 15A, (h) inphase of cured HNBR with 1 phr 15A.

While imaging the surface of a nanocomposite provides an indication of particle dispersion, examination of the bulk of the nanocomposite is necessary to determine the distribution of filler throughout the sample. AFM images of fracture surfaces for the unfilled rubber and nanocomposite samples are shown in Figure 42. The unfilled HNBR fracture surface image (Figure 42 a, b) shows features attributed to zinc oxide aggregates, as observed on the surface image. APMMT/HNBR (Figure 42 c, d) and 15A/HNBR (Figure 42 g, h) fracture surfaces show large, hard features consistent with clay particle aggregates, similar to those observed in surface images. The TSPMMT/HNBR nanocomposite fracture surface, on the other hand, shows finely dispersed particles, consistent with the features observed on the surface image.

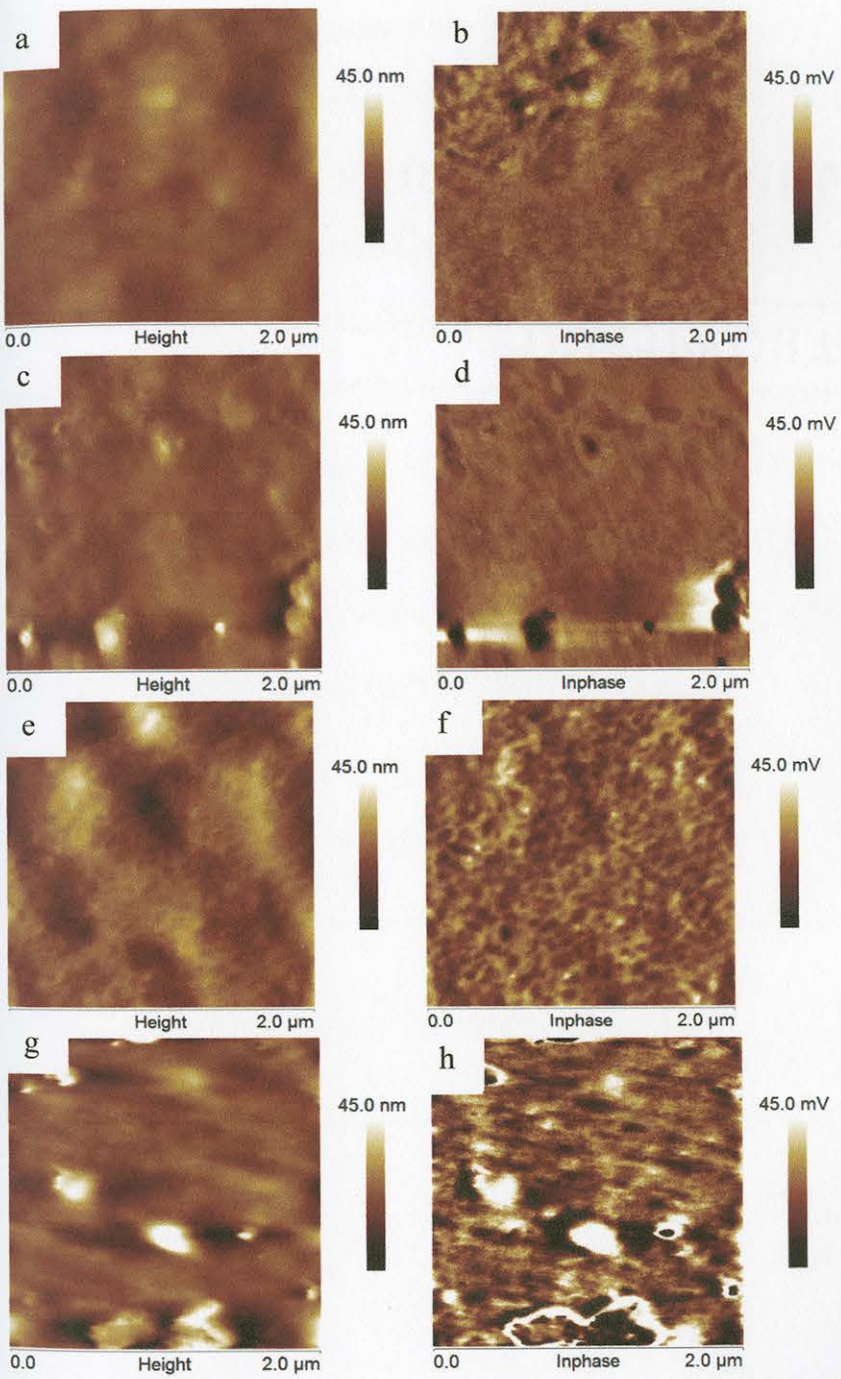

Figure 42. AFM images of fracture surface of (a) height of cured HNBR, (b) inphase of cured HNBR, (c) height of cured HNBR with 1 phr APMMT, (d) inphase of cured HNBR with 1 phr APMMT, (e) height of cured HNBR with 1 phr TSPMMT, (f) inphase of cured HNBR with 1 phr APMMT, (g) height of cured HNBR with 1 phr 15A, (h) inphase of cured HNBR with 1 phr 15A.

Table 4 tabulates particle size and surface roughness data obtained from AFM analysis for the cured samples. Fillers increase the root mean square roughness of the as-cured samples, with TSPMMT providing the smallest increase and APMMT producing the highest increase. Aggregate particle size of the fillers increases in the same order, both on the surface and in the bulk. Surface roughness and aggregate size are inversely related to the dispersion of filler in the composite matrix. Collectively, the as-cured surface and fracture surface AFM images indicate that the TSP modified clay is well dispersed in the rubber matrix, while the APMMT has a strong tendency to aggregate and phase separate. The AFM analysis provides complementary evidence to the rheological and XRD data of the strong TSPMMT/HNBR interactions.

Table 4

RMS roughness values and average particle size of surface and fracture surface of cured HNBR composites

	HNBR	HNBR 1 APMMT	HNBR 1 TSPMMT	HNBR 1 15A
Surface Roughness (nm)	1.2	6.1	2.3	4.0
Average particle size on surface (s.d) (nm)		279.1 (32)	8.53 (1)	11.8 (4)
Average particle size in bulk (s.d) (nm)		70.4 (21)	14.5 (8)	65.5 (18)

Transmission electron microscopy

Figure 43 shows a TEM image of HNBR with 1 phr of APMMT. Dark lines observed in the TEM image represent the cross-sections of single or multiple clay platelets. The average length of the APMMT platelets in HNBR is 150 nm. There is evidence of clay tactoids, or bundles of clay platelets, of various sizes. Tactoids consisting of 3-4 APMMT platelets indicate the presence of intercalated HNBR in the APMMT layers. Large, agglomerated tactoids of APMMT are also observed. Single platelets, evident of exfoliation of the clay layers, are not observed. The TEM images complement the AFM and XRD data presented in the previous sections.

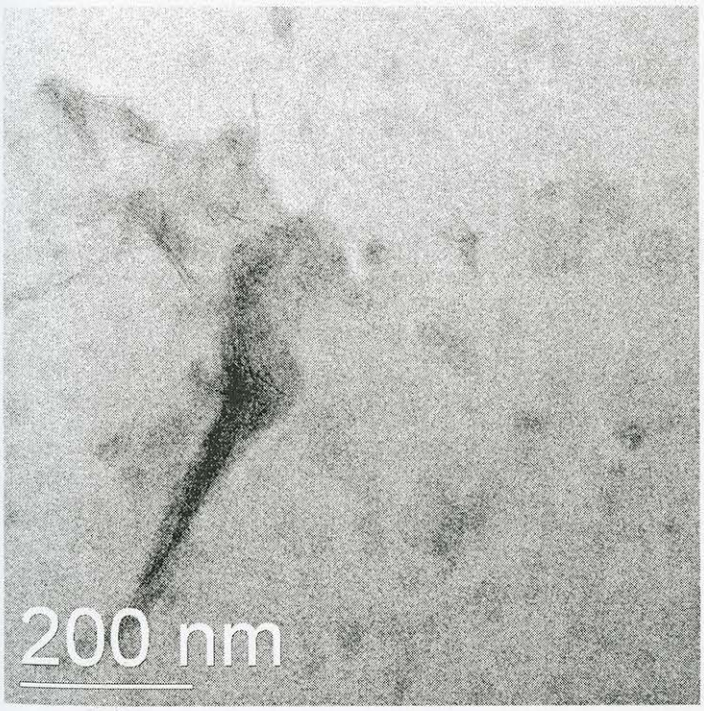

Figure 43. TEM image of cured HNBR with 1 phr APMMT.

Figure 44 shows a TEM image of the TSPMMT HNBR composite. Again, the TEM data supports XRD and AFM analysis of the system. Single, unaligned clay platelets are observed in some portions of the grid, indicating exfoliation. Small tactoids

of 3-4 TSPMMT layers are also observed, indicating intercalation. The length of TSPMMT platelets is on the order of 100 nm. Also important to note is the absence of voids in the micrograph, providing evidence for strong adhesion between the TSPMMT platelets and the HNBR (12).

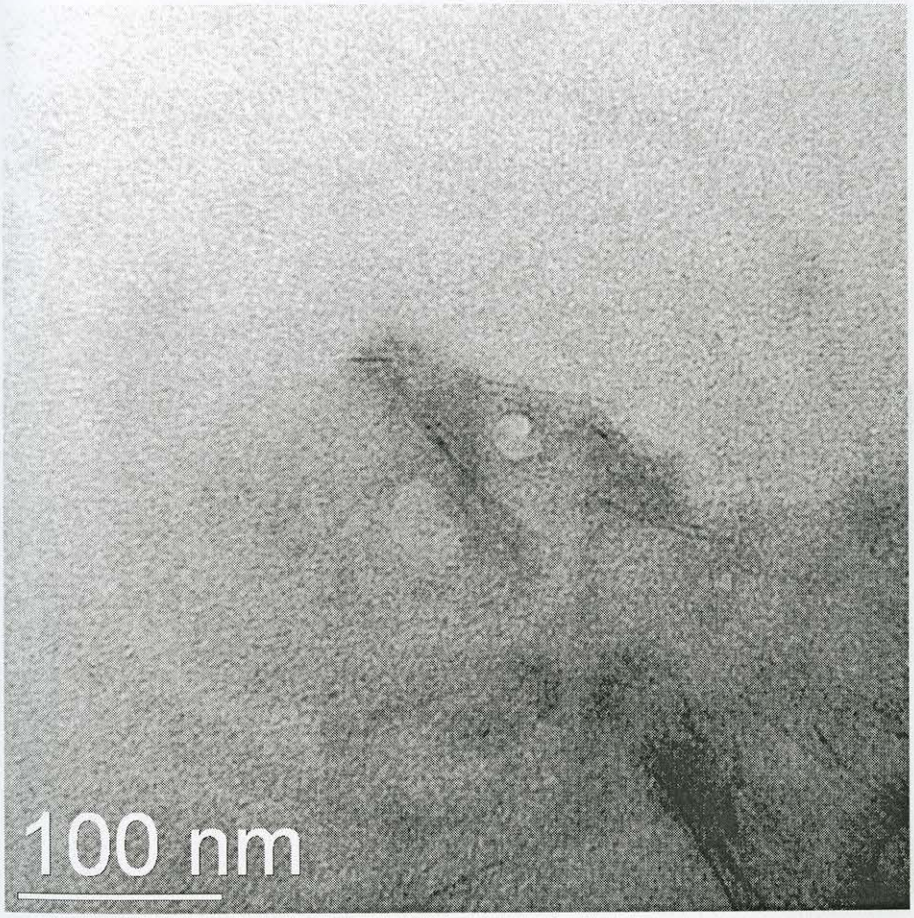

Figure 44. TEM image of cured HNBR with 1 phr TSPMMT.

Viscoelastic Properties

Good mechanical properties of nanocomposites are produced by strong polymer-filler interaction and a high interfacial area of the filler. Generally, the storage modulus increases with the addition of well dispersed nanofillers (6). Figure 45 shows the storage modulus as a function of temperature for cured HNBR and HNBR composites with 1 phr loading of APMMT, TSPMMT and 15A. Below T_g, in the glassy region, all fillers

improve the storage modulus as compared to the unfilled HNBR. This improvement is attributed to mechanical shear mixing which causes a 'house of cards' morphology of exfoliated clay fillers. The increase in modulus of HNBR with all fillers is a reflection of the confinement of the fillers in the rubber after curing. In the rubbery plateau, the largest increase in storage modulus is seen for the TSPMMT composite due to the strong rubber-filler interactions (6). This further reinforces the postulation that hydrogen bonding is present between HNBR and TSPMMT.

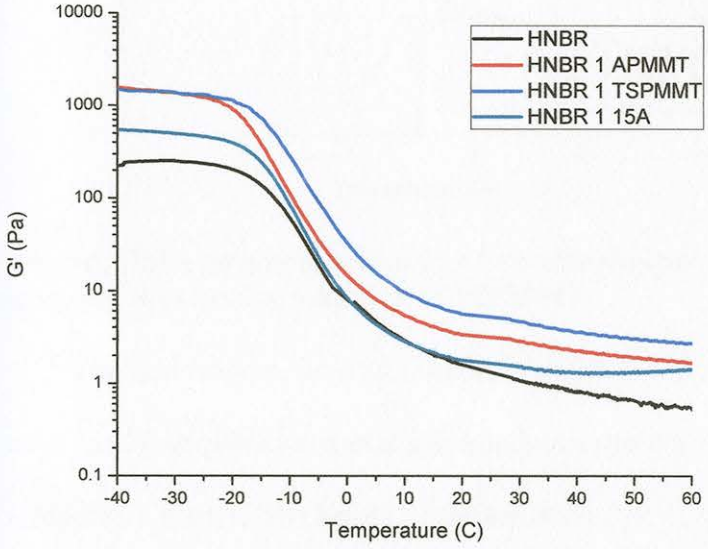

Figure 45. DMA storage modulus results as a function of temperature of cured HNBR composites with 1 phr filler.

Since TSPMMT provides the greatest improvement in storage modulus of the selected fillers, higher loading levels were examined using DMA. All loading levels of TSPMMT produced increases in G' over the unfilled rubber at low strain rates, as shown in Figure 46. In the glassy region, 4 phr loading exhibited the greatest increase, indicating that the saturation point of loading has been reached (5a). Above T_g, 7 TSPMMT loading

provided the largest improvement in modulus. This can be ascribed to the large surface area of the filler, which allows strong rubber-filler interactions (13).

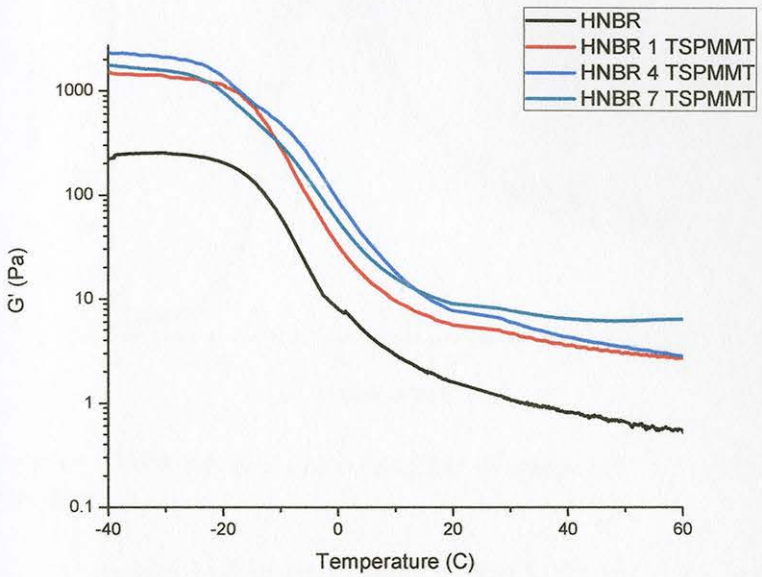

Figure 46. DMA storage modulus as a function of temperature of cured HNBR composites with loading variation of TSPMMT.

The loss tangent, tan delta, which is defined as the loss modulus divided by the storage modulus, provides useful information regarding the damping and reinforcement of a filler in a matrix. The height of the tan delta curve can be correlated to adhesion between the filler and the matrix (13). A reduction in the maximum tan delta height, as seen with the addition of TSPMMT in Figure 47, implies a strong adhesion between TSPMMT and HNBR and indicates that sliding of the filler is suppressed and chain slipping is impeded by the filler (13). The addition of 15A produces no change in the height of tan delta, implying little adhesion. The inclusion of APMMT increases the tan delta peak, implying that there is extremely poor adhesion and interaction between APMMT and HNBR.

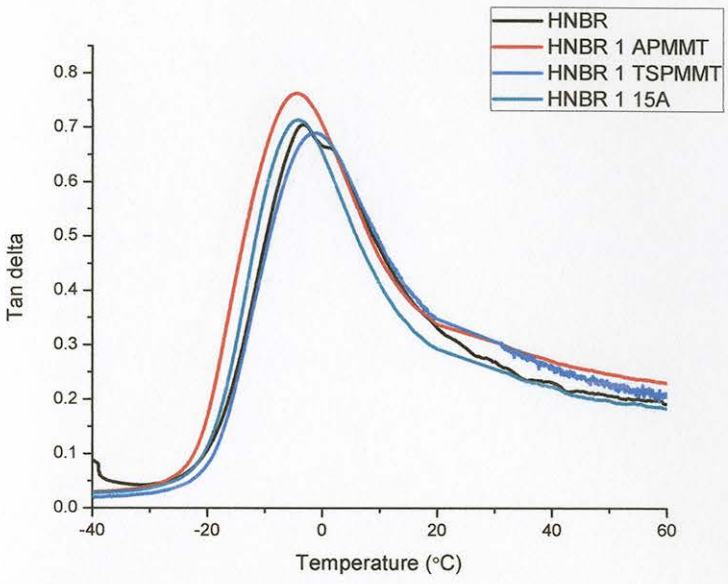

Figure 47. DMA tan delta as a function of temperature of cured HNBR composites with 1 phr filler.

At higher loading levels of TSPMMT, the tan delta maximum decreased, and the T_g and G' increased in comparison to the values obtained for1 phr loading, as shown in Figure 48. However, the T_g decreases at 7 phr loading, indicating that not all property improvements are retained at this loading level.

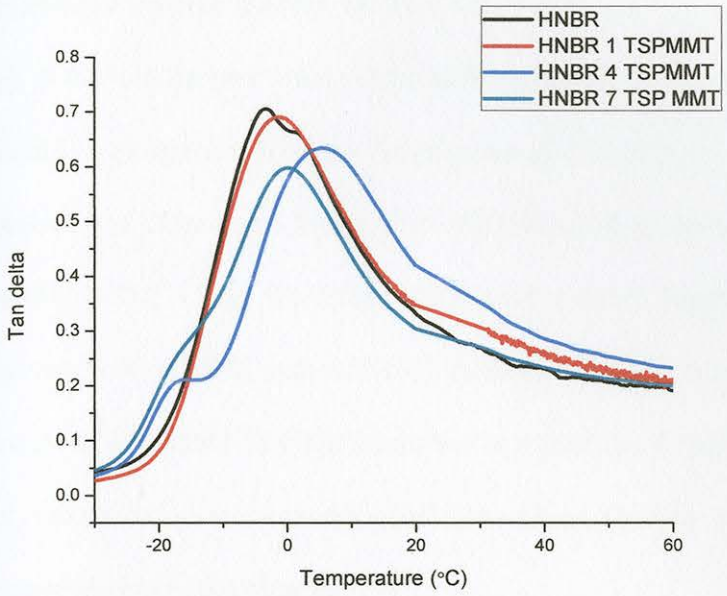

Figure 48. DMA tan delta as a function of temperature of cured HNBR composites with loading variation of TSPMMT.

The shift in glass transition determined by DMA signifies interaction and mobility changes (13). As shown in Table 5, the T_g of unfilled HNBR was -3.6°C. 1 phr TSPMMT caused an increase in glass transition to -2.5°C. This is attributed to the limited mobility of the polymer chains (5b). In contrast, the addition of APMMT and 15A causes a decrease in the glass transition temperature, once again indicating poor polymer-filler interaction. Bhowmick suggests that the plasticization effect may be due to the orientation of clay platelets, which allows slippage of the polymer chains (5b). The parameter B enables us to gauge the interaction between polymer and filler more accurately [9]. The equation:

$$\tan \delta = \frac{\tan \delta_m}{1+1.5B\varphi} \tag{7}$$

can be used to determine polymer-filler interactions. B is a phenomenological interaction parameter which determines the interfacial interaction between the polymer matrix and

filler, φ is the volume fraction of filler, tan δ is the loss tangent of the filled polymer and tan δ_m is the loss tangent value of the unfilled polymer matrix. The larger the B value, the stronger the interaction between the polymer and the filler surface (14). The interaction parameter was determined for the three fillers, and it was found to increase in the order APMMT (-0.79) < 15A (-0.012) < TSPMMT (0.029). Negative B values indicate poor interaction with HNBR, with APMMT demonstrating the lowest level of interaction. The inclusion of TSPMMT in HNBR resulted in a positive B parameter which indicates strong interfacial interaction and good dispersion (14). This analysis reinforces the results discussed earlier in the chapter.

The apparent crosslink density of HNBR with fillers can be determined from the storage modulus at 40°C.The equation:

$$\eta = \frac{G'}{3RT} \tag{8}$$

where η is the crosslink density, G' is the storage modulus at 40°C, R is the gas constant (8.314 J* $(mol*K)^{-1}$), and T is the temperature in Kelvin, can be used to determine the apparent crosslink density (14-15). The crosslink density can be explained by the flexible nature of the filler-polymer interaction. The apparent crosslink density of HNBR is increased with the addition of TSPMMT and APMMT (Table 4). The increase in density can be attributed to strong interaction between the polymer and filler. As expected from rheological studies, the addition of TSPMMT produces the greatest increase in apparent crosslink density, particularly as the loading level increases. At a 1 phr loading level, the apparent crosslink density of HNBR with TSPMMT increases by 173% as compared to the unfilled rubber. The addition of 1 phr APMMT caused a 73% increase. It is important to note that the apparent crosslink density values reflect not only the chemical

crosslinking but also different interactions between the components of the hybrid system (15b).

Table 5

Storage modulus at 50°C, glass transition temperature, and crosslink density of cured HNBR composites

HNBR	1 TSPMMT	4 TSPMMT	7 TSPMMT	1 15A	1 APMMT
Tg (°C)	-3.6	-2.5	5.7	0.2	-4.2	-4.4
G' (MPa) at 50°C	0.66	3.01	3.52	6.34	1.30	1.92
Crosslink density ($*10^5$)	16.8	45.8	55.3	82.8	10.5	29.1

Mechanical Properties

The strain at break of cured HNBR with different loading levels of filler is shown in Figure 49. Although there is large variability in the data, TSPMMT provides an increase in the average strain at break of the cured nanocomposites. As seen with rheological data, a plateau occurs at 4 weight percent loading, and no further improvements are observed at higher loading levels. It is thought that the threshold of loading has occurred, but aggregation has not yet occurred. Due to strong polymer-filler interactions in the TSPMMT system, it is proposed that the polymer can absorb more energy, which is used to decoil the polymer to a high extent (1). The other fillers show decreases in average strain at break at high loading levels. These findings are consistent

with data obtained in previous sections indicating strong interactions and good dispersion for the TSPMMT system, but aggregation and phase separation for the other systems.

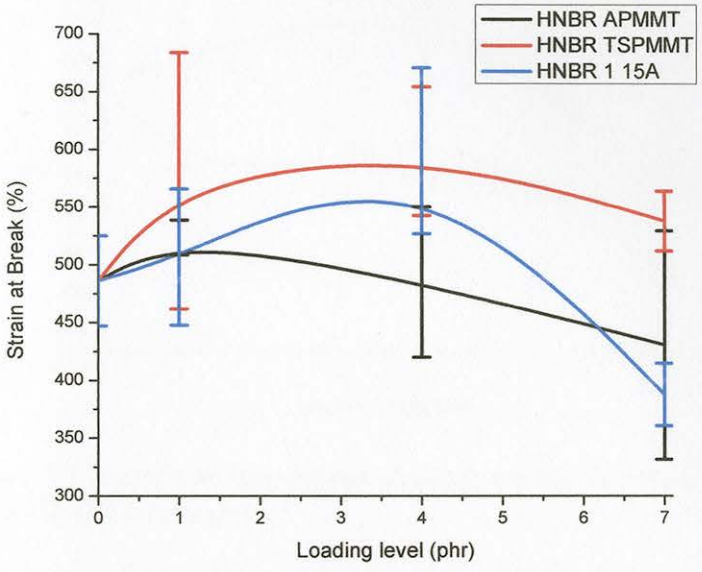

Figure 49. Tensile testing strain at break results as a function of loading level of filler in cured HNBR composites.

Tensile strength at failure data is shown in Figure 50. The data shows high variation, and in general the average strength at break decreases upon addition of filler.

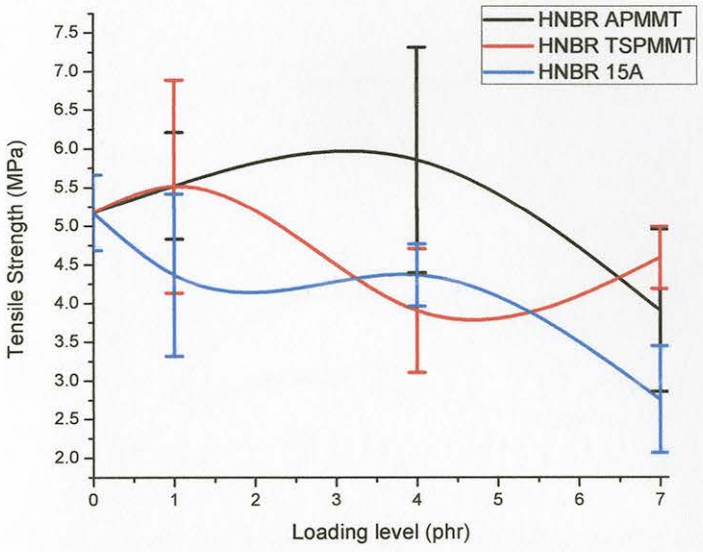

Figure 50. Tensile testing tensile strength results as a function of loading level of filler in cured HNBR composites.

Tensile modulus at 100% strain data is shown in Figure 51. Tensile modulus is improved 136% in comparison to neat rubber on the addition of 7 phr TSPMMT.

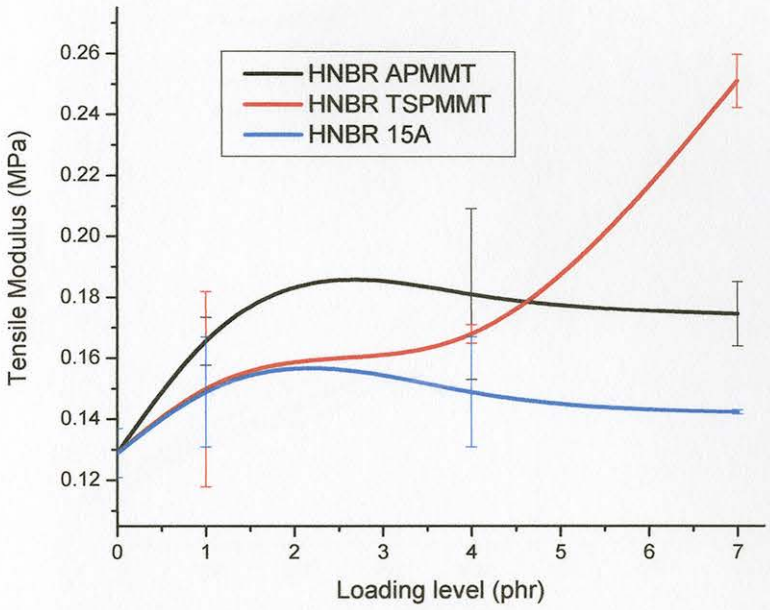

Figure 51. Tensile testing tensile modulus at 100% strain results as a function of loading level of filler in cured HNBR composites.

Stress-strain curves for 1 phr loaded nanocomposites are presented in Figure 52. All of the fillers promote an increase in the stress at failure, and both of the POSS-modified systems provide an increase in strain at failure. TSPMMT provides the greatest improvement in the properties, consistent with all previous analysis.

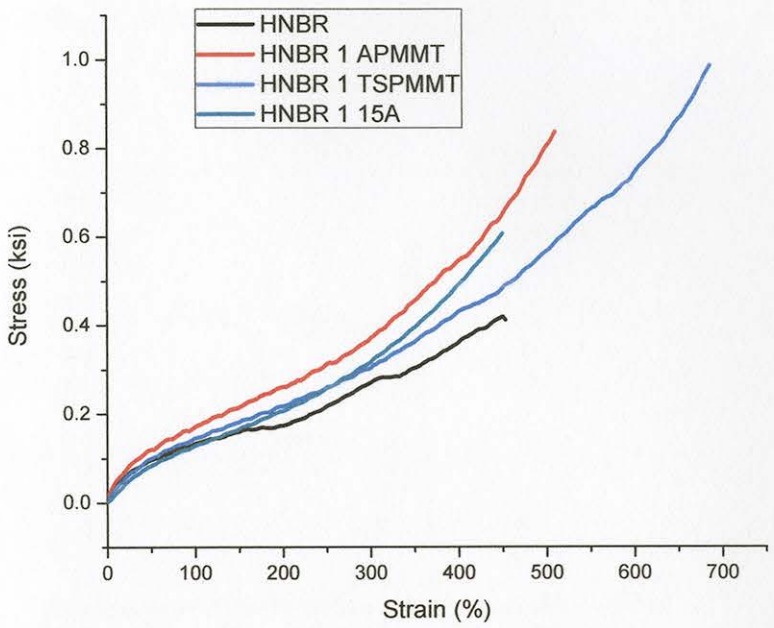

Figure 52. Tensile testing stress-strain curves of cured HNBR composites with 1 phr filler.

Thermal Properties

The effect of fillers on the thermal degradation behavior of HNBR in nitrogen is shown in Figure 53 and Table 6. The temperature at which the maximum rate of degradation occurs for unfilled HNBR is 431.1°C. While all of the fillers increased the degradation temperature, TSPMMT provided the largest increase. The increase of 6.2°C can be attributed to the strong polymer-filler interactions and good dispersion (6). Higher loading levels of TSPMMT do not provide any further improvement in degradation temperature. It should also be noted that although it has been shown that APMMT has poor compatibility with HNBR, the addition of APMMT provides a similar increase in degradation temperature as 15A. POSS has been shown to improve the thermal degradation temperature of rubber, regardless of the aggregation state (16). The use of 15A provides the smallest increase in temperature. It is known that longer alkyl chains,

such as those present in 15A, are less thermally stable compared to shorter chains, such as the isobutyl substituents in APMMT (5b).

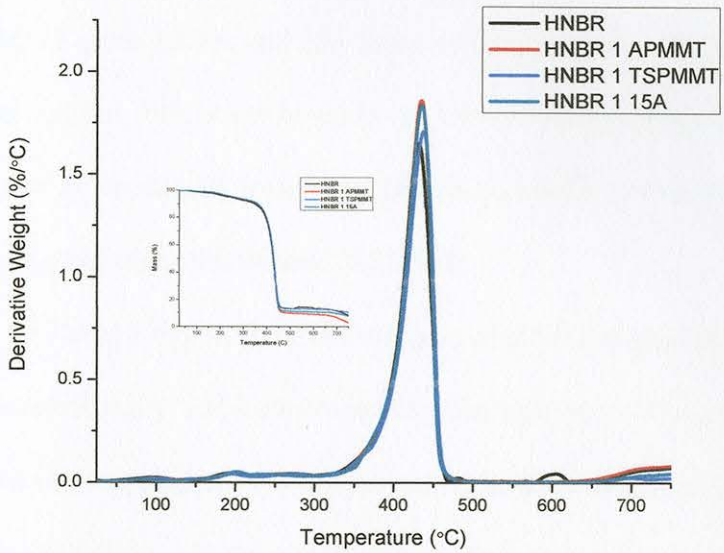

Figure 53. TGA derivative weight of cured HNBR composites with 1 phr filler in nitrogen.

Table 6

Temperature at maximum rate of degradation of cured HNBR with fillers in nitrogen

	HNBR	HNBR 1 APMMT	HNBR 1 TSPMMT	HNBR 4 TSPMMT	HNBR 7 TSPMMT	HNBR 1 15A
Degradation Temperature (°C)	431.1	434.8	437.3	437.5	437.4	434.9

Water Uptake

Water sorption data presented in Chapter III indicate that in a 25°C and 90% relative humidity environment TSPMMT absorbs 17.4% of its original mass, while APMMT gains 10.7% and 15A has a 4.9% mass gain. TSPMMT has the largest degree of water uptake. This is attributed to the low efficiency of the TSPMMT reaction, which resulted in residual hydroxyl groups. These results further reinforce the idea of hydrogen bonding between HNBR and TSPMMT.

Table 7 shows the mass increase of HNBR composites when placed into a 90% relative humidity, 25°C environment. The high permeability of HNBR to water vapor is due to the association of water molecules with the acrylonitrile group. This weakens the rubber cohesion, allowing more water vapor transmission (17). At 1 phr loading, TSPMMT increases the water sorption of HNBR, while APMMT and 15A decrease water sorption. This increase is attributed to the hydrophilicity of the TSPMMT filler. However, at a loading of 4 phr TSPMMT, the water sorption is similar to that of the other fillers at 1phr. It is hypothesized that at 1 phr of TSPMMT, the exposed hydroxyl groups of TSP have not undergone sufficient hydrogen bonding with HNBR, but at 4 phr, the hydrogen bonding level with the nitrile groups of HNBR is high enough to eliminate the exposed hydroxyl groups and decrease the water uptake level. Additionally, the fillers decrease the water uptake of HNBR due to the increased tortuousity of water molecule migration path through the intercalated and exfoliated clay layers (17).

Table 7

Percent mass gain of cured HNBR with fillers at 90% relative humidity and 25°C

Sample	HNBR	HNBR 1 APMMT	HNBR 1 TSPMMT	HNBR 4 TSPMMT	HNBR 1 15A
Mass increase (%)	11.9	11.2	12.7	10.8	9.6

Solvent Uptake

Only 15A causes a reduction in solvent uptake as compared to the unfilled rubber. The interaction of POSS with MEK causes an increase in the swelling with the addition of POSS modified MMT.

The molecular weight between crosslinks was determined using the following equation (18):

$$-[\ln(1-V_r)+V_r)+\chi V_r^2] = \frac{\rho_r V(V_r^{\frac{1}{3}}-\frac{V_r}{2})}{2M_c} \quad (9)$$

Where χ = Flory-Huggins interaction parameter; V= molar volume of swelling solvent; M_c= number average molecular weight of the chain between two crosslinks and $\frac{1}{2}M_c$ = apparent crosslink density, in mol/cc of rubber hydrocarbon. The interaction of solvents with cross-linked rubbers is expressed as a function of concentration in the swollen rubber network and the degree of cross-linking. More details on this equation can be found in the experimental section. With the addition of POSS-modified clay fillers, the molecular weight between crosslinks increases, implying a decrease in crosslink density.

We hypothesize that the partial solubility of POSS in MEK contributes to the low apparent crosslink density. It should be noted that using the solvent sorption technique, there is no way to differentiate a cluster of crosslinks (due to aggregation of the filler) from average crosslinking of the rubber (19).

The difference in crosslink density values from DMA and MEK uptake studies, as seen in Table 8, is due to the effect of the filler on the rubber matrix. DMA crosslink density values are based upon the storage modulus values. This method takes into account the effect of the filler on the matrix, the filler and the cure agent, as well as the crosslinking of the rubber. There is insufficient evidence that this technique is reliable. The solvent uptake technique is reliant upon the percentage of cure the system undergoes. However, there is no method to determine whether the crosslinking is due to the rubber-rubber or rubber-filler crosslinking.

Table 8

Percent mass gain of cured HNBR composites due to MEK, molecular weight between crosslinks, and crosslink density from MEK uptake and DMA

	HNBR	HNBR 1 APMMT	HNBR 1 TSPMMT	HNBR 4 TSPMMT	HNBR 7 TSPMMT	HNBR 1 15A
Percent mass uptake	260	272	271	264	253	246
Molecular weight between crosslinks	20588	22046	21331	25182	20583	16943
Apparent crosslink density from MEK sorption(*10^5)	2.43	2.27	2.34	1.99	2.43	2.95
Apparent crosslink density from DMA (*10^5)	16.8	29.1	45.8	55.3	82.8	10.5

Solubility Parameters

Solubility parameters for the surface modifying agents and the matrix were calculated using the Hoy and Van Krevelen group contribution methods, in an attempt to predict compatibility of the fillers with the rubber. The Hoy method employs the formula:

$$\delta = \frac{\rho \Sigma G_i}{M_0} \tag{10}$$

where δ is the theoretical solubility parameter, ρ is the material density, G_i is a molar attraction constant representing one of the various structural groups present in the molecule, and *Mo* is the molecular weight of the material (20).

Using this equation, a solubility parameter of 12 $(cal/cm^{-3})^{1/2}$ was calculated for TSP and a solubility parameter of 9.3 $(cal/cm^{-3})^{1/2}$ for AP. Solubility parameters were also calculated ignoring the siloxane cage using the van Krevelen group contribution method (20-21), and estimates of 10.78 $(cal/cm^{-3})^{1/2}$ for TSP and 6.90 $(cal/cm^{-3})^{1/2}$ for AP were obtained. Using the Hoy method, Krikorian et al determined that Cloisite 15A has a solubility parameter of 8.37 $(cal/cm^{-3})^{1/2}$ and 8.46 $(cal/cm^{-3})^{1/2}$ using the van Krevelen method (22). Reports indicate that the solubility parameter of HNBR increases from 8.5 $(cal/cm^{-3})^{1/2}$ to 10.5 $(cal/cm^{-3})^{1/2}$ with increasing nitrile content from 10 to 40% (23). These values are summarized in Table 9.

Table 9

Theoretical solubility parameters of HNBR and fillers $(cal/cm^{-3})^{1/2}$

Material	Hoy	Van Krevelen	Average	Reported
HNBR				8.5-10.5
15A	8.4	8.5	8.4	
AP	9.3	6.9	8.1	
TSP	12.0	10.8	11.4	

Misra et al. showed that in a nylon matrix, calculated solubility parameters adequately predicted dispersion levels of selected POSS molecules (24). Due to the high acrylonitrile content of the HNBR used in this study, it can be assumed that the solubility parameter of HNBR is approximately 10 $(cal/cm^{-31/2}$. If the average solubility parameter

value is used, the differences in solubility parameters for the surface modifiers and the HNBR are very close, with that of AP and HNBR equal to 1.9, that of TSP and HNBR equal to1.4 and the difference between 15A and HNBR equal 1.6. The calculated solubility parameters do not adequately distinguish between polymer/filler interactions in the nonpolar hydrocarbon segments and the more polar acrylonitrile domains. Experimental data indicate that the interactions between the acrylonitrile moieties and the fillers dominate nanocomposite performance.

REFERENCES

1. Sadhu, S.; Bhowmick, A. K. Preparation and Properties of Nanocomposites Based on Acrylonitrile-Butadiene Rubber, Styrene-Butadiene Rubber, and Polybutadiene Rubber. *Journal of Polymer Science: Part B: Polymer Physics* **2004,** *42*, 1573-1585.
2. Jeon, H. S.; Rameshwaram, J. K.; Kim, G.; Weinkauf, D. H. Characterization of polyisoprene-clay nanocomposites prepared by solution blending. *Polymer* **2003,** *44*, 5749-5758.
3. Maiti, M.; Bhattacharya, M.; Bhowmick, A. Elastomer Nanocomposites. *Rubber Chemistry and Technology* **2008,** *81*, 384-469.
4. Leuenberger, H. The application of percolation theory in powder technology. *Advanced Powder Technology* **1999,** *10* (4), 323-352.
5. (a) Klafke de Azerdo, L.; Schuster, R. H. NBR/Layered Silicate-Nanocomposites Prepared by Continuous Dynamic Latex Compounding. *Elastomers and Plastics* **2010**, 130-138; (b) Bhowmick, A.; Bhattacharya, M.; Mitra, S. Exfoliation of Nanolayer Assemblies for Inmproved Natural Rubber Properties: Methods and THeory. *Journal of Elastomers and Plastics* **2010,** *00*, 1-21.
6. Bhowmick, A.; Bhattacharya, M.; Mitra, S.; Kumar, K. D.; Maji, P. K.; Choudhury, A.; George, J. J.; Basak, G. C. Morphology-Property Relationship in Rubber-Based Nanocomposites: Some Recent Developments. *Advanced Polymer Science* **2010,** *239*, 1-83.

7. Marrucci, G.; Greco, F.; Ianniruberto, G. Rheology of polymer melts and concentrated solutions. *Current Opinion in Colloid & Interface Science* **1999,** *4* (4), 283-287.

8. Bhattacharya, M.; Bhowmick, A. Correlation of Vulcanization and Viscoelastic Properties of Nanocomposites Based on Natural Rubber and DIfferent Nanofillers, with Molecular and Supramolecular Structure. *Rubber Chemistry and Technology* **2010**, *83* (1), 16-34.

9. Bhattacharya, M.; Maiti, M.; Bhowmick, A. Tailoring Properties of Styrene Butadiene Rubber Nanocomposite by Various Nanofillers and Their Dispersion. *Polymer Engineering and Science* **2008**, 1-18.

10. Gatos, K. G.; Szazdi, L.; Pukanszky, B.; Karger-Kocsis, J. Controlling the Deintercalation in Hydrogenated Nitrile Rubber (HNBR)/Organo-Montmorillonite Nanocomposites by Curing with Peroxide. *Macromolecular Rapid Communications* **2005,** *26*, 915-919.

11. Wang, X.; Huang, A.; Jia, D.; Li, Y. From exfoliation to intercalation- changes in morphology of HNBR/organoclay nanocomposites. *European Polymer Journal* **2008,** *44*, 2784-2789.

12. Valadares, L. F.; Leite, C. A. P.; Galembeck, F. Preparation of natural rubber–montmorillonite nanocomposite in aqueous medium: evidence for polymer–platelet adhesion. *Polymer* **2006,** *47* (2), 672-678.

13. Varghese, S.; Karger-Kocsis, J. Natural rubber-based nanocomposites by latex compounding with layered silicates. *Polymer* **2003,** *44*, 4921-4927.

14. Rooj, S.; Das, A.; Sto¨ckelhuber, K. W.; Reuter, U.; Heinrich, G. Highly Exfoliated Natural Rubber/Clay Composites by ''Propping-Open Procedure'': The Influence of Fatty-Acid Chain Length on Exfoliation. *Macromolecular Materials Engineering* **2012,** *297*, 369-383.

15. (a) Xu, D.; Karger-Kocsis, J.; Apostolov, A. A. Hybrids from HNBR and in situ polymerizable cyclic butylene terephthalate (CBT): Structure and rolling wear properties. *European Polymer Journal* **2009,** *45* (4), 1270-1281; (b) Karger-Kocsis, J.; Felhös, D.; Xu, D. Mechanical and tribological properties of rubber blends composed of HNBR and in situ produced polyurethane. *Wear* **2010,** *268* (3–4), 464-472; (c) Lakshmi, M. S.; Narmadha, B.; Reddy, B. S. R. Enhanced thermal stability and structural characteristics of different MMT-Clay/epoxy-nanocomposite materials. *Polymer Degradation and Stability* **2008,** *93* (1), 201-213.

16. Yang, D.; Zhang, W.; Yao, R. L.; Jiang, B. Z. Thermal Degradation Characteristics and Kinetics of High Temperature Vulcanized (HTV) Silicon Rubber/POSS Hybrid. *Applied Mechanics and Materials* **2012,** *105-107*, 1657-1661.

17. Gatos, K. G.; Karger-Kocsis, J. Effect of the aspect ratio of silicate platelets on the mechanical and barrier properties of hydrogenated acrylonitrile butadiene rubber (HNBR)/layered silicate nanocomposites. *European Polymer Journal* **2007,** *43*, 1097-1104.

18. Flory, P. J.; Rehner, J. H. Statistical mechanics of crosslinked polymer networks II. Swelling. *Journal of Chem Phys* **1943,** *11*, 521-526.

19. Vijayabaskar, V.; Tikku, V. K.; Bhowmick, A. K. Electron beam modification and crosslinking: Influence of nitrile and carboxyl contents and level of unsaturation on structure and properties of nitrile rubber. *Radiation Physics and Chemistry* **2006,** *75* (7), 779-792.

20. van Krevelen, D. W. *Cohesive properties and solubility*. lsevier: New York, 2009.

21. Van Krevelen, D. W.; Nijenhuis, K. *Properties of Polymers: Their Correlation with Chemical Structure; their Numerical Estimation and Prediction from Additive Group Contributions*. Elsevier: The Netherlands, 2009.

22. Krikorian, V.; Pochan, D. J. Poly (L-Lactic Acid)/Layered SIlicate Nanocomposite: Fabrication, Characterization, and Properties. *Chem Mater* **2003,** *15*, 4317-4324.

23. (a) White, J. L.; Kim, K.-J. *Thermoplastic and Rubber Compounds: Technology and Physical Chemistry*. Ohio, 2008; (b) Choudhury, A.; Bhowmick, A.; Ong, C. Novel role of polymer-solvent and clay-solvent interaction parameters on the thermal, mechanical and optical properties of polymer nanocomposites. *Polymer* **2009,** *50*, 201-210.

24. Misra, R.; Fu, B. X.; Plagge, A.; Morgan, S. POSS-Nylon 6 Nanocomposites: Influence of POSS Structure on Surface and Bulk Properties. *Journal of Polymer Science: Part B: Polymer Physics* **2009,** *47*, 1088-1102.

CHAPTER V

STYRENE BUTADIENE RUBBER NANOCOMPOSITES

A comparison study of POSS-MMT/rubber nanocomposites was performed using SBR as the matrix. SBR, shown in Figure 54, is one of the most common rubbers used in industry. SBR's different structure, with a pendant phenyl group in place of the nitrile group in HNBR, allows exploration of the effects of polymer structure on POSSMMT/rubber interactions and dispersion. Additionally, the bulky pendant phenyl group on the SBR polymer chain is known to cause difficulty in SBR intercalation between clay layers (1).

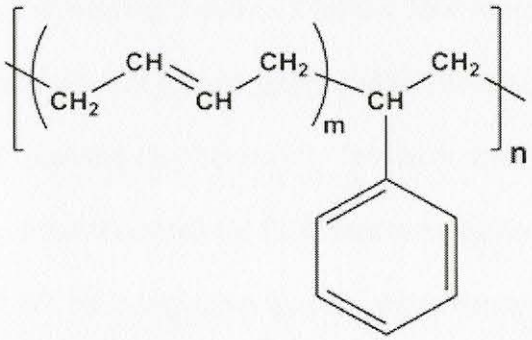

Figure 54. Structure of SBR.

Uncured SBR Composite Rheology

Parallel plate rheology studies of uncured SBR latex/clay blends were performed to evaluate the dispersion and interaction properties of the fillers with the rubber matrix. Figure 55 shows the storage modulus of SBR uncured latex with 1 phr filler. Both TSPMMT and 15A improve the storage modulus of SBR, while APMMT decreases the property. The 20 kPa increase in storage modulus upon the addition of TSPMMT is attributed to the exfoliation of the filler, which will be explored more with XRD analysis. Increased interaction of TSPMMT with SBR is attributed to π–π interactions between the

phenyl rings of the TSP and the SBR, as has been observed previously in studies of POSS with polystyrene (2). Additionally, it is hypothesized that physical connectivity of TSPMMT with SBR is improved due to the large surface area of the filler. The smaller enhancement of approximately 10 kPa observed with 15A is due to the lesser extent of exfoliation when incorporated into SBR and the absence of π-π stacking. The decrease in storage modulus with APMMT as a filler implies the incompatibility between the organic polymer chains and the APMMT. This incompatibility leads to poor dispersion and agglomeration of POSS-modified clay particles that decreases the storage modulus (3). As noted in earlier chapters, the spacing of APMMT is constrained in the (002) and (003) planes, making it difficult for the SBR to intercalate between the clay layers. It is known that the bulky phenyl group on the SBR polymer chain inhibits intercalation of the rubber between the clay layers (1). This may contribute to the smaller enhancement in storage modulus observed for SBR nanocomposites in comparison to those obtained with the HNBR nancomposites discussed in Chapter IV.

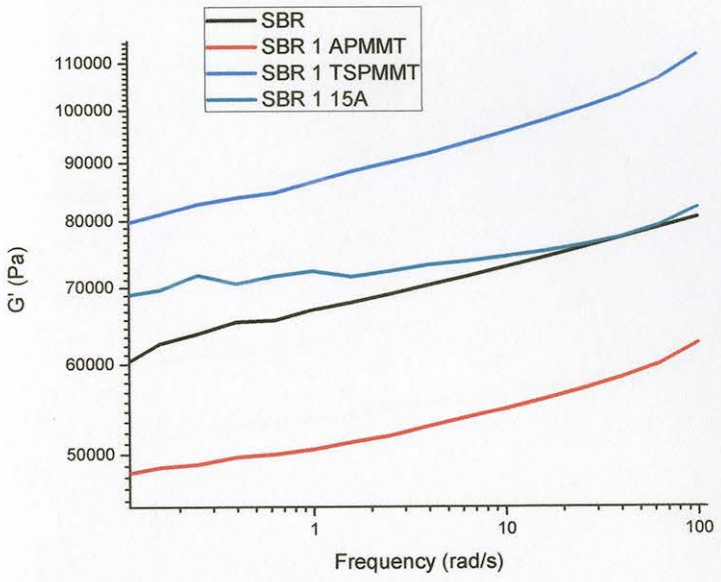

Figure 55. 120°C parallel plate rheology storage modulus as a function of frequency for uncured SBR composites with 1 phr of filler.

The effect of TSPMMT loading level on modulus is shown in Figure 56. The largest improvement in storage modulus, 1.7 times that of the unfilled SBR at low frequencies, is observed at 2 phr TSPMMT loading. At high frequencies the modulus increment increases to three times that of the neat resin. The modulus improvement is attributed to the presence of highly dispersed filler particles in intimate contact with polymer chains that limit polymer relaxation (4).

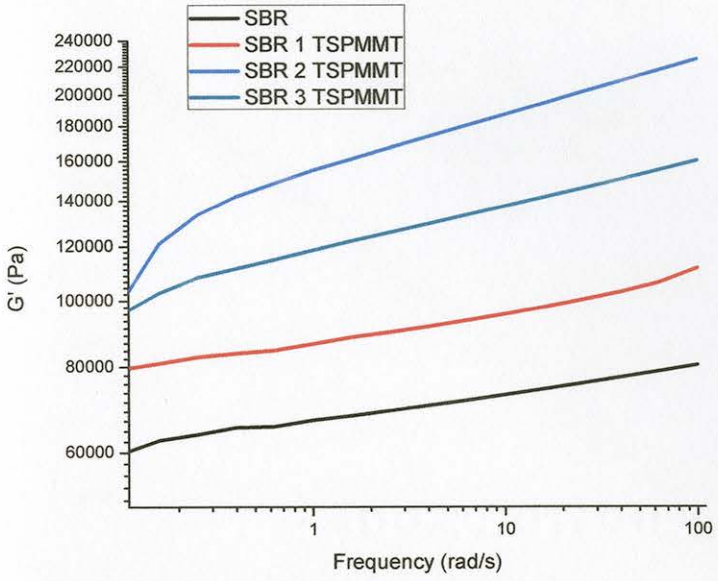

Figure 56. 120°C parallel plate rheology storage modulus as a function of frequency for uncured SBR composites with loading variation of TSPMMT.

Similar trends were observed in the complex viscosity measurements of uncured SBR composites, shown in Figure 57. Both TSPMMT and 15A incorporation resulted in increased viscosity in comparison to the neat resin, while APMMT incorporation resulted in decreased viscosity. This decrease in viscosity is attributed to the smaller available surface area of APMMT interacting with SBR. The decrease in filler-matrix interaction results in increased flow behavior (5). The viscosity increase upon the addition of TSPMMT and 15A is indicative of the resistance to shear deformation that exfoliated clay particles create. Good dispersion and the large surface area of the exfoliated TSPMMT and 15A clay particles contribute to viscosity increases (5). The largest increase in viscosity exhibited by TSPMMT composites provides further evidence of the strong polymer-filler interactions for the SBR/TSPMMT system mentioned previously.

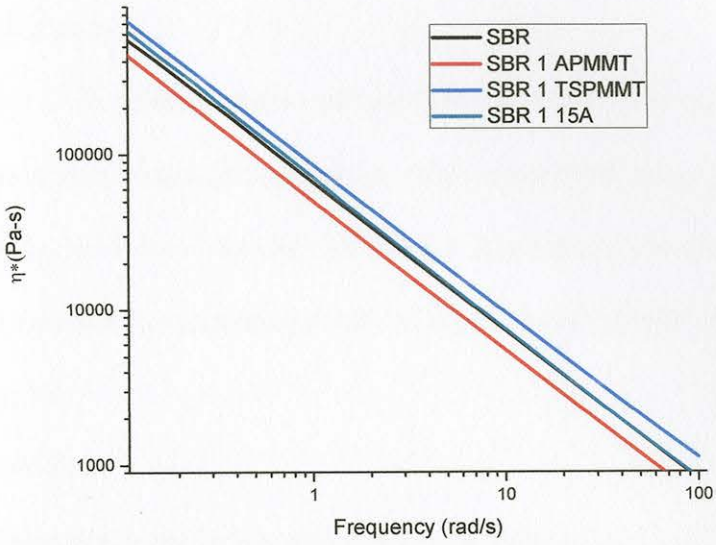

Figure 57. 120°C parallel plate rheology complex viscosity as a function of frequency for uncured SBR composites with 1 phr filler.

The complex viscosity is assumed to follow power law behavior against frequency (6). The linear relationship between log (frequency) and log (complex viscosity) follows the model:

$$\eta^* = K(\omega)^{n-1} \tag{11}$$

Where η* is the complex viscosity, K is the consistency coefficient (Pa s^n), ω is the frequency (rad/s) and n is the flow behavior index. The K values ranged from 4.7 to 5.2 Pa s^n. The flow behavior index, n, ranged from 0.89 to 0.97 (Table 10). Decreases in consistency coefficient indicate increases in flow. The smaller the n value, the larger the departure from Newtonian behavior (7). Calculated K values were substantially higher for the TSPMMT composites than for the neat rubber latex or for systems with the other fillers at the same loading level. High K values indicate constraint of flow due to strong

polymer-filler interactions, providing further evidence of the strong TSPMMT/SBR interactions.

In general, the power law index was lower for the filled systems than for the neat latex, implying a greater degree of deviation from Newtonian flow behavior. In contrast to the behavior observed with HNBR/clay blends, incorporation of fillers in SBR appears to increase the pseudoplasticity of the composites, with the exception of the 1 phr 15A blend.

Table 10

Consistency coefficient and power law index of uncured SBR nanocomposites

	K (Pa s^n)	n	R^2
SBR	4.82	0.96	1.00
SBR 1 APMMT	4.70	0.96	0.99
SBR 4 APMMT	4.74	0.89	0.99
SBR 7 APMMT	4.94	0.90	0.99
SBR 1 TSPMMT	4.93	0.95	0.99
SBR 2 TSPMMT	5.20	0.92	1.00
SBR 3 TSPMMT	5.08	0.93	1.00
SBR 1 15A	4.85	0.97	1.00
SBR 4 15A	4.80	0.93	0.99
SBR 7 15A	4.74	0.91	0.99

Overall, the degree of improvement in modulus behavior on incorporation of modified MMT is dramatically greater for HNBR than for SBR, as illustrated in Table 11. We propose that there is a competition between the π-π stacking of SBR and TSPMMT and the tendency of the bulky phenyl group on the SBR chain to limit the rubber migration between the clay layers and limit the contact between polymer and filler. In contrast, the nitrile groups of HNBR facilitate intercalation and exposure of clay hydroxyl groups, allowing increased TSPMMT/clay hydrogen bonding interactions, as discussed in the previous chapter.

Table 11

Rheological storage modulus of uncured rubbers with 1 phr TSPMMT at 0.1 rad/s and 120°C

% improvement in G' from unmodified rubber	HNBR 1 TSPMMT	SBR 1 TSPMMT
	565.7%	22.7%

Structural Properties of Cured Composites

XRD provides information regarding the structure of the cured composite. XRD spectra for neat SBR and composites with 1 phr filler loading are shown in Figure 58. The neat SBR spectrum shows no peaks, indicating the lack of crystallinity in the matrix (8). Peaks are present in the APMMT, TSPMMT and 15A SBR composites due to the incorporation of the crystalline MMT. The intensity and location of the peaks indicate the degree to which the filler has been exfoliated and/or intercalated into the network (9). All

of the fillers have a peak at approximately 4.0 2θ which signifies that SBR has become intercalated between the clay layers. 15A and APMMT have sharper peaks at this position, which is indicative of a more ordered, intercalated structure within SBR (9). The peak at 6.0 2θ is sharp for SBR with APMMT and SBR, while the SBR/TSPMMT blend has a broad halo. The broad peaks of the XRD spectra of SBR with TSPMMT are indicative of a more exfoliated clay structure (9). However, it is very difficult to achieve pure exfoliation of a filler, and there is most likely a combination of intercalated and exfoliated clay layers. As mentioned in previous chapters, exfoliated fillers generally provide the best properties of a nanocomposite.

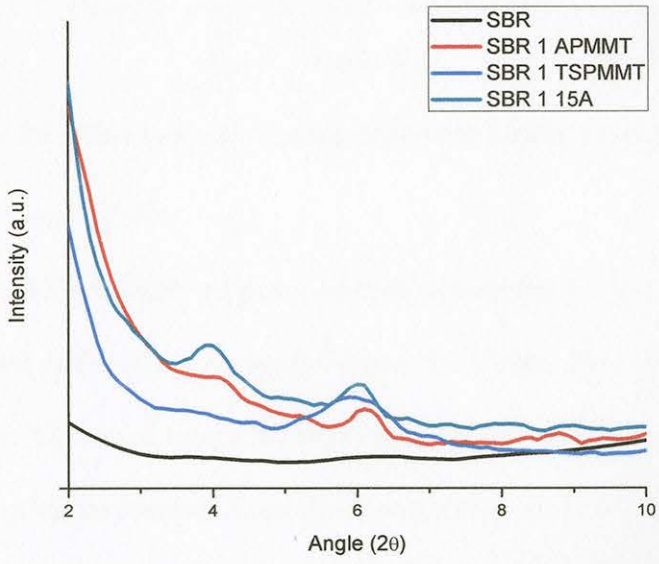

Figure 58. XRD spectra of cured SBR with 1 phr filler.

The XRD analysis of composites with higher loading levels of TSPMMT is presented in Figure 59. In the 2 phr loading of TSPMMT in the cured SBR composite, a peak at 2.1 2θ is apparent which corresponds to a d-spacing of 4.2 nm. This large increase in d-spacing as compared to lower loading levels of filler indicates that more rubber

particles have become intercalated between the TSPMMT layers. Additionally, sharper peaks are observed at 4.0 and 6.0 2θ which indicate strong, intercalated interaction between the filler and matrix at both 2 and 3 weight percent loading of TSPMMT.

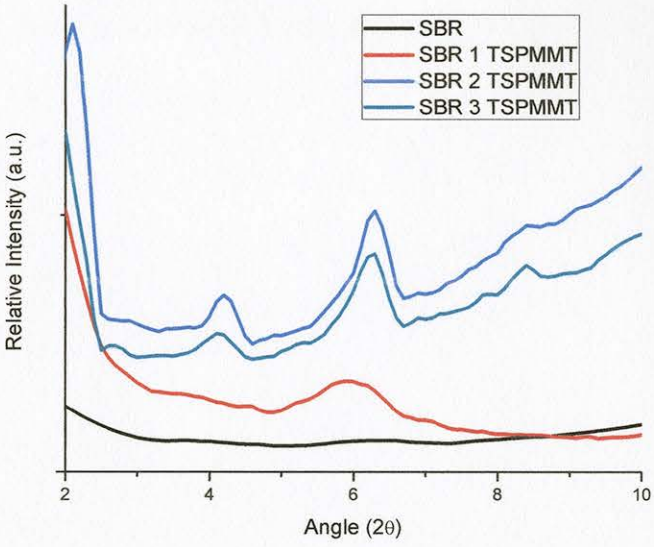

Figure 59. XRD spectra of cured SBR with loading variation of TSPMMT.

Dispersion of Filler

AFM height and phase images of samples of neat SBR and SBR 1 phr composite as-cured surfaces are shown in Figure 60. Figure 60a and 60b show the neat SBR sample. The small bright features observed in the height image are attributed to zinc oxide particles residual from the cure package used. Figure 60c and 60d shows the APMMT/SBR composite surface. Bright, oblongate features of approximately 300 nm diameter appearing in the height image are attributed to aggregates of APMMT.

The surface of the TSPMMT/SBR composite, in contrast, appears very smooth with no apparent aggregation (Figure 60e and 60f). The 15A composite surface again shows large, oblongate bright features over the entire surface, indicating the presence of

15A aggregates (Figure 60g and 60h). These images indicate that the TSPMMT is more finely dispersed than the APMMT and 15A fillers, and shows decreased tendency to segregate to the surface of the rubber. These findings complement the rheological and XRD data, which suggested greater interaction between the TSPMMT filler and the SBR rubber than that exhibited by the APMMT and 15A systems.

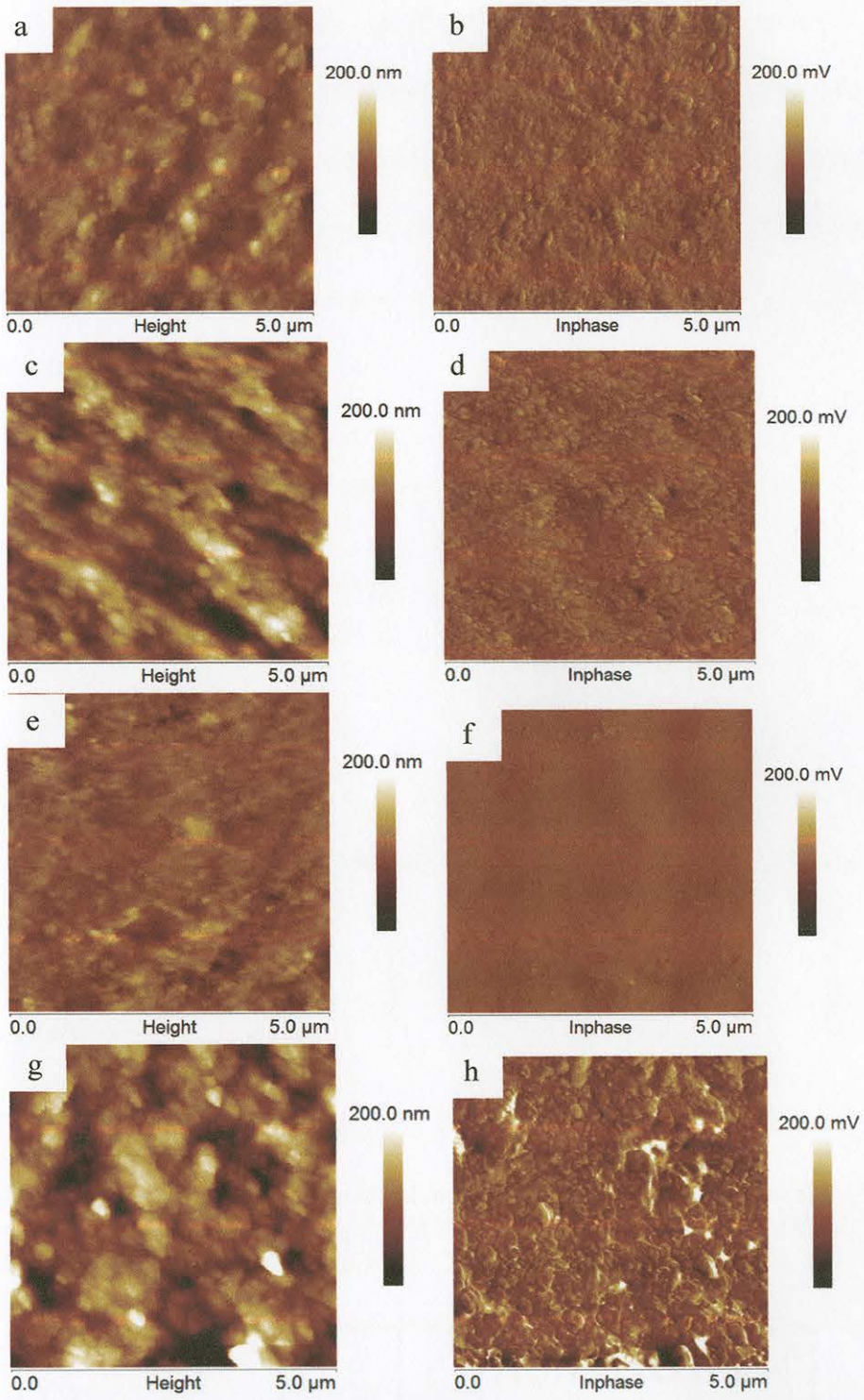

Figure 60. AFM images of surface of (a) height of cured SBR, (b) phase of cured SBR, (c) height of cured SBR with 1 phr APMMT, (d) phase of cured SBR with 1 phr APMMT, (e) height of cured SBR with 1 phr TSPMMT, (f) phase of cured SBR with 1 phr TSPMMT, (g) height of cured SBR with 1 phr 15A, (h) phase of cured SBR with 1 phr 15A.

Figure 61 a, b and 61 c, d show AFM images of the 2 phr and 3 phr TSPMMT/SBR composites, respectively. Non-uniform bright features are apparent on the 2 phr composite surface, while smaller, evenly distributed raised features are observed on the 3 phr composite surface. The raised features are attributed to TSPMMT aggregates, indicating that higher loading levels promote clay aggregation in the SBR system.

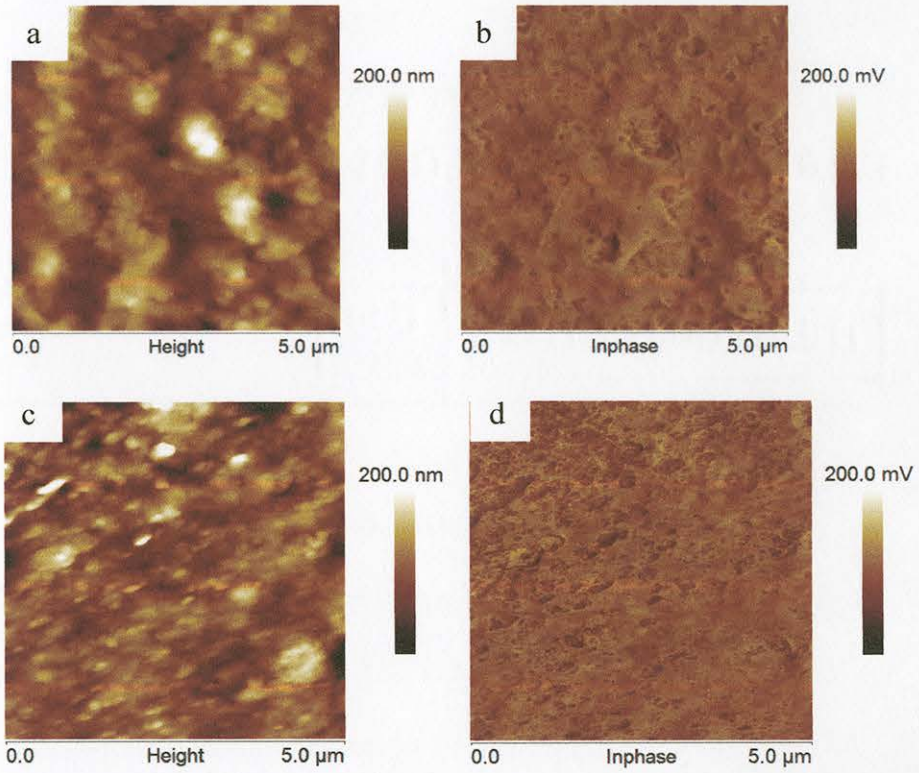

Figure 61. AFM images of surface of (a) height of cured SBR with 2 phr TSPMMT, (b) phase of cured SBR with 2 phr TSPMMT, (c) height of cured SBR with 3 phr TSPMMT, (d) phase of cured SBR with 3 phr TSPMMT.

Root mean square roughness and the average particle size of the fillers observed on the surface of the cured SBR composite samples are shown in Table 12. At 1 phr loading, the measured roughness and particle size values are dramatically lower for TSPMMT than for APMMT and 15A, indicating greater dispersion and interaction of the particle with the rubber for the TSP-modified MMT. With increasing loading levels, the

TSPMMT composites reveal higher roughness and aggregate size, indicating a saturation level for clay dispersion with TSP modification.

Table 12

RMS roughness values and average particle size of surfaces of cured SBR composites

	SBR	SBR 1 APMMT	SBR 1 TSPMMT	SBR 2 TSPMMT	SBR 3 TSPMMT	SBR 1 15A
RMS Roughness (nm)	16.1	28.3	12.3	27.4	27.9	42.0
Average particle size (s.d.) (nm)		318.3 (62)	48.4 (11)	184.5 (30)	124.3 (29)	406.1 (89)

A TEM image of a microtomed 1 phr TSPMMT/SBR composite is shown in Figure 62. Exfoliated silicate layers, tactoids of 4-5 sheets as well as agglomerates in a range of sizes are observed. The TEM analysis is consistent with the XRD findings. The relatively small improvements in viscoelastic properties result from the variable composite morphology, which consists of a combination of exfoliated, intercalated and aggregated TSPMMT structures. While strong interaction between the rubber and TSPMMT is indicated by the contorted positions of the aggregates in the TEM image, intercalation is limited, most likely due to the bulky phenyl substituent on the SBR chain. (10).

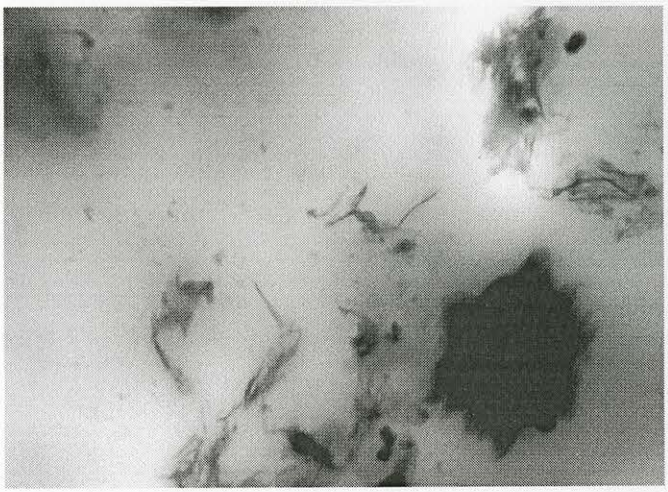

Figure 62. TEM image of cured SBR with 1 phr TSPMMT.

Rheology of cured composites

The rheological properties of vulcanized SBR composites were examined using parallel plate rheology at 120 °C at 1% strain. Figure 63 shows storage modulus as a function of frequency for cured SBR samples. All fillers provided an increase in the modulus in comparison to the neat SBR, with TSPMMT showing the greatest improvement, 15A showing intermediate improvement and APMMT providing only minor increase in G'. In the uncured samples, addition of APMMT resulted in a decrease of G' in comparison to that of the neat SBR. The small increase observed after curing for this system is attributed to stronger physical connectivity between APMMT and SBR upon crosslinking. The increase in storage modulus is very slight, indicative of the poor compatibility of APMMT with SBR.

15A and TSPMMT composites showed improvement in storage modulus in comparison to the neat resin both pre- and post-cure, with TSPMMT composites showing the greatest improvement. Increases in modulus are attributed to exfoliated clay layers, good dispersion, and high levels of interaction between the modified clay and the rubber matrix as discussed previously (11). After curing, the storage modulus of the SBR/ 1 phr

TSPMMT composite increased by 30 kPa as compared to the unfilled SBR. The improvements in properties of the vulcanized system indicate that no damage was created by the sulfur cure system.

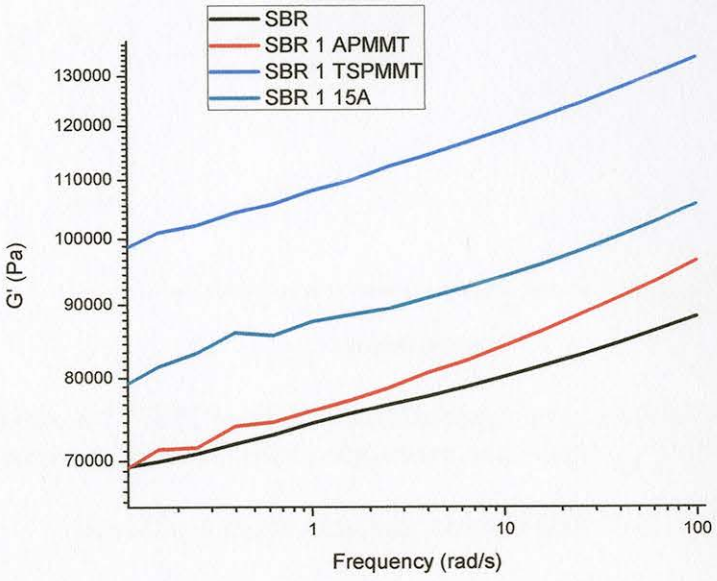

Figure 63. 120°C parallel plate rheology storage modulus as a function of frequency for cured SBR composites with 1 phr of filler.

The effects of higher loading levels of APMMT on SBR modulus are shown in Figure 64. As APMMT loading level increases, G' of the composite decreases, and the composite with 7 phr APMMT shows a 50% reduction in G' in comparison to that of the neat resin. This is attributed to APMMT aggregation and poor interaction of the modified clay with the SBR matrix.

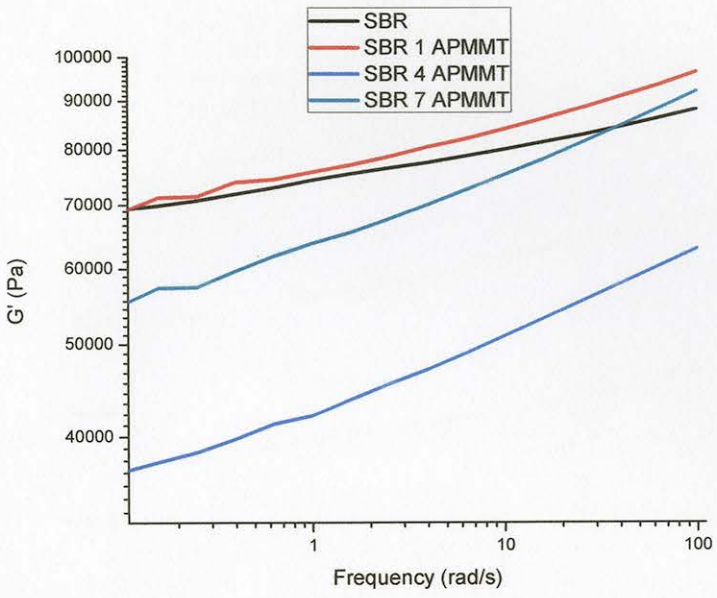

Figure 64. 120°C parallel plate rheology storage modulus of SBR as a function of frequency for cured SBR composites with loading variation of APMMT.

In contrast, higher loading levels of TSPMMT in SBR provide further increases in the storage modulus of the composite, shown in Figure 65. This behavior is indicative of the strong polymer-filler interaction as well as good dispersion of the filler in SBR, even at high loading levels (4). The increase in storage modulus at high loading levels is in contrast to the surface segregation and aggregation at higher loading levels that was noted with AFM.

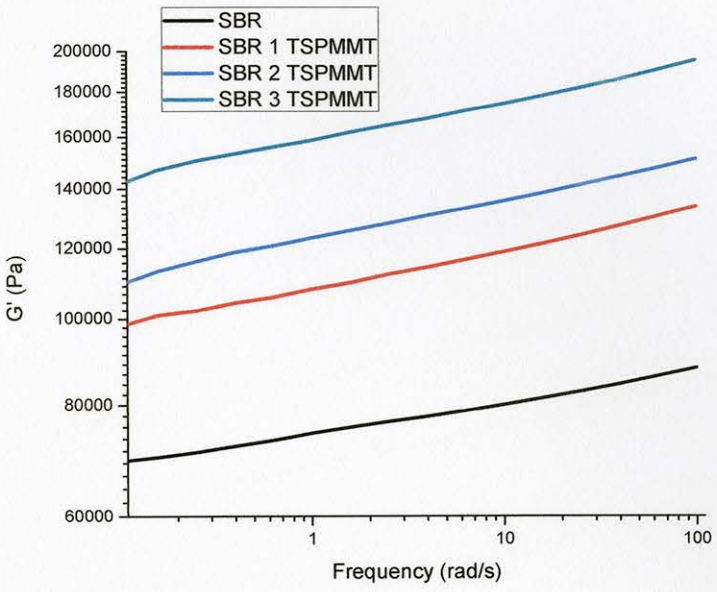

Figure 65. 120°C parallel plate rheology storage modulus as a function of frequency for cured SBR composites with loading variation of TSPMMT.

Increasing loading of 15A in SBR also results in an increase in storage modulus, as shown in Figure 66. However, at a loading level of 7 phr of 15A, the storage modulus is well below that of 3 phr of TSPMMT. It is apparent that high loading levels of 15A are needed to match the viscoelastic properties that are obtained with low loadings of TSPMMT.

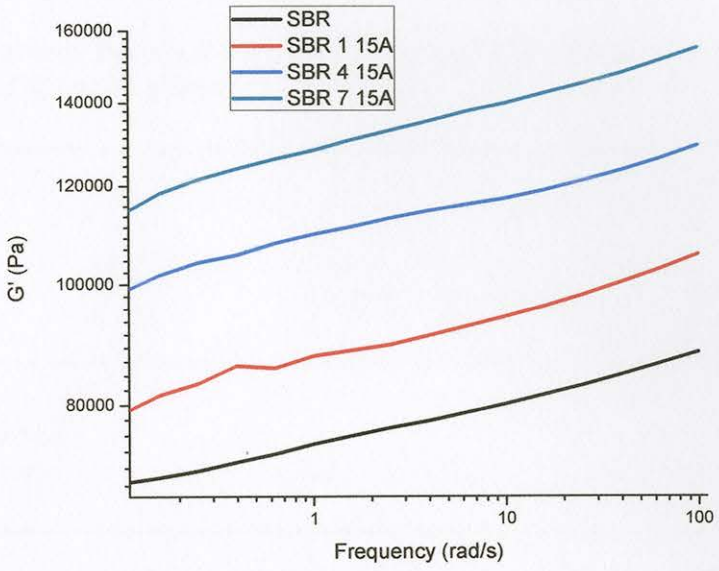

Figure 66. 120°C parallel plate rheology storage modulus as a function of frequency for cured SBR composites with loading variation of 15A.

Water Sorption

Water sorption studies were performed to determine the hydrophobicity of the nanocomposites. Table 13 shows the change in mass when the composite is inserted into a 25°C, 90% relative humidity environment. Due to its non-polar nature, the neat SBR displays a very low water sorption value of 2.3% of its original weight. The addition of fillers results in reduced water uptake, with 15A providing the greatest reduction. The 30% reduction in water uptake observed for this nanocomposite is attributed to the fact that 15A is the most hydrophobic of the three fillers evaluated. The decrease in water uptake upon the addition of fillers is attributed to the increased tortuousity for water vapor transport in the presence of nanofillers (12).

Table 13

Percent mass gain of cured SBR composites and fillers at 90% relative humidity and 25°C environment

	SBR	SBR 1 APMMT	SBR 1 TSPMMT	SBR 1 15A	15A	APMMT	TSPMMT
% Mass Gain	2.3	2.2	2.1	1.6	4.9	10.7	17.4

Solvent Uptake

By placing samples of SBR into toluene, the crosslink density of SBR with the three different fillers was determined. The Flory-Rehner equation used for these calculations can be found in Chapter 4. The crosslink density provides an indication of the curing properties of the rubber. Additionally, these results give an indication of the barrier properties of the material, since well dispersed nanoclays restrict the movement of solvent through the material due to the tortuous pathways that are formed (4). Table 14 shows that upon incorporation of fillers, the crosslink density increased for all samples. This increase implies that the addition of fillers does not interrupt the curing process of SBR. Following the trend in viscoelastic and morphological properties, the largest increase in crosslink density is seen for TSPMMT. This increase corresponds to the greater exfoliation level of TSPMMT. The reliability of the solvent sorption method is mitigated by the uncertainty of the distribution of crosslinks throughout the composite due to possible aggregation of the fillers.

Table 14

Cured SBR composite volume of bound rubber, molecular weight between crosslinks, and apparent crosslink density from MEK uptake

	SBR	SBR 1 APMMT	SBR 1 TSPMMT	SBR 1 15A
Volume bound rubber	0.381	0.385	0.396	0.387
Mass between crosslinks	501..3	486.1	423.7	434.9
Crosslink density ($*10^5$)	99.8	102.9	118.0	115.0

Solubility Parameters

Solubility parameters were calculated by the group contribution method of Hoy in an attempt to predict the compatibility of the clay modifiers with the SBR matrix (13). It was determined that AP had an average solubility parameter of $8.1(cal/cm^{-3})^{1/2}$, while TSP was $11.4\ (cal/cm^{-3})^{1/2}$ and 15A was $8.4\ (cal/cm^{-3})^{1/2}$. The solubility parameters reported in the literature for SBR range from 8.1 to $8.85\ (cal/cm^{-3})^{1/2}$ (14). These values indicate that APMMT and 15A should be the most compatible with SBR. However, it is clear through our studies that this is not the case. As was the case with the HNBR systems, the calculated solubility parameters for these systems appear to overestimate the importance of the alkyl group interactions in the rubber/filler systems, while under-predicting the importance of the interactions with the pendant phenyl group.

Our studies highlight the importance of tailoring the clay surface modification to provide maximal interaction with the rubber matrix. POSS nanostructured chemicals, with their wide range of functional structures, provide an opportunity for precisely tuning clay surface composition to maximize rubber nanocomposite performance.

REFERENCES

1. Sadhu, S.; Bhowmick, A. K. Preparation and Properties of Nanocomposites Based on Acrylonitrile-Butadiene Rubber, Styrene-Butadiene Rubber, and Polybutadiene Rubber. *Journal of Polymer Science: Part B: Polymer Physics* **2004,** *42*, 1573-1585.

2. (a) Dintcheva, N. T.; Morici, E.; Arrigo, R.; La Mantia, F. P.; Malatesta, V.; Schwab, J. J. Structure-properties relationships of polyhedral oligomeric silsesquioxane (POSS) filled PS nanocomposites. *Express Polymer Letter* **2012,** *6* (7), 561-571; (b) Misra, R.; Alidedeoglu, A. H.; Jarrett, W. L.; Morgan, S. E. Molecular miscibility and chain dynamics in POSS/polystyrene blends: Control of POSS preferential dispersion states. *Polymer* **2009,** *50* (13), 2906-2918.

3. Jeon, H. S.; Rameshwaram, J. K.; Kim, G.; Weinkauf, D. H. Characterization of polyisoprene-clay nanocomposites prepared by solution blending. *Polymer* **2003,** *44*, 5749-5758.

4. Bhowmick, A.; Bhattacharya, M.; Mitra, S.; Kumar, K. D.; Maji, P. K.; Choudhury, A.; George, J. J.; Basak, G. C. Morphology-Property Relationship in Rubber-Based Nanocomposites: Some Recent Developments. *Advanced Polymer Science* **2010,** *239*, 1-83.

5. Klafke de Azerdo, L.; Schuster, R. H. NBR/Layered Silicate-Nanocomposites Prepared by Continuous Dynamic Latex Compounding. *Elastomers and Plastics* **2010**, 130-138.

6. Marrucci, G.; Greco, F.; Ianniruberto, G. Rheology of polymer melts and concentrated solutions. *Current Opinion in Colloid & Interface Science* **1999,** *4* (4), 283-287.

7. Bhattacharya, M.; Bhowmick, A. Correlation of Vulcanization and Viscoelastic Properties of Nanocomposites Based on Natural Rubber and DIfferent Nanofillers, with Molecular and Supramolecular Structure.

8. Dai, J.; Huang, J. Surface modification of clays and clay-rubber composite. *Applied Clay Science* **1999,** *15*, 51-65.

9. Gatos, K. G.; Szazdi, L.; Pukanszky, B.; Karger-Kocsis, J. Controlling the Deintercalation in Hydrogenated Nitrile Rubber (HNBR)/Organo-Montmorillonite Nanocomposites by Curing with Peroxide. *Macromolecular Rapid Communications* **2005,** *26*, 915-919.

10. Gu, Z.; Song, G.; Liu, W.; Li, P.; Gao, L.; Li, H.; Hu, X. Preparation and properties of styrene butadiene rubber/natural rubber/organo-bentonite nanocomposites prepared from latex dispersions. *Applied Clay Science* **2009,** *46* (3), 241-244.

11. Lu, Y.-L.; Li, Z.; Yu, Z.-Z.; Tian, M.; Zhang, L.-Q.; Mai, Y.-W. Microstructure and properties of highly filled rubber/clay nanocomposites prepared by melt blending. *Composites Science and Technology* **2007,** *67*, 2903-2913.

12. Gatos, K. G.; Karger-Kocsis, J. Effect of the aspect ratio of silicate platelets on the mechanical and barrier properties of hydrogenated acrylonitrile butadiene rubber (HNBR)/layered silicate nanocomposites. *European Polymer Journal* **2007,** *43*, 1097-1104.

13. van Krevelen, D. W. *Cohesive properties and solubility*. lsevier: New York, 2009.

14. Barton, A. F. *CRC Handbook of Polymer-Liquid Interaction Parameters*. CRC Press: USA, 1990.

CHAPTER VI

CONCLUSIONS

Clay nanofillers provide the possibility of improving the viscoelastic, mechanical and thermal properties of rubbers using cost-effective materials with reduced environmental impact in comparison to that of traditional fillers. The challenge in replacing traditional carbon black fillers is achieving desired properties through even, nanoscale dispersion of clay platelets in the rubber matrix. The use of POSS modified clay fillers to aid in dispersion has been examined in this paper.

Three montmorillonite based fillers in two rubber matrices were examined in an attempt to define structure-property relationships of rubber nanocomposites. The surface modification of two MMT fillers was successfully completed. The first, an ion exchange reaction of AP with MMT, resulted in an expanded interlayer of the clay. XRD studies and molecular simulation studies suggested that there is a tilted bilayer packing of AP within MMT layers, indicated by a shift in the (001) plane from 1.17 nm in MMT to 3.93 nm in APMMT. Although this filler expanded the *a* plane, the *b* and *c* planes were not fully expanded due to the short aliphatic chains present on the amino-POSS.

The incorporation of an open caged POSS molecule, TSP, in the clay system was achieved through a condensation reaction. XRD studies indicated that the silanol-POSS was grafted onto the outside surfaces of the MMT. The small particle size and flaky nature of the TSPMMT particles observed by SEM suggested that the surface area was greater than that of the AP- modified MMT. Water sorption studies indicated that not all of the exposed hydroxyl groups of TSP underwent condensation reactions with MMT during the surface modification process. These unreacted hydroxyls thus remained

available for subsequent reaction with the polymer matrix. As a control filler, a commercially available ion exchanged MMT, 15A, was studied.

Nanocomposites produced from incorporation of the three fillers in HNBR demonstrated very different mechanical, viscoelastic and adsorption properties. TSPMMT provided the largest property improvements in the uncured state. Rheological studies indicated that TSPMMT had the greatest degree of interaction with the HNBR, presumably due to hydrogen bonding of the POSS silanol groups with the HNBR acrylonitrile. Additionally, the open cage POSS molecules demonstrated a lower degree of aggregation than the fully condensed POSS, consistent with previous reports of POSS behavior in selected polymer matrices. In the cured state, XRD analysis indicated that HNBR intercalated in the TSPMMT layers through a shear-adsorption mechanism, even though expanded interlayers were not observed in the TSPMMT in the absence of the rubber. Observed levels of intercalation and exfoliation were greater for the TSPMMT than for the 15A and APMMT systems, attributed to hydrogen bonding in the TSPMMT nanocomposite. Atomic force microscopy and TEM analysis indicated that TSPMMT was better dispersed in the matrix than the other fillers. The increase in glass transition temperature, tensile modulus, and increased temperature of maximum degradation measured for TSPMMT nanocomposites demonstrated the property improvements obtained through incorporation of TSPMMT in HNBR. Small decreases in water uptake were observed for all of the systems tested.

As a comparison study, SBR nanocomposites were evaluated. Again, TSPMMT provided the largest improvements in dispersion and rheological properties. The π-π stacking of the phenyl rings in SBR and TSPMMT is postulated to improve interaction of

this filler with the rubber matrix in comparison to the other modified clays. The rheological and mechanical property improvements observed for SBR nanocomposites were dramatically lower than those observed for HNBR nanocomposites. This was attributed to the general difficulty of intercalating SBR due to the presence of the bulky phenyl substituent.

The exceptional performance of trisilanol POSS modified MMT/rubber nanocomposites was unexpected, as it was assumed that the alkylamine POSS system would provide the greatest degree of clay dispersion. In fact, XRD studies of the modified clays in the absence of the rubber showed significant intercalation for the APMMT, but no evidence of intercalation for the TSPMMT. These findings indicate that the mechanisms of clay incorporation in the rubber matrix are more complicated than originally assumed, and simple hydrophobic modification of the clay surface does not provide optimized properties. This is a potential area for further research.

The use of water vapor and solvent sorption studies provided valuable insight into the continuity of the rubber-filler matrix. In both the HNBR and SBIR filled rubber systems, the addition of fillers resulted in a decrease of the water uptake. This is indicative of the tortuosity effect introduced by the clay fillers in the rubber matrix. Solvent sorption studies revealed differences in the two rubber systems. In the HNBR matrix, at low loading levels MEK uptake increased, and reductions in solvent sorption were observed only at high filler levels. In the SBR matrix, on the other hand, fillers produced appreciable decreases in MEK uptake. Apparent crosslink density was calculated using the Flory-Rehner equation. In the HNBR matrix, the calculated apparent crosslink density was lower in the filled systems than in the neat rubber, while in the SBR

matrix the apparent crosslink density was higher in the filled systems. These estimates of crosslink density do not differentiate between rubber crosslinking, filler interactions and filler-rubber crosslinking. It is likely that the fillers change the distribution of crosslinks within the matrix, and this influences water and solvent uptake. This is another potentially fruitful area for future research.

Theoretical solubility parameters were calculated for the rubber matrices and the fillers. It is interesting to note that the solubility parameters did not correspond to the fillers with the greatest interaction and dispersion in the rubber. Using group contribution methods, the interactions of the phenyl group of SBR and the nitrile group of SBR with the fillers was not taken into account. It is important to note that the examination of a filler before introduction into a rubber matrix is not an accurate method to determine the compatibility and dispersion of a rubber nanocomposite. Calculated solubility parameters, water sorption and XRD analysis of modified clay fillers are not sufficient to predict compatibility with rubber. Further understanding of the physical and chemical interactions of the modified clay surfaces with the rubber matrix is necessary to accurately predict nanocomposite performance.

The studies highlight the importance of tailoring the clay surface modification to provide maximal interaction with the rubber matrix. POSS nanostructured chemicals, with their wide range of functional structures, provide an opportunity for precisely tuning clay surface composition to maximize rubber nanocomposite performance.

Further Research Considerations

The experiments and discussions of this thesis have enabled basic understanding of the properties of POSS modified clays in a rubber matrix. Other aspects of the fundamental understanding of the relationship between POSS, clay and rubber remain unknown and need to be investigated further. The following experiments may be considered for future study.

The examination of POSS and clay separately as fillers may allow for a better understanding of the benefits of the two fillers. Additionally, first modifying clay with the amino based POSS and then grafting with the open caged POSS could provide clay with hydrophobic surfaces at the interlayer as well as the edges and outside surfaces. The chain length of the ion exchanged alkyl ammonium has been shown to determine material properties. Further studies into the alkyl chain length of the amino POSS can be explored.

The effect of the modified clays on rubber crosslinking is not well understood. Controlled processing studies combined with evaluation of the nanoscale morphology might provide better information on this process, and produce better barrier properties in the nanocomposites.

There are a variety of characterization techniques that can be used to study rubber nanocomposites. Gas and water permeation studies could be used to correlate with the solvent and water sorption studies that have been previously conducted. NMR studies may be helpful in determining the exact bonding mechanisms between POSS and clay. Additionally, the exploration of how rubber vulcanization is affected by fillers can be compared using vacuum oven curing to compression molding methods.